UC Irvine

UC Irvine Electronic Theses and Dissertations

Title

Multiproxy speleothem analyses applied to late Pleistocene and Holocene hydrologic reconstruction in Southeast Asia

Permalink

https://escholarship.org/uc/item/1k76f87j

Author

Wood, Christopher Thompson

Publication Date

2019

Peer reviewed|Thesis/dissertation

eScholarship.org Powered by the California Digital Library
University of California

UNIVERSITY OF CALIFORNIA,
IRVINE

Multiproxy speleothem analyses applied to late Pleistocene and Holocene hydrologic reconstruction in Southeast Asia

DISSERTATION

submitted in partial satisfaction of the requirements
for the degree of

DOCTOR OF PHILOSOPHY

in Earth System Science

by

Christopher Thompson Wood

Dissertation Committee:
Dr. Kathleen Johnson, Chair
Dr. Claudia Czimczik
Dr. Francois Primeau

2019

Fig. 4.5 (Morrill et al., 2013a) is available through the Creative Commons Attribution 3.0 License (https://creativecommons.org/licenses/by/3.0/legalcode)

All other materials © 2019 Christopher T. Wood

TABLE OF CONTENTS

LIST OF FIGURES

LIST OF TABLES

ACKNOWLEDGMENTS

Chapter 2 is being prepared for submission to *Quaternary Science Reviews*. Wood, C. T., Johnson, K. R., Griffiths, M. L., Borsato, A. The dissertation author is the primary investigator and author of this manuscript.

Chapter 3 is being prepared for submission to *Geochimica et Cosmochimica Acta*. Wood, C. T., Johnson, K. R., Griffiths, M. L., Borsato, A., Czimcik, C., Walker, J., Xu, X. (author list not finalized). The dissertation author is the primary investigator and author of this manuscript.

Chapter 4 is being prepared for eventual submission and publication. Wood, C. T., Johnson, K. R., Lewis, L. E., Mason, A., Wright, K, Wang, J. K., Griffiths, M. L., Borsato, A. (author list not finalized). The dissertation author is the primary investigator and author of this manuscript.

The love of my parents, William and Becky Wood, despite my increasing distance from home, is very appreciated. I will make my best effort to stay in non-digital contact in the future, as the distance is only going to get larger with my next career move. Thank you for supporting my life and career choices.

I would like to thank my advisor, Dr. Kathleen Johnson, for taking a chance on a scrappy 30-something year old who decided to go back to school, as well as everyone in the Department of Earth System Science at the University of California, Irvine over the last ~5 years. The opportunities and experiences I have had here are immeasurable in value. I appreciate everyone, including faculty, staff, and peers (especially the 2014 PhD cohort) that helped shape my experiences here.

Finally, I thank my cat, Rusty. With or without human-level sentience or decision-making skills, he has nonetheless put up with the travel and cat-sitting adventures necessary during my PhD journey. It is only going to get stranger for you, my friend.

CURRICULUM VITAE

Christopher T. Wood

Upcoming appointment:

University of Waikato; Hamilton, New Zealand (January 2020)

Postdoctoral Research Fellow, Faculty of Science (Waikato Environmental Geochemistry)

EDUCATION

University of California, Irvine (2014 – 2019)

Doctor of Philosophy in Earth System Science, **December 2019**
Department of Earth System Science
Advisor: Dr. Kathleen Johnson
Advanced to Candidacy: September 2016
Master's Degree conferred: December 2016

University of North Carolina at Wilmington (2000-2004)

Bachelor of Arts in Geology, magna cum laude, May 2004
University Honors and Honors in Geology
Minor in Creative Writing
Honors Thesis: "Evidence for recent hydrothermal activity in Endeavor Deep, Juan Fernandez Microplate, Southeast Pacific Ocean"
(Advisor: Dr. Lewis Abrams)

AWARDS AND ACTIVITIES (UC Irvine, 2014 – 2018)

Teaching Assistant – Seven quarters completed (academic years 2015-2018); courses include:
The Atmosphere (ESS5)
Physical Geology (ESS7)
Catastrophes (ESS17)
Paleoclimatology (ESS101)
Field Methods (ESS114)
Advanced Geology (ESS140; two appointments)

AGS Travel Grant – (Associated Graduate Students, UCI) Awarded summer 2018 for travel to Goldschmidt conference (Boston, MA)

MAPS Honorary Fellow – (Machine Learning and Physical Sciences) 2017-2018
Honorary (unfunded) fellow: participation in NSF program included a group project, presentation, and a year-long team science course

ARCS Scholar – (Achievement Awards for College Scientists) Awarded 2016-2018
Orange County Chapter (https://orange-county.arcsfoundation.org/); two-year merit based supplementary scholarship award

Graduate Student Representative (2016-2017) Official graduate student liaison between faculty and graduate students in the Department of Earth System Science; organization of many events
and official activities (position elected by peers)

CLEAN Education Outreach (Climate, Learning, Empowerment, Action, and iNquiry)
2014-2018; Lead presenter (2016) and frequent volunteer in local middle school outreach initiative run by graduate students

AISIESS Teaching Assistant – (American Indian Summer Institute in Earth System Science)
Summer 2016 – Two-week summer institute for American Indian high school students

Jenkins Family Graduate Fellowship – Awarded 2014-2015
(http://www.ess.uci.edu/grad/fellowships/jenkins)

PUBLICATIONS AND PRESENTATIONS

Publications (*in prep. or in revision*):

Wood C., Johnson K., Griffiths M., Borsato A. Speleothem trace element responses over the last deglaciation and Holocene in Northern Laos. (in prep; target journal: *Quaternary Science Reviews*)

Wood C., Johnson K., Borsato A., Frisia S., Griffiths, M. Speleothem radiocarbon evidence for paleohydrologic changes in Mainland Southeast Asia. (in prep.; target journal: *Geochimica et Cosmochimica Acta*)

Johnson, K. R., Griffiths, M., Bhattacharya, T., Borsato, A., **Wood, C. T.**, Frisia, S., Henderson, G., LeGrande, A., Lewis, M., Mason, A., Syed, S., Tierney, J., Wang, J. K., Yang, H. (in revision). Orbital and millennial variability of Southeast Asian hydroclimate over the past 38,000 years. (in revision for submission to *Nature Geoscience*)

Griffiths, M. L., Johnson, K. R., Pausata, F. S. R., White, J. C., Henderson, G. M., **Wood, C. T.**, Yang, H., Ersek, V., Conrad, C., Sekhon, N. (in revision). Holocene megadroughts in the middle Mekong basin linked to global climate changes. (in revision for submission to *Science Advances*)

Publications:

Bergel, S., Carlson, P. E., Larson, T. E., **Wood, C. T.**, Johnson, K. R., Banner, J. L., Breecker, D. O. (2017). A subsoil carbon source to cave-air CO_2 and speleothem calcite in central Texas. *Geochimica et Cosmochimica Acta*, **Volume 217**, 112-127.

Conference Abstracts and Presentations:

2019

Guest Lecture: Minerals and an introduction to the rock cycle (October 10, 2019). ESS 140: Advanced Geology; Department of Earth System Science, University of California, Irvine.

Radiocarbon Short Course 2019 (August 12-17, 2019). University of California, Irvine; Department of Earth System Science (Irvine, CA)
Wood C. (2019) Radiocarbon utilization in speleothems.
(oral presentation)

Southeast Asian Paleoclimate Workshop: Isotopes in the Environment (January 5-6, 2019) International Center for Tropical Highlands Ecosystems Research (Bidoup-Nui Ba National Park, Vietnam)
Wood C. (2019) Speleothems and paleoclimate: multiproxy studies over the last deglaciation and Holocene in Northern Laos.
(oral presentation)

2018

AGU Fall Meeting 2018 (Washington, D.C.)
Wood C., Johnson K., Griffiths M., Borsato A., Frisia S. (2018) Deglacial and Holocene hydrologic shifts in Southeast Asia inferred from speleothem trace elements and ^{14}C. [Abstract #380419; final paper #PP33D-1743]
(poster presentation)

Goldschmidt 2018 (Boston, MA):
Wood C., Johnson K., Borsato A., Frisia S., & Griffiths M. (2018) Speleothem ^{14}C as a paleoclimate proxy in Northern Laos: comparisons with multiproxy data. *Goldschmidt Abstracts*, **2018**
(poster presentation)

2017

Goldschmidt 2017 (Paris, France):
Wood C., Johnson K., Griffiths M., & Henderson G. (2017) Speleothem Trace element responses over the last deglaciation and Holocene in Northern Laos. *Goldschmidt Abstracts*, 2017 **4288**
(oral presentation)

Summer School for Speleothem Science ("S4") (Burgos, Spain):
Attendance, participation, and a brief poster presentation

Climate Change: The Karst Record VIII ("KR8") (Austin, TX):
Wood C., Johnson K., Griffiths M., & Henderson G. (2017) Speleothem Trace element responses over the last deglaciation and Holocene in Northern Laos.
(poster presentation)

ABSTRACT OF THE DISSERTATION

Multiproxy speleothem analyses applied to late Pleistocene and Holocene hydrologic reconstruction in Southeast Asia

By

Christopher Thompson Wood

Doctor of Philosophy in Earth System Science

University of California, Irvine, 2019

Dr. Kathleen Johnson, Chair

Paleoclimate proxy records from U-Th dated speleothems (cave deposits) provide evidence of past climate change on a range of timescales. The oxygen isotope composition ($\delta^{18}O$) of speleothems from the East Asian Summer Monsoon (EASM) region have been critical in confirming large-scale changes in monsoon intensity linked to Earth's orbital variations, which influence the spatial and temporal patterns of incoming solar radiation, and to abrupt millennial-scale changes in ocean circulation, which influence the meridional temperature gradient. However, multiple controls affect speleothem $\delta^{18}O$, and significant debate continues about the precise interpretation of these records in regard to monsoon precipitation patterns. Furthermore, a scarcity of records from Mainland Southeast Asia (MSEA) has thus far prevented confident reconstructions of past monsoon and precipitation changes across the entire Asian Monsoon region. The research presented in this dissertation addresses these issues through: (1) extending the spatiotemporal coverage of speleothem paleoclimate records in MSEA, and (2) developing more robust records of past monsoon history and local water balance through the use of multiple proxies in a ~38,000 year old stalagmite from Tham Doun Mai Cave, Laos.

Through the application of cave monitoring data and geochemical modeling of the local environment, trace element ratios (Mg/Ca and Sr/Ca) and carbon isotopes ($\delta^{13}C$ and ^{14}C) in stalagmite TM-17 are determined to be responsive to local hydrology through various controls: prior calcite precipitation (PCP) increases trace elements and $\delta^{13}C$ during drier periods, while the dead carbon proportion (DCP), calculated from ^{14}C data, reveals a significant bedrock dissolution control on TM-17 carbon. DCP data also reveals alternate $\delta^{13}C$ controls as dominant during disparate abrupt climate events during the last deglaciation and Holocene. During the Holocene, when PCP is likely a shared control, trace element ratios and $\delta^{13}C$ provide evidence for a mid-Holocene peak in rainfall amounts, which is at odds with interpretations of EASM $\delta^{18}O$ records that suggest an earlier peak in monsoon intensity during the Northern Hemisphere summer insolation maximum. The results of these studies emphasize the importance of multiproxy approaches to speleothem-based climate reconstruction and provide new data for comparison with other records and climate model simulations.

Chapter 1

Introduction

1.1 Introduction to hydrologic reconstruction using multiproxy speleothem records

Despite providing significant advances on past climate change on a variety of timescales, traditional speleothem proxies, such as $\delta^{18}O$ and $\delta^{13}C$, remain controversial in their interpretations, especially in the greater Asian Monsoon (AM) domain. Despite the difficulty in ascertaining rainfall amount interpretations from changes in $\delta^{18}O$, localized reconstructions of rainfall and/or moisture conditions may be possible via multiproxy speleothem analyses involving additional hydrologically responsive proxies. The purpose of this research is to reconstruct the past hydrology of Mainland Southeast Asia (MSEA) as seen through a stalagmite record from Northern Laos. This well-dated sample, TM-17, spanning the most recent ~38,000 years, is analyzed using a new record of trace element ratios (Mg/Ca and Sr/Ca), new measurements of the dead carbon proportion (DCP - evidenced by ^{14}C measurements), and modern monitoring samples collected on multiple field campaigns. These new data assist in interpretations of the local hydrologic history via proxy interpretations enhanced by simple models of the cave's geochemical environment. Additionally, the 8.2 ka event, a major, relatively recent global climate anomaly is investigated at greater resolution using all available proxies. The controls and interplay of multiple speleothem proxies assists in the interpretation of each element or isotope, and the methods used can be applied towards developing other cave climate records. These new records and the corresponding analyses aim to assist in the

reconstruction of ever-growing global paleoclimate records of terrestrial environments, providing a comparison framework for climate models and enhancing future predictions of the AM's response under anthropogenically-induced climate change.

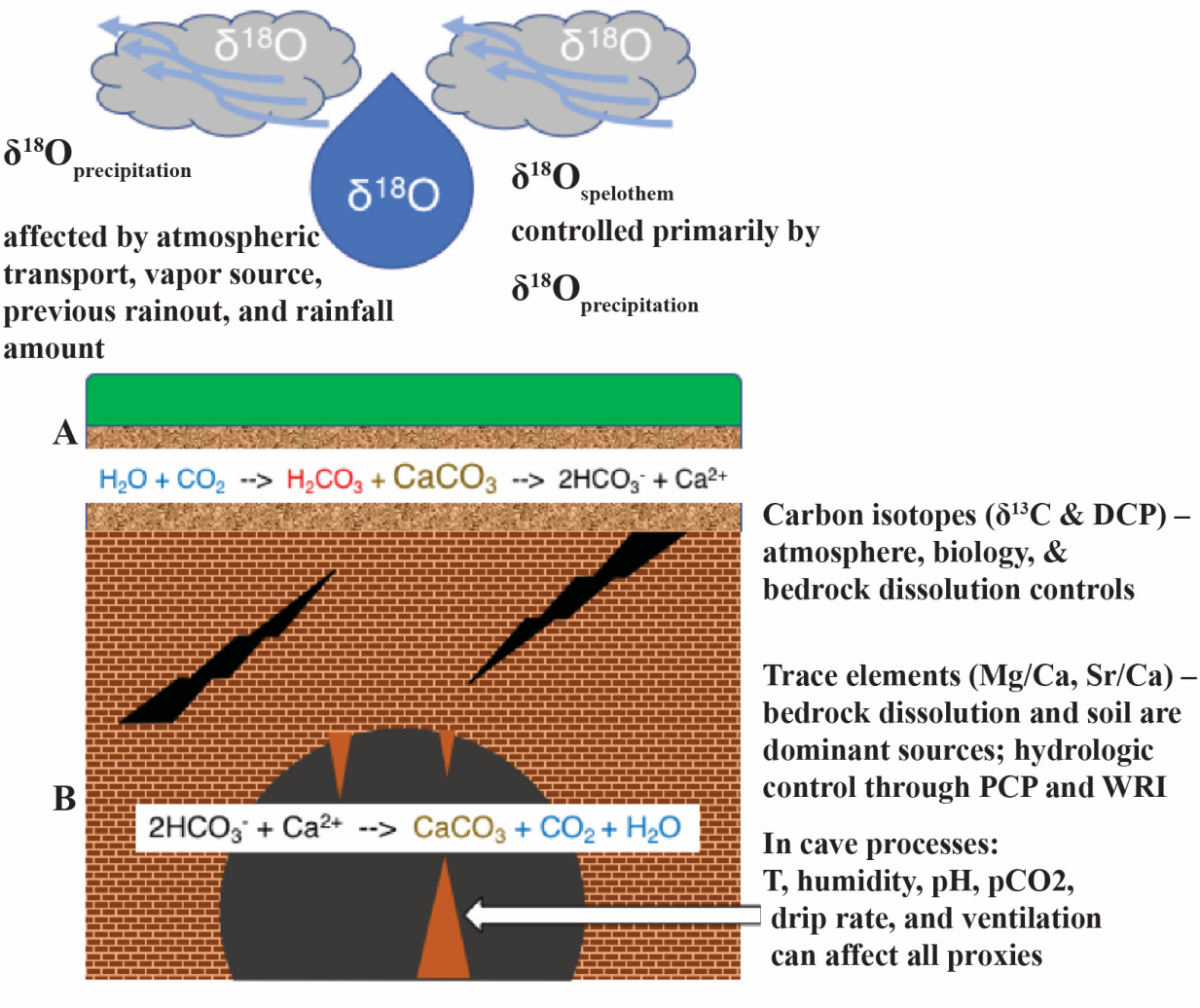

Figure 1.1 – Cave proxy schematic - *Schematic of precipitation / water vapor, the vegetation and soil zones, the epikarst (sub-soil zone of fractured and highly weathered bedrock), bedrock (brick symbols represent calcite and/or dolomite bedrock) and speleothem (stalagmite) proxy sources and controls.* ***A*** *–* ***Eq. 1*** *from text expanded to include carbonic acid (H_2CO_3) step ($CaCO_3$ is encountered after acid formation and is not a chemical product of the first reaction).* ***B – Eq. 1*** *reversed when calcium carbonate is precipitated from drip water due to lowered pCO_2 in cave air. (Figure not to scale.)*

1.2 Speleothems as paleoclimate archives: an overview

In order to better predict the future of Earth's climate under changing conditions, modern observations are best matched with past evidence or records of specific events that mimic current or future climate scenarios. The study of ancient climate, or paleoclimate, is therefore more than just a fascinating look into Earth's natural history. A major function of paleoclimate studies is to improve the general understanding of how the Earth System works, how sensitive to specific forcings the Earth may be, and what consequences the response(s) will have on human civilization and the natural world. Even with a plethora of modern observations and modeled future scenarios, such as those reported in the Intergovernmental Panel on Climate Change ("IPCC;" Stocker et al., 2013), the evidence of abrupt and/or significant climate change in Earth's history is not fully understood or well-represented by climate models, and these instances paint scenarios that may be more extreme than any currently predicted changes (Alley, 2003). Thus, many paleoclimate archives and their corresponding climate proxies have been studied by scientists. These include ice cores, ocean sediment cores, tree rings, fossil corals, lake sediments, and many others. As the capabilities and time ranges for paleoclimate archives are exceptionally variable, the focus here is on an archive relatively new to science, the speleothem, and its relationship to reconstructing monsoonal rainfall histories in the greater AM region.

The term speleothem simply means cave deposit (Moore, 1952), and it may refer to any of the numerous shapes and sizes of secondary mineral depositions found inside of a cave. Speleothems form through the degassing of CO_2 from drip waters previously acidified in the soil zone (**Fig. 1.1**), as the degassing reaction precipitates $CaCO_3$ (**eq. 1**; Fairchild & Baker, 2012):

$$Ca^{2+} + 2HCO_3^- \underset{\substack{precipitation\ to\ right \\ dissolution\ to\ left}}{\longleftrightarrow} CaCO_3 + CO_2 + H_2O \qquad \textit{eq. 1}$$

Eq. 1 can also be reversed (moving to the left) to represent the dissolution of limestone in the above-cave environment as rain or ground water is acidified and creates a weak carbonic acid (step assumed in arrow; **Fig. 1.1**). Calcite and aragonite are the main minerals found in most speleothems, with calcite typically being much more abundant, and they form slowly (usually a maximum of 1 mm yr^{-1} for stalagmites) from mineral crystals that aggregate with or overgrow previous crystals, at least in the case of "hard" calcite (Ford & Williams, 2013). The growth of layered calcite, with older portions resting below more recently deposited ones, is the feature which allows paleoclimatic study, as the chemistry and/or fabric of each layer may change with the external climate. Paleoclimatic interest in speleothems ramped up in the 1960's, and efforts to understand the isotopic systems began around this time, focused mainly on the stable isotope measurements of $\delta^{18}O$ and $\delta^{13}C$ (e.g. Hendy, 1971 and sources within).

The potential for absolute dates and a corresponding age model of past growth is a primary reason that speleothems can be reliable archives of paleoclimatic information. The most widely used and accurate method for dating samples up to ~600,000 years old is U-Th disequilibrium dating, which utilizes the decay of ^{234}U to ^{230}Th as the principal indicator of the age of deposition. This natural, radiogenic process is feasible for dating since thorium (Th) is non-water soluble, so that, in an ideal speleothem sample, most of the thorium present will have come from the decay of ^{234}U, which was present in the original drip water (Fairchild & Baker, 2012). Prior to the late 1980's, decay counting methods were used, which were then replaced by thermal ionization mass spectrometry (TIMS), and even these have subsequently been improved by inductively coupled plasma mass spectrometry (ICP-MS) techniques, including multi-collector and sector-field instruments (Cheng et al., 2013 and refernces within; Edwards et al., 1987).

Detrital thorium, or thorium sourced from deposition and not decay, causes uncertainty in speleothem dates, but this complication can be accounted for by measuring $^{230}Th/^{232}Th$ (radiogenic / detrital), especially in 'clean' samples where the ratio is greater than 300 (Fairchild & Baker, 2012). A robust age model may require many U-Th dates to reduce uncertainty and resolve potential changes in growth rate and/or growth hiatuses, and even with modern techniques that require relatively small sample sizes, it is often unfeasible to date as many points as a researcher might desire. However, modeling programs, such as StalAge (Scholz & Hoffmann, 2011) or COPRA (Breitenbach et al., 2012) provide age models using statistical methods and a knowledge of common data problems encountered in speleothem U-Th-based age models.

Proxies inside a speleothem archive can be difficult to interpret due to the numerous controls that may be active on any single proxy, as the observed proxy signal has five major realms of potential influence: the atmosphere, the soil zone and upper epikarst, the lower epikarst and cave environment, mineral precipitation dynamics, and post-deposition or secondary change (Fairchild & Baker, 2012). Each of these, in turn, have many potential complicating factors, including temperature, vegetation, precipitation and moisture content, pCO_2, soil and bedrock chemistry, etc. As each proxy may be governed by more than one control, monitoring efforts can sometimes allow the researcher(s) to know the specific, active control or controls in a particular cave or specific sample (Breecker et al., 2012; Frisia et al., 2011; Hu et al., 2008; Mattey et al., 2010). However, perhaps the best method for understanding the information inside a speleothem archive is a multi-proxy analysis, involving two or more proxies, in order to duplicate findings,

separate controls, or provide additional information not readily deduced from a single proxy analysis.

1.3 Speleothem stable isotopes in the Asian Monsoon region

1.3.1 $\delta^{18}O$: controls and controversies

Speleothem $\delta^{18}O$ variations have been widely utilized to investigate past changes in tropical precipitation and monsoon strength. While in some regions, speleothem $\delta^{18}O$ variations are controlled by the so-called "amount effect", whereby more negative (or 'depleted') values are associated with increased local or regional precipitation amounts (e.g. Dansgaard, 1964; Fleitmann et al., 2004; Medina-Elizalde et al., 2010), this is not the case in much of the AM region. In the East Asian summer monsoon (EASM) region, speleothem $\delta^{18}O$ records have been interpreted as a proxy for large-scale, regional monsoon intensity and moisture transport, not necessarily representing changes in local rainfall amount, while the significance of any amount effect also likely changes by region (Chiang et al., 2015; Dayem et al., 2010; Johnson & Ingram, 2004).

Numerous mechanisms have been proposed to explain EASM $\delta^{18}O$ variability. $\delta^{18}O$ of precipitation is depleted as distance from the moisture source region increases due to the progressive removal of water vapor, as seen in global measurements of $\delta^{18}O$ (Yuan et al., 2004). Additionally, a changing source region may alter the $\delta^{18}O$ by possessing a different original value, a changing source path, and/or the distance traveled (Dayem et al., 2010). Changes in EASM $\delta^{18}O$ may originate in the Indian Monsoon, closer to the major moisture source of the Indian Ocean, representing large scale, distal changes in precipitation source combined with

upstream rainout as opposed to any significant local change in amount (Cheng et al., 2012; Johnson, 2011; J. Liu et al., 2015; Pausata et al., 2011; Yang et al., 2016). Other possibilities, such as differing types of precipitation and/or atmospheric cycles of condensation and evaporation could also be important factors in $\delta^{18}O$ variability (Dayem et al., 2010).

Interpretations of $\delta^{18}O$ are potentially weighted towards summer rainfall values during the monsoon season, and the seasonality of rainfall, including the changes in the monsoon onset and demise and/or wintertime rainfall contributions could affect the $\delta^{18}O$ signal (Chiang et al., 2015; Clemens et al., 2010; Dayem et al., 2010). As an example, the seasonality of the monsoon (the ratio of summer vs. winter rainfall and/or source of water vapor) may have changed in the Holocene compared to deglacial times, thus increasing the $\delta^{18}O$ variability seen in a stalagmite from Northeast India (Lechleitner et al., 2017). For the monsoon intensity interpretation of $\delta^{18}O$, previous studies have concluded that for a more intense monsoon, the $\delta^{18}O$ recorded in speleothems will be depleted (more negative $\delta^{18}O$ values) compared to a less intense monsoon (e.g. Clemens et al., 2010; Y. Wang et al., 2001; Y. Wang et al., 2008). In light of all the possibilities for $\delta^{18}O$ variability, other proxies are needed to construct a local hydrologic history.

1.3.2 $\delta^{13}C$ and its potential controls

The majority of carbon incorporated in speleothems comes from the overlying soil and epikarst (Fairchild et al., 2006), so carbon isotope ($\delta^{13}C$) values, while potentially affected by rainfall amounts, reveal less about the large scale atmospheric / climatic conditions and more about the immediate overlying vegetation, soil zone processes, and changes in the vadose zone water balance above the cave (Wong & Breecker, 2015). Changes in vegetation, such as a shift from

C3 to C4 photosynthetic species (or a change in the ratio of C3:C4 plants) during drier or hotter conditions, may increase speleothem $\delta^{13}C$, and a dry period could also decrease soil respiration, which would also shift $\delta^{13}C$ more positive (Dorale, 1998; Genty et al., 2001; Partin et al, 2013). In addition to the initial inputs of carbon from the soil zone and bedrock, processes in the cave, including CO_2 degassing, equilibration with cave air, the associated kinetic fractionations, are all driven by pCO_2 differences between the drip water and cave air, and these processes may enrich speleothem $\delta^{13}C$ well above the original drip water values (Frisia et al., 2011). Precipitation of calcite from the drip water at any stage prior to stalagmite formation, known as prior calcite precipitation (PCP), is often a significant factor in $\delta^{13}C$ interpretations that can tie the proxy directly to hydrology, as PCP can increase in dry periods (Fairchild et al., 2006; Johnson et al., 2006). PCP enriches $\delta^{13}C$, as ^{12}C is preferentially lost in the degassed CO_2 (Fairchild et al., 2006). Degassing and PCP often drive $\delta^{13}C$ in the same direction, and this allows the combined effects to sometimes work as a proxy for past rainfall amounts (Oster et al., 2010).

Different $\delta^{18}O$ and $\delta^{13}C$ controls can sometimes be distinguished through cave monitoring efforts (Breecker et al., 2012; Frisia et al., 2011; Hu et al., 2008; Mattey et al., 2010), but it is challenging to conduct detailed monitoring studies over multiple seasons or years at remote field locations. However, the measurement of multiple speleothem proxies can help distinguish the various controls. For instance, speleothem trace element (e.g. Mg/Ca and Sr/Ca) variations can provide more direct evidence of local hydrologic change and can be used as additional constraints on $\delta^{18}O$ and $\delta^{13}C$ interpretations (Johnson et al., 2006; Y. H. Liu et al., 2013; Tremaine & Froelich, 2013).

1.4 Additional hydrologically responsive speleothem proxies and their controls

1.4.1 Trace elements

Mg and Sr are the most common of trace-level elements that are found in speleothem samples, although many others have been detected and used for various studies (Ford & Williams, 2013). Bedrock dissolution is the main source of the most commonly used trace elements in speleothem studies (e.g. Mg, Sr, Ba, U), although detrital inputs from soil and dust, volcanic ash, or sea-salt aerosols can also be minor contributors (Belli et al., 2017; Borsato et al., 2007; Fairchild & Treble, 2009; Frisia et al., 2005). While controls on trace element variation in a speleothem time series can be highly variable by cave site and even within a single cave, one mechanism commonly cited for a hydrological response in trace element ratios (e.g. Mg/Ca, Sr/Ca) is PCP, as mentioned before in relation to $\delta^{13}C$ (Fairchild et al., 2000). During dry periods, PCP is theorized to increase the ratio of these trace elements in drip water, as the precipitation of calcite will prefer Ca over the trace elements, which substitute for Ca at a much lower rate. Obtaining evidence for PCP or closely-related water-rock interactions (WRI) that affect trace elements similarly is possible through cave monitoring of drip waters and/or the analysis of Mg/Ca and Sr/Ca data (e.g. Sinclair et al., 2012; Wong et al., 2011).

Due to the heterogeneity of cave chemistry and cave environmental factors, monitoring data or comparisons with other proxies are necessary to make robust conclusions about trace element concentrations or ratios. Similarities among trace elements themselves, such as a strong correlation between Mg/Ca and Sr/Ca, can be one strong indication that hydrology and/or PCP was a dominant control (Tremaine & Froelich, 2013). Additionally, as PCP affects $\delta^{13}C$ in similar ways, a correlation between these proxies has been used as evidence for hydrological

control of both (e.g. Griffiths et al., 2016). If $\delta^{18}O$ is interpreted as a proxy for rainfall amount (e.g. Ayliffe et al., 2013), then similarities between trace elements and $\delta^{18}O$ could also be used to the same purpose, although this is not likely to be of value in much of Asia, as $\delta^{18}O$ is interpreted as a more regional monsoon strength proxy not necessarily tied to local rainfall (Chiang et al., 2015; Dayem et al., 2010; Johnson & Ingram, 2004).

Evidence for seasonal variations of trace elements in a monsoonal climate allows a hypothesis that a long-term climate change could also cause similar increases or decreases of trace element ratios (Johnson et al., 2006). Therefore, for a lower-resolution record, an increase over decades or centuries could be caused by a control such as PCP. For trace element interpretations, it is crucial to note that, during a typical monsoon year, an increase in trace element ratios caused by PCP or prolonged WRI might be more significant during the dry season, thus potentially biasing the trace element proxies to the winter season. This is in contrast to $\delta^{18}O$, which is most likely weighted by summer monsoon precipitation, although the understanding of seasonal differences in speleothem proxy control is incomplete (Chiang et al., 2015). Therefore, a long-term shift in trace element ratios could be difficult to interpret, as it could represent less wet season rainfall, a shorter monsoon season, and/or a longer or drier dry season. But in any of these cases, less rainfall over several years or decades would result in an increase of trace element ratios.

1.4.2 ^{14}C and the Dead Carbon Proportion

Radiocarbon (^{14}C) measurements in stalagmites have been used previously in order to calibrate atmospheric ^{14}C history, investigate soil organic matter (SOM) ages and turnover times, and to analyze potential climate change over time due to a link with hydrology and bedrock dissolution

(e.g. Fohlmeister et al., 2011; Griffiths et al., 2012; Southon et al., 2012). Age model development using ^{14}C is possible, yet the uncertainties are much higher than U-Th dating methods (Lechleitner et al., 2016a), but by comparing ^{14}C to U-Th dates and calculating the dead carbon proportion (DCP) in a speleothem, one may examine the amount of decayed organic matter and/or fully decayed bedrock carbon that enters the drip water pool and the speleothem (Genty & Massault, 1997). Changes in the amount of the DCP can then be traced to above-cave changes in ecology and SOM or open vs. closed system dissolution regimes, both tied to local hydroclimate and rainfall (Hendy, 1971; Oster et al., 2010). DCP is especially useful as part of a multiproxy approach to analysis, as it may help untangle the many controls potentially active on $\delta^{13}C$ that make it difficult to interpret on its own (Lechleitner et al., 2016b; Rudzka et al., 2011).

Table 1.1 Speleothem proxies, controls, and interpretations[1] cited often in the presented research

Proxy	Source(s)	Control	Interpretation
$\delta^{18}O$	Precipitation	rainfall amount	more negative = higher rainfall amt.
		source region	changing source of atmospheric water vapor
		monsoon intensity (moisture transport distance, previous rainout)	more negative = more intense monsoon
$\delta^{13}C$	drip water DIC via soil and epikarst CO_2, bedrock dissolution	CO_2 degassing, PCP, cave air pCO_2, drip rate	more positive = drier conditions
		Vegetation	more negative = C3 plants; more positive = C4 plants
		open vs. closed system dissolution	more negative = open system (CO_2 source); more positive = closed system (bedrock source)
Mg/Ca & Sr/Ca	Bedrock, soil, dust and ash, aerosols	PCP and WRI	ratio increases during dry periods
DCP	bedrock dissolution, aged SOM	open vs. closed system dissolution	higher DCP = closed system and wet conditions lower DCP = open system and dry conditions
		SOM age spectrum	higher DCP = older SOM (wet periods) lower DCP = younger SOM (drier periods)

[1]See text for additional details and references

1.4.3 Other isotopic systems and emergent proxies

A summary of the proxies commonly referenced in this research with their associated sources, controls, and interpretations is in **Table 1**. Several other speleothem proxies have been investigated and used for evidence for past hydrological change. As one of the elements forming all $CaCO_3$, isotopes of Ca are a somewhat obvious candidate for potential information. However, the first systematic study of the Ca isotopic dynamics in a cave setting was in 2016 (Owen et al., 2016). The Owen et al. (2016) study linked $\delta^{44/42}Ca$ change to effective rainfall via the PCP mechanism that is known to affect trace elements and $\delta^{13}C$, as the lighter ^{42}Ca will be preferentially incorporated in the initial calcite. This study also provided a quantitative estimate of rainfall change in the monsoon region of Central China over the 8.2 ka event, which is notable as quantitative reconstructions using other PCP proxies has been elusive. Isotopes of strontium ($^{87}Sr/^{86}Sr$) have also been utilized to look at past rainfall amounts and recharge in aquifers, and although still relatively new in speleothem studies, this proxy has been investigated to a higher degree, with the first study in 1996. $^{87}Sr/^{86}Sr$ is a potentially useful proxy for water recharge, as the mineral precipitate may reflect the chemistry of the water directly in lieu of fractionation or temperature effects (Banner et al., 1996). In addition to rainfall recharge, Sr isotopes have been effectively used as tracers of climate through dust influx in the Sahara-East Mediterranean and in China, as more radiogenic Sr (^{87}Sr) is deposited in the soil zone during times of higher dust input (Frumkin & Stein, 2004; Zhou et al., 2009). Relevant to monsoon studies, the Zhou et al. (2009) study linked higher dust input to colder, drier conditions that are linked to a strong Asian winter monsoon. The $^{87}Sr/^{86}Sr$ system has also been applied to separating the regional signal of speleothem $\delta^{18}O$ records from local hydrologic conditions in Brazil, where variations were interpreted as changes in water residence times (Ward et al., 2019).

Any potential "new" proxy likely adds weight to the recommendation of multi-proxy analysis in speleothem research, as it would need to be compared to the more readily measurable or "classic" proxies, such as stable isotopes ($\delta^{18}O$ and $\delta^{13}C$) or the most abundant trace elements (Mg and Sr), in order to test their accuracy or improve the interpretations of the previously established and well-studied proxies. In addition to novel proxies, improvements to age models or increased resolution in sampling may also increase the potential for hydrologic reconstruction in speleothems. While U-Th dating has improved significantly in recent years (Cheng et al., 2013), including new estimates of half-lives and smaller sample sizes required, the issue of detrital Th remains in many samples. Recent work towards assigning better or multiple values of detrital Th to a single speleothem sample may allow more accurate age models (Hellstrom, 2006; Ridley et al., 2015; Wong & Breecker, 2015). Increased resolution of proxy sampling to seasonal or smaller time slices could also aid the interpretation of proxies over all time scales. For example, seasonal resolution of $\delta^{18}O$ has been analyzed using an ion microprobe, which was then interpreted as a signal of two components of AM rainfall: source effects (Indian vs. Pacific Ocean) and the proportion of summer vs. winter rainfall (Orland et al., 2015). Seasonal variations in drip water proxies due to a highly seasonal monsoonal rainfall regime (e.g. Johnson et al., 2006) could potentially be matched in a seasonally or sub-seasonally resolved speleothem record, adding confidence to all interpretations.

1.5 Theoretical mechanisms behind Asian Monsoon variability

Speleothem paleoclimate records from the AM, often focusing on $\delta^{18}O$ as a proxy of monsoon intensity, show similarities to other records of global change throughout glacial and interglacial

periods over the last several ice ages in the Pleistocene, such as $\delta^{18}O$ of the atmosphere from ice cores, which responds to global ice volume and the hydrologic cycle (Petit et al., 1999; Y. Wang et al., 2008). Incoming incident solar radiation, which changes over time due to cyclic changes in Earth's orbit and spinning axis over orbital timescales of ~23 – 100 kyr, is often hypothesized to be responsible for changes in AM intensity, with Chinese $\delta^{18}O$ displaying the most similarities with the precessional (~23 kyr) band of orbital frequency (e.g. Cheng et al., 2016). Abrupt, millennial to centennial-scale changes in monsoon intensity are also possible. Insolation change is likely still a primary driver, while associated climate responses and feedbacks, such as ice volume and iceberg / freshwater release, affect sea level and both oceanic and atmospheric circulation (Cheng et al., 2016; McManus et al., 2004).

In the Holocene, $\delta^{18}O$ across the AM region roughly coincides with Northern Hemisphere summer insolation, which maximized around 8% higher than present day at ~10 – 11 kyr BP (Cheng et al., 2016; Prell & Kutzbach, 1987). However, the timing of maximum monsoon intensity varies across the EASM region (An et al., 2000; Chiang et al., 2015; Clemens et al., 2010). For example, the precipitation or effective moisture maximum for the middle and lower Yangtze River regions in China is between 5-7 kyr BP, yet Southwest China had a much earlier peak in maximum rainfall at ~11 kyr BP (An et al., 2000). The discrepancies may be attributed to some areas having closer ties to the Indian Monsoon vs. East Asian Monsoon moisture sources. In any case, the timing of monsoon maxima across all regions is still a debated topic and a focus of ongoing work.

The North Atlantic region and the rapid melting or release of freshwater from ice or ice-dammed reservoirs is long-thought to be a catalyst for abrupt climate changes during the last deglaciation and the Pleistocene. Clues such as the accumulation of ice rafted debris (IRD) in marine sediments, decreases in foraminifera in ocean cores, or temperature changes evidenced by ice and ocean cores give robust evidence for such events (e.g. Bond et al., 1992; Broecker et al., 1992; Heinrich, 1988; McManus et al., 2004). The "Heinrich events," first defined by IRD in marine sediment cores, were thought to be tied to more frequent Dansgaard-Oeschger (D-O) cycles of rapid temperature change and possibly linked to external forcings (i.e. orbital-solar) or internal ice sheet dynamics, and they appeared to be linked to global climate responses (Broecker, 1994). The cause of global responses to Heinrich events, or Heinrich Stadials, is now thought to be slowing or cessations of the Atlantic Meridional Overturning Circulation (AMOC) (Broecker, 1994; McManus et al., 2004). While the cause and effects of Heinrich Stadials is still debated and/or subject to ongoing research, the global effects on millennial timescales, as opposed to climate changing more slowly due solely to orbital forcing, are striking, as they mark evidence for rapid changes that occur within decades and can last for several millennia.

Global, centennial to millennial-scale climate events such as Heinrich Stadials also affect the $\delta^{18}O$ measurements in speleothems of the AM region (e.g. Dykoski et al., 2005; McManus et al., 2004; Y. Wang et al., 2001). The most notable of these events since the last glacial maximum (LGM: 26.5 - 19 kyr BP) are Heinrich Stadial 1 (HS1; ~17.5 – 14.5 kyr BP) and the Younger Dryas (~12.7 – 11.7 kyr BP), both millennial-scale cooling events in the Northern Hemisphere, with the Bølling-Allerød interstadial, a relatively warm period, in between (Clark et al., 2009; McGee et al., 2014; McManus et al., 2004; Zhang et al., 2016). A third major event is the 8.2 kyr

Event, which is the most striking abrupt climate change event of global scale since the start of the more stable Holocene Epoch (Alley et al., 1997; Alley & Ágústsdóttir, 2005; Cheng et al., 2009b; Y. H. Liu et al., 2013). During these large-scale climate events, the AM is hypothesized to respond to a Northern Hemisphere and/or North Atlantic Ocean forcing via a climate teleconnection (An et al., 2000; Gupta et al., 2003; Y. H. Liu et al., 2013; Y. Wang et al., 2005), in which anomalies of the Intertropical Convergence Zone (ITCZ) (Broccoli et al., 2006; Chiang & Bitz, 2005; Schneider et al., 2014), caused by a weakening or cessation of the AMOC (McGee et al., 2014; McManus et al., 2004). These oceanic and atmospheric changes may create changes in monsoon intensity on a decadal to millennial scale (Cheng et al., 2009a; Y. Wang et al., 2008). In this hypothesis, the AMOC is weakened, slowed, or halted by ice melt and/or freshwater release into the North Atlantic, causing cooler Northern Hemisphere temperatures, a southern shift of the ITCZ, and a less intense AM (**Fig. 1.2**). The extent of possible shifts or changes in the ITCZ as a mechanism for monsoon variability is an ongoing focus for speleothem studies of all monsoon regions.

A more recent theory on AM variability involves the position of the westerlies throughout the monsoon season (Chiang et al., 2015; Zhang et al., 2018). In this view, millennial-scale stadials, and potentially longer-term responses to orbital forcing, may change the signal seen in paleo-records due to changes in the timing and extent sub-seasonal evolutionary stages of the monsoon. The westerly jet migrates to the North each Boreal Summer, and the position of the jet causes distinct changes in rainfall location maxima as the prevailing winds encounter the high altitude of the Tibetan plateau and evolve in a stepwise manner (Chiang et al., 2015) (**Fig. 1.2**). Another

hypothesis on orbital variability involves low-latitude gradients in interhemispheric (north vs. south) insolation which influences atmospheric outflow from the AM, which may alternate flow to the North Pacific or Southern Indian Ocean (Beck et al., 2018). In this hypothesis, the low latitudes could potentially influence higher latitudes to a greater degree. In light of the many hypotheses on past monsoon and hydrologic variability in the AM, determining the history of rainfall in specific AM regions and the climatic controls on variability is challenging, and

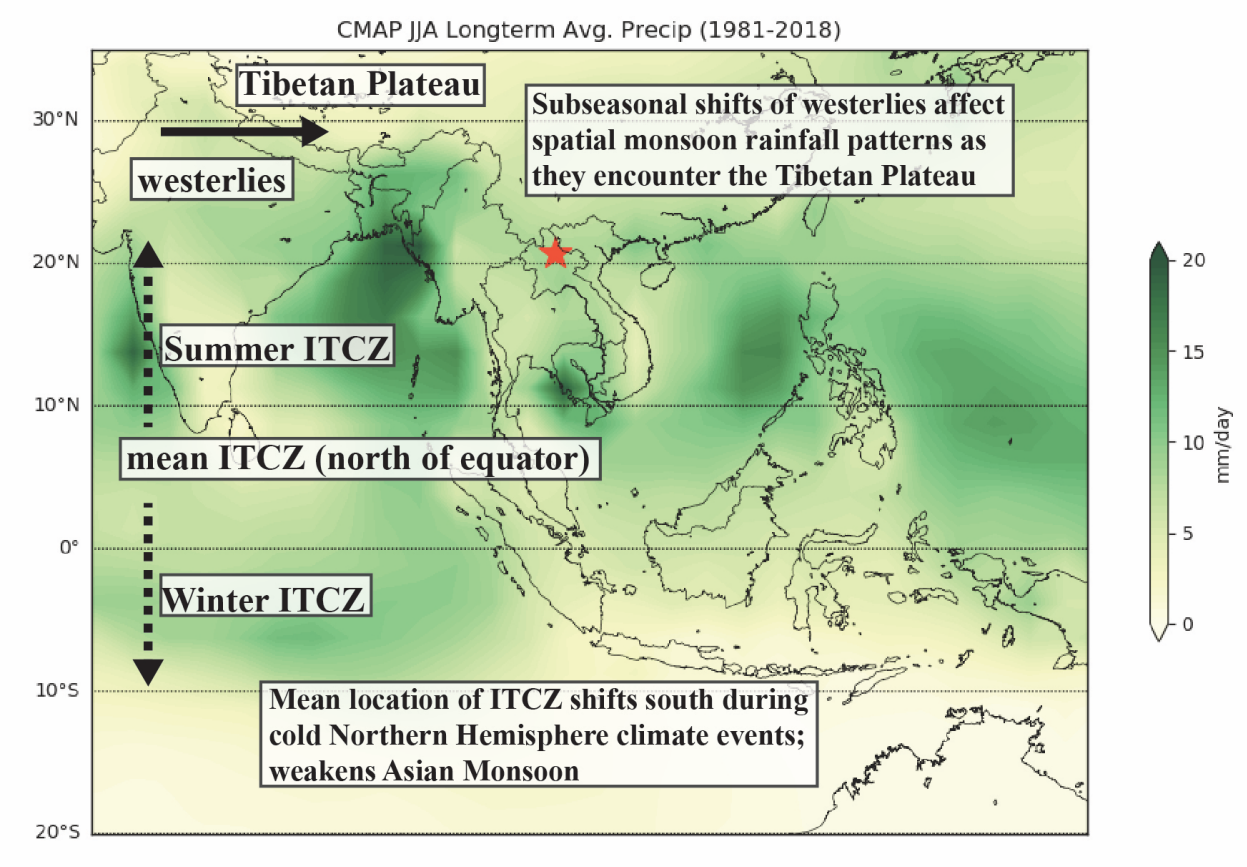

Figure 1.2 – Asian Monsoon variability overview – *Location of Tham Doun Mai Cave (red star) and theories of monsoon variability during abrupt climate events. See text for discussion and references for ITCZ hypotheses. Plot shows mean June, July, and August daily precipitation for dates shown from CMAP Precipitation data provided by the NOAA/OAR/ESRL PSD, Boulder, Colorado, USA, from their Web site at* https://www.esrl.noaa.gov/psd (Xie & Arkin, 1997)*. Summer and Winter refer to Boreal seasonality.*

debates continue on the interpretations of existing records. More paleoclimate records, especially from low latitudes, could eventually shed light on which mechanism(s) control both orbital and millennial monsoon and rainfall responses.

1.6 Introduction to the research chapters

1.6.1 Chapter 2: Speleothem trace element responses across the last deglaciation and Holocene in Northern Laos

Trace elements in speleothem paleoclimate records have the potential to provide a local history of rainfall and hydrology due to their governing controls in the cave and above-cave environment. Mg/Ca and Sr/Ca ratios are analyzed over a 38,000-year record developed from TM-17, a stalagmite from Tham Doun Mai in Northern Laos (**Fig. 1.2**). The new trace element record of local hydrology is the first of its scope in MSEA and contributes to a growing archive of cave records from this location. Through additional data from cave drip waters, bedrock, soil, and modern calcite, a hydrologic control for trace elements is established, likely dominated by prior calcite precipitation (PCP). Comparisons between multiple proxy records from TM-17 reveal when previously analyzed stable isotope controls beyond rainfall amount ($\delta^{18}O$) or PCP ($\delta^{13}C$) may have dominated these more commonly analyzed speleothem proxies, namely in HS1 and during the early to mid-Holocene. $\delta^{13}C$ and trace element agreement during the Holocene suggests a shared PCP/hydrologic control, and these proxies display a mid-Holocene rainfall maximum, contrary to the regionally controlled $\delta^{18}O$, representing monsoon strength, that maximizes earlier in the Holocene. Trace elements also suggest a potential dry period prior to HS1, which is compared to other potentially related low-latitude speleothem records displaying similar features.

1.6.2 Chapter 3: Speleothem radiocarbon evidence for paleohydrologic changes in Mainland Southeast Asia

The dead carbon proportion (DCP) of stalagmite TM-17 is analyzed and compared with monitoring data and other proxies, which reveal its use as a hydrologic climate proxy. TM-17 DCP is abnormally high for a stalagmite (often >50%) and varies substantially through the record with notable shifts around known climate events such as HS1 and the 8.2 ka event. An estimate of potential organic matter influence on the DCP shows that bedrock dissolution and corresponding open vs. closed system dissolution changes are the dominant control on DCP variability, potentially enhanced by sulfuric acid dissolution mechanisms in the epikarst. The DCP record is used to assess multiple potential controls on $\delta^{13}C$ and contrasting controls during HS1 and 8.2. Modeling of calcite precipitation in the CaveCalc geochemical program, utilizing local monitoring input, reinforces these findings. This work demonstrates the ability of DCP measurements to contribute to a multiproxy speleothem study as an additional proxy responsive to hydroclimate, and the data assists in the interpretations of controls on other proxies, thus improving the record of local hydrology from our cave site in Northern Laos over the last ~35,000 years.

1.6.3 Chapter 4: A high resolution, multi-proxy speleothem record of the 8.2 ka event from Mainland Southeast Asia

The 8.2 ka event is the most prominent abrupt climate change event of the Holocene Epoch (or the last ~11,700 years). Documented as a cold, dry event in the North Atlantic and Europe, its effects have shown up in paleoclimate proxy records of the AM. This relatively short-lived event requires a rapid, atmospheric teleconnection for global climate responses between the North

Atlantic Ocean and the AM region. Using additional U-Th series dates across the event, higher resolution stable isotope measurements, and new LA-ICP-MS trace element analyses, the event is examined for timing and climatological impacts on MSEA via the speleothem sample TM-17 from Northern Laos. Previously established controls on TM-17 proxies are applied to this centennial scale event and reveal a response of at least 173 years ($\delta^{18}O$ data) on MSEA, similar to proxy records around the globe. $\delta^{13}C$ and Mg respond decades earlier and provide evidence of an extended hydrologic response after the event, suggesting the response in $\delta^{18}O$ alone may be insufficient to define event boundaries in speleothem samples. Outside of dating estimates, the weak monsoon / drying is similar to EASM records of the 8.2 and provides new information on the spatial extent of the event that can be incorporated when analyzing model simulations of climate sensitivity to AMOC changes.

1.7 Summary

The Southeast Asian Monsoon region is less extensively covered by terrestrial archives compared to the East Asian Monsoon, and its proximity to the tropics and potential ITCZ effects, as well as its primary source of moisture from the Indian Ocean and Bay of Bengal (Johnson et al., in revision), make MSEA a prime region to study for a more complete picture of ancient monsoon behavior. These new records of trace elements, ^{14}C, and the high-resolution documentation of the 8.2 ka event from Tham Doun Mai showcase the climate impacts of the deglaciation period and associated abrupt climate events in a region in need of additional terrestrial archives. The effects of global change during HS1 display a long-term weak monsoon response in MSEA tracible to a multi-millennial cessation or slowing of the AMOC, and the hydrological proxies of focus in this dissertation give insight into the local effects on rainfall and

moisture. The Holocene monsoon strength maximum differs from the precipitation maxima of the trace elements and carbon isotopes, showing how the interpretation of speleothem proxies benefits from multiproxy analyses. These new records and interpretations add to the global effort to understand past climate change, and they provide location-specific data that may be compared beside or incorporated in models that mimic both past and future climate changes in the Earth System.

Chapter 2

Speleothem trace element responses across the last deglaciation and Holocene in Northern Laos

2.1 Abstract

Despite significant progress in recent years in understanding the history and variability of the Asian Monsoon (AM) system, there is still a paucity of paleoclimate records from Mainland Southeast Asia (MSEA). Furthermore, significant debate still exists regarding the paleoclimate interpretation of speleothem $\delta^{18}O$ records from the AM region and the response of regional rainfall patterns to orbital forcing and abrupt climate events. Given these issues, an approach that incorporates additional proxies, such as speleothem trace element ratios (e.g. Mg/Ca), can provide more robust information about past hydroclimate change. Towards this end, we present here a new speleothem trace element record from Tham Doun Mai cave, Laos, that spans the last 37.8 kyr BP. We find a significant positive correlation ($R^2 = 0.44$) between Mg/Ca and Sr/Ca, consistent with a strong hydrologic control on trace element ratios through the prior calcite precipitation (PCP) mechanism, whereby trace element ratios increase during drier periods. Cave monitoring results, including analyses of drip waters, modern calcite, bedrock, and soil provide further evidence for a local hydrologic control on speleothem Mg/Ca and Sr/Ca ratios. Sharp positive excursions occur near the onset of abrupt climate events, including Heinrich Stadial 1, the Younger Dryas, and the 8.2 ka event, suggesting dry conditions at these times. On orbital

timescales, Mg/Ca and Sr/Ca values are elevated during the early Holocene (~10.2 – 8.2 kyr BP), consistent with locally drier conditions as previously inferred from the Tham Doun Mai $\delta^{13}C$ record. This contrasts with more negative values of speleothem $\delta^{18}O$ that suggest a more intense AM during Northern Hemisphere summer insolation maxima. A prominently dry 8.2 ka event response, which displays the highest individual trace element ratios in the record, separates the early Holocene from a relatively wetter mid-Holocene. These results suggest the wettest conditions of the Holocene occurred around 5 kyr BP at our site, providing evidence for a decoupling of large-scale AM strength from past precipitation amounts in MSEA. While the trace element data provide overall support for the interpretation of stable isotope records from the same cave, some key differences in the duration and magnitude of the proxy responses potentially reflect the combined effects of karst hydrology, differing proxy response times, and multiple environmental controls on each proxy.

2.2 Introduction

Mainland Southeast Asia (MSEA) is a key region that sits at the interface of the East Asian Summer Monsoon (EASM) and Indian Summer Monsoon (ISM) regions, yet recent studies suggest that the hydroclimate response to orbital forcing and millennial scale abrupt climate events, such as Heinrich stadials, may differ between these highly-populated monsoon sub-regions (Johnson et al., in revision; Zhang et al., 2018;). The speleothem oxygen isotope record of Asian Monsoon (AM) variability now extends back to 640 kyr BP and indicates a strong influence of Northern Hemisphere summer insolation (NHSI) on AM strength, with more negative $\delta^{18}O$ values interpreted as reflecting a stronger monsoon during NHSI maxima, and vice versa (Cheng et al., 2016; Yuan et al., 2004). Similarly, more positive $\delta^{18}O$ values during

Heinrich stadials and other abrupt climate events linked with weakening of the Atlantic Meridional Overturning Circulation (AMOC) indicate a strong atmospheric teleconnection between the North Atlantic and the AM region, with weak monsoon periods occurring during times of weakened AMOC (Broecker, 1994; Cheng et al., 2012; Y. H. Liu et al., 2013; McManus et al., 2004). The strong coherence of orbital and millennial scale speleothem $\delta^{18}O$ records from cave sites spanning the broad AM region, where modern precipitation exhibits no significant correlations (Dayem et al., 2010), indicates that the speleothem $\delta^{18}O$ records are likely recording large-scale variations in AM intensity, though they do not necessarily reflect local or regional precipitation at all sites. This has been investigated by both proxy and modeling studies, which suggest other factors such as the degree of upstream rainout, the strength and position of the mid-latitude westerlies, the seasonality of precipitation, and/or changes in moisture source region may dominate the precipitation $\delta^{18}O$ variations that are recorded by speleothem calcite (e.g. Chiang et al., 2015; Johnson, 2011; Pausata et al., 2011). Given the significant interest in understanding regional precipitation variability across the AM region, the use of additional speleothem proxies, such as $\delta^{13}C$ and trace element ratios (e.g. Mg/Ca, Sr/Ca), which are more sensitive to local hydrology than $\delta^{18}O$ (Fairchild et al., 2006; Fairchild & Treble, 2009; Johnson et al., 2006; Wong & Breecker, 2015), are becoming increasingly utilized.

The majority of carbon incorporated in speleothem calcite comes from the local soil and epikarst zones (Fairchild et al., 2006), and carbon isotope ($\delta^{13}C$) controls often depend on an individual cave site's environmental setting and conditions. Low respiration rates in the soil may shift $\delta^{13}C$ to more positive values, closer to atmospheric CO_2 (~ -8‰) than to soil CO_2 (-25‰) produced by

respiration (Genty et al., 2001). The type of vegetation, such as a change in the ratio of C3 to C4 plants, could also affect speleothem $\delta^{13}C$ values, as C4 plants create more positive $\delta^{13}C$ (Dorale, 1998; Partin et al., 2013). Within cave processes, such as variable CO_2 degassing due to changing drip rate can also enrich ^{13}C in the dissolved inorganic carbon, and thus, in speleothem calcite, during periods of slower drip rate (Frisia et al., 2011; Mühlinghaus et al., 2007). Precipitation of calcite from the drip water at any stage prior to stalagmite formation, referred to as prior calcite precipitation (PCP), is another control on $\delta^{13}C$ that can tie the proxy directly to the local water balance, as PCP increases $\delta^{13}C$ during dry periods when ^{12}C is preferentially lost during CO_2 degassing (Fairchild et al., 2006; Johnson et al., 2006; Oster et al., 2010). Drier conditions increase the likelihood of PCP, as there will be more air space in the fractures and cavities above a cave, while a wetter period will fill pore space and fractures, decreasing the exposure of drip waters to low pCO_2 gas. The combination of all of these controls typically creates a more positive stalagmite $\delta^{13}C$ when conditions are drier locally (Wong & Breecker, 2015; Johnson et al., in revision), signifying local rainfall amounts and water balance as opposed to the large scale atmospheric or regional climatic conditions controlling $\delta^{18}O$. Different $\delta^{18}O$ and $\delta^{13}C$ controls can sometimes be distinguished through cave monitoring efforts (e.g. Breecker et al., 2012; Frisia et al., 2011; Hu et al., 2008; Mattey et al., 2010), but it is challenging to conduct detailed monitoring studies at remote field locations, creating the need for additional hydrologically responsive proxies such as trace element ratios which can help distinguish between the above mechanisms.

Local hydrology in and above a cave system is also a major control on trace element concentrations in drip waters and speleothems (e.g. Mg, Sr, Ba) through PCP and/or extended

water-rock interaction times (WRI), which increase trace element concentrations in drip water during drier periods (Fairchild et al., 2006; Sinclair et al., 2012). Seasonal or long-term changes in hydrology can affect both $\delta^{13}C$ and trace elements through PCP, which may occur anytime waters with higher pCO_2 encounter a lower pCO_2 up-flow from speleothem formation (Fairchild & Treble, 2009). During drier periods, slower drip rates and more degassing at the site of speleothem formation may also occur, which can increase trace element ratios in the remaining solution. Such an increase would co-occur with the increased chance of PCP up-flow from the sample in question (Huang et al., 2001b; Johnson et al., 2006). Therefore, the interpretation of a drier period can be correct regardless of whether the increase in trace elements is caused by PCP, changes to the CO_2 degassing rate that accompany slow drip rates, or increased WRI, which would all increase trace elements in the solution and represent local hydrologic variability (Fairchild et al., 2000; Sinclair et al., 2012).

Trace element (e.g. Mg/Ca and Sr/Ca) ratios can thus provide direct evidence of local hydrologic change and be used as additional constraints on $\delta^{18}O$ and $\delta^{13}C$ interpretations (Johnson et al., 2006; Y. H. Liu et al., 2013; Tremaine & Froelich, 2013). In the EASM, hydrologically-controlled trace elements have recently been used as evidence for past regional precipitation patterns and monsoon dynamics that differ from the signal of monsoon strength evidenced by the $\delta^{18}O$ record (Zhang et al., 2018). Here we present a new ~37,800 year long trace element record from a precisely-dated speleothem collected from Tham Doun Mai Cave, Laos (N20°45.24', E102°39.09', 352 m asl; **Fig. 2.1**). Through analysis and comparison of our speleothem Mg/Ca and Sr/Ca time series with modern cave monitoring data and stable isotope ($\delta^{18}O$ and $\delta^{13}C$) records from the same stalagmite (Johnson et al., in revision), we present a robust, multi-proxy

record of past hydrologic changes from MSEA that covers the late glacial, last deglaciation, and Holocene time periods.

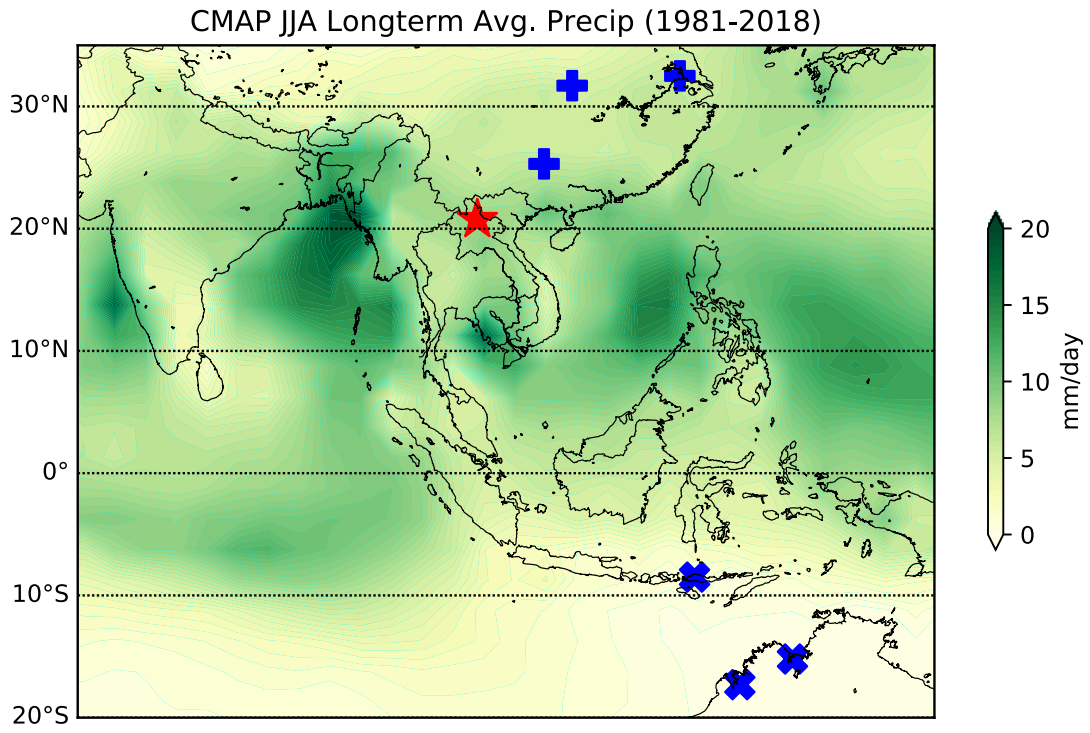

Figure 2.1 – Tham Doun Mai Cave, Northern Laos - *Location of Tham Doun Mai Cave (N20°45.24', E102°39.09', 352 m asl) is marked by red star. Blue crosses represent the caves used to construct the composite Chinese $\delta^{18}O$ record referenced in this study (Cheng et al., 2013), and blue x's mark the locations of Liang Luar, Indonesia (Ayliffe et al., 2013) and KNI-51 and Ball Gown Caves, Australia (Denniston et al., 2017). Map is overlaid with the region's long-term daily precipitation average from June, July, and August (JJA) from CMAP Precipitation data provided by the NOAA/OAR/ESRL PSD, Boulder, Colorado, USA, from their Web site at https://www.esrl.noaa.gov/psd* (Xie & Arkin, 1997).

2.3 Setting and Materials

Laos is a landlocked country on the Indochina Peninsula where the regional climate is dominated by the seasonal Southeast Asian Monsoon (SEAM). While connected to the larger AM systems, which affect a large percentage of the world's population, the SEAM is a system with behavior that differs from the East Asian Monsoon and the Indian Monsoon, and it directly affects the

countries of Cambodia, Laos, Myanmar, Thailand, Vietnam, and parts of Southern China (Lau & Yang, 1997; Misra & Dinapoli, 2014). Northern Laos has a humid subtropical and tropical monsoonal climate, and rainfall in the Nam Ou River Basin averages 1,700 mm yr^{-1} (Shrestha et al., 2018). The months of maximum rainfall are May through August, and temperature in the region close to our study site ranges from 17.8° C to 26.2° C (January and June, respectively) (Kiernan, 2015).

Tham Doun Mai (TM) cave (N20°45', E102°39'; 352 m asl; **Fig. 2.1**) is a ~3.75 km long solution cave consisting of a relic streambed above an active river channel. The entrance is ~ 30 m above the water level of the Nam Ou river, the largest Laotian tributary to the greater Mekong river system, near the village of Muang Ngoi in Nong Khiaw District, Luang Prabang Province, Laos (Dreybrodt et al., 2013a; Kiernan, 2015). Most outcrops in this area of the Nam Ou are massive to well-bedded limestones of Carboniferous-Permian age found on steep karst hills and towers, the highest of which is 1902 m asl (Kiernan, 2015). TM stays above the river channel sections of the cave for the first several hundred meters, after which there is a steep drop-off to the river level, and the cave continues both up and downstream. The soil overlying the cave is rocky and shallow, as is typical of karst environments, with spatially variable thicknesses ranging from <10 to ~70 cm with an average of less than 30 cm. The areas between the river and cave entrance, as well as the areas above the cave, are covered by dense tropical forest vegetation that continues along the steep, rocky slope of the karst tower above. Year-round temperature in the cave is similar to the mean annual temperature for the region (~22° C; HOBO logger data) and relative humidity is ~95% (HOBO logger data). Measured cave air pCO_2 is around 600-630

ppm in January – March (Vaisala CO_2 probe), though we cannot rule out seasonal fluctuations in cave ventilation as all field campaigns have occurred during the winter.

TM-17, a ~60 cm long fossil stalagmite consisting primarily of columnar calcite, was collected from a steep wall / slope where TM drops towards the river level, ~250-300 m from the single known cave entrance. The growth history of TM-17 was constrained by 25 U-Th MC-ICPMS dates (University of Oxford), which show that it formed continuously between 37,880 and 76 yrs BP (years before 1950) at an average growth rate of 19 μm/year (Johnson et al., in revision). The slow, steady growth of the stalagmite, candlestick-like morphology, and columnar fabric throughout the sample suggest that it formed from diffuse flow allowed by matrix porosity that remained fairly constant over time (e.g. Treble et al., 2013). From available topographic maps (Dreybrodt and Laumanns, 2013b), the sampling area is under at least 100 m of bedrock, although the steep karst tower outside could make the overburden higher above the sampling location, as parts of the cave are under as much as 400 m of bedrock. $\delta^{18}O$ data from drip waters and modern calcite suggest a residence time of at least one year for drip waters in this section of the cave (Johnson et al., in revision).

Bedrock, cave drip waters, and soil samples were collected in and around TM cave in 2013, 2015, and 2017. Bedrock samples were taken from inside and outside of the cave, and both the bulk rock, consisting of dark grey limestone, as well as mineral crusts and weathered surfaces on bedrock samples were drilled into powder for sampling. Soil samples were taken from locations approximately 10-20 m above the cave entrance on a heavily vegetated, rocky slope at depths of 10, 20, and 30 cm. Beyond this region, areas more directly above in-cave sampling sites are

beyond a near-vertical limestone cliff of at least 100 m, making sampling of areas directly above the deeper cave sites inaccessible. Drip waters were collected from several locations in the cave for trace element analysis. Two drip sites are singled out for analysis and discussion: the D-10 site, a hydrologically active multi-drip site that has been sampled over multiple field campaigns for water chemistry and modern calcite grown on glass plates placed under the drip; and the D-17 site, which consists of drip waters taken from the closest active drip to the TM-17 growth site. As TM-17 was an inactively growing (fossil) stalagmite, these waters are used as the closest modern analogue to the drip that directly contributed to TM-17 growth.

2.4 Methods

All water, calcite, soil, and rock samples were prepared and analyzed for trace elements in The Center for Isotope Tracers in Earth Science (CITIES) at UC Irvine utilizing a Nu Instruments Attom high resolution inductively coupled plasma mass spectrometer (HR-ICPMS).

The TM-17 stalagmite was sectioned in half, polished, and drilled at 0.5 mm resolution utilizing a Sherline Micromill with a diamond dental drill bit. 1,213 samples were collected, covering a timeframe of approximately 37.8 kyr, creating an average resolution of ~30 years per sample. Splits from these samples were analyzed previously for stable isotopes ($\delta^{18}O$ and $\delta^{13}C$) (Johnson et al., in revision), and the archived powders were subsequently weighed for trace element analyses presented here. ~30-70 μg of calcite powder was diluted with 500 μL of a 2% HNO_3 solution to bring the samples to ~20 ppm Ca prior to instrumental analysis. The samples were run with either a "wet" method (probe-based autosampler and a 200 μL min^{-1} glass nebulizer) or a "dry" method (probe-based autosampler prior to a desolvating nebulizer (DSN) and a 100 μL min^{-1} glass nebulizer) for input to the ICP-MS. For soil sampling, separate aliquots of ~5 g each

were leached with 18.2 milli-Q water or a 4% acetic acid solution for ~72 hours. After removal of the liquid portion, water leachates were then acidified to 2% HNO_3, and acetic acid samples were dried completely on a hotplate and then re-dissolved in 2% HNO_3 prior to ICP-MS analysis. Water samples were acidified to 2% HNO_3 and run with a custom standard containing trace element concentrations similar to TM cave waters.

A standard was created from elemental solutions to mimic the average concentrations of measured elements: Ca, Mg, and Sr were mixed at levels comparable to stalagmite TM-17 calcite. A standard was analyzed every 4 samples, and a blank sample (2% HNO_3, 98% 18.2 MQ H_2O) was run every 8 samples. Standard bracketing and linear interpolation between both standards and blanks were used to correct for instrumental noise, drift, and memory effects following the methods of Rosenthal et al. (1999). After blank subtraction, measured trace element intensity ratios were compared to the known standard to generate a correction factor that was used to calculate sample trace element ratios. Powders drilled from bedrock samples, powder from glass plate calcite, and soil leachate samples were tested for trace elemental ratios with the same method and standard as speleothem calcite. Waters were collected in 5-10 mL acid-washed polyethylene (LDPE) screw-cap vials, which were tightened and sealed with Parafilm prior to transport. Some drip sites consist of one drip (higher drip rates), while other sites contain multiple drips (slower drip rates) under a small section of the cave or single section of stalactites that had similar feeding water. Trace element ratios for cave waters were determined using a drip water standard-based correction factor similar to the bedrock and stalagmite analyses.

The error estimate reported for stalagmite Mg/Ca and Sr/Ca is based on repeated analyses of the custom elemental standard aliquots during each batch run; the standard deviation during a particular run was weighted by the number of successfully analyzed samples and then averaged over all batch runs. Individual samples with RSDs above 10% were either reanalyzed at a later date or rejected. Additionally, z-scores from the interpolated time series for Mg/Ca, Sr/Ca, and $\delta^{13}C$ were calculated to investigate multi-proxy agreement. The relative change in proxies, shown by the variance in terms of standard deviations from the mean (z-score), is considered in some plotting and discussion since the $\delta^{13}C$ unit is dissimilar from trace element ratios, and the Mg/Ca and Sr/Ca ratios are of different baseline magnitudes. All coefficients of correlation (R^2) and p-values reported utilize interpolated data for missing points and were calculated using the methods of Macias-Fauria et al. (2012), which consider the possible effects of autocorrelation of time series data for the Pearson correlation coefficient.

2.5 Results

Mg/Ca and Sr/Ca values for cave monitoring samples, including bedrock, soil leachates, drip waters, and modern glass plate calcite values are shown in **Table 1.1**. TM-17 stalagmite Mg/Ca and Sr/Ca data cover the full time series (~38,000 years) (**Fig. 2.2**), with 1,209 Mg/Ca and 1,165 Sr/Ca analyses. The estimated error for trace element ratios, based on repeated runs of the test standard, is 5.46% for Mg/Ca and 5.56% for Sr/Ca. Mg/Ca ranges from 21.2 to 57.4 mmol/mol, while Sr/Ca ranges from 0.25 to 0.59 mmol/mol, and substantial variability is seen from decadal to orbital timescales. Mg/Ca and Sr/Ca are significantly correlated over the entire time series ($R^2 = 0.44$, $p < 0.001$), visually apparent especially on orbital and millennial timescales (**Fig. 2.2**). Discrepancies occur during decadal to centennial timescales, such as elevated Sr/Ca between 10

Table 2.1 – Tham Doun Mai monitoring results: trace element ratios

Sample type	Sample ID	Year collected	Mg/Ca (mmol/mol)	Sr/Ca (mmol/mol)
Bedrock	TM-BR-C-1	2013	11.42	0.60
	TM-BR-C-2	2013	12.10	0.58
	TM-BR-C-3	2013	8.98	0.30
	TM-BR-1	2013	106.18	0.45
	TM-BR-2	2013	104.18	0.46
	TM-BR-2A	2013	75.29	0.47
	TM-BR-B1-1-R	2013	70.89	0.25
	TM-BR-B1-2-R	2013	27.86	0.30
	TM-BR-B1-2A	2013	196.96	0.54
	TM-BR-B2-1	2013	79.51	0.41
	TM-BR-B2-2-R	2013	122.58	0.21
	TM-BR-B2-3	2013	38.96	0.41
Soil (water leachate)	TM-S-1-1-W	2015	275.73	0.66
	TM-S-1-2-W-R	2015	260.34	0.71
	TM-S-2-W	2015	240.27	0.54
Soil (acid leachate)	TM-S-1-1A-R_d20	2015	132.81	0.36
	TM-S-1-2A-R_d20r	2015	218.83	0.67
	TM-S-2A-R_d20	2015	203.41	0.47
Drip Water (D10 site)	TM-D10a	2013	256.26	1.93
	TM-D10b	2013	243.65	1.83
	TM-2015-D10-i	2015	194.91	1.48
	TM-2015-D10-ii	2015	237.66	1.81
	TM-2015-D10-iii	2015	147.96	1.13
	TM17-D10a	2017	149.02	1.18
	TM17-D10b	2017	208.67	1.65
Drip Water (D17 site)	TM17-D17	2017	920.14	2.94
	TM17-D17-DUPd50	2017	971.16	2.56
Glass Plate Calcite	TM-GP-H-C	2013-2015	2.68	0.08
	TM-GP-H-M	2013-2015	3.01	0.06
	TM-GP-H-O	2013-2015	3.36	0.05
	TM-GP-H-B	2013-2015	3.02	0.06
	TM-GP-D10-1a	2015-2017	8.01	0.08
	TM-GP-D10-1b	2015-2017	8.21	0.08
	TM-GP-D10-2a	2015-2017	8.73	0.09
	TM-GP-D10-2b	2015-2017	8.24	0.08
	TM-GP-D10-3a	2015-2017	2.89	0.06
	TM-GP-D10-3b	2015-2017	3.21	0.06
Stalagmite (mean)	TM-17	2013	38.47	0.38

– 11 kyr BP, as well as an apparent increased offset between the two proxies from ~2 kyr BP to the near-present. The Sr/Mg ratio rarely extends beyond 2 standard deviations from the average, showing a consistent relationship over time (**Fig. 2.2**). A principal component analysis involving only Mg/Ca and Sr/Ca combines Mg/Ca and Sr/Ca signals into one proxy (TM17 PC1) for discussion and plotting (**Fig. 2.4**). Time series data were interpolated to fill missing data points and standardized using a z-score prior to principal component analysis (PCA), resulting in a 1,211 point data array for Mg/Ca and Sr/Ca data, which is used for the creation of TM17 PC1. The effectiveness of this component representing both trace elements is evidenced by identical loadings of 0.71 for both Mg/Ca and Sr/Ca and 83% of total variance explained.

Large amplitude variations are observed between ~33-31 kyr BP, prominent structures at the end of a general decline in values between 38-33 kyr BP (**Fig. 2.2**). From ~30 kyr BP and through the Last Glacial Maximum (LGM, ~22 kyr BP), there is an overall increasing trend in trace elements at the orbital to millennial scale. This concurrent increasing trend ends around 18.5 kyr BP, when higher levels remain steady for around 1,000 years. This excursion is near the beginning of Heinrich Stadial 1 (HS1; ~17.5 – 14.5 kyr BP), and Mg/Ca and Sr/Ca display sharp increases prior to or at the start of other well-documented, global events, including the Younger Dryas (YD; ~12.7 – 11.7 kyr BP) and the 8.2 ka event**.** The highest recorded individual values of both proxies occur between 8 – 8.5 kyr BP. While there are several other shorter departures from averages and trends in the deglaciation and Holocene, the trend in Mg/Ca and Sr/Ca displays an overall millennial scale decrease from ~17.5 to ~4.5 kyr BP, followed by an increase towards the present day.

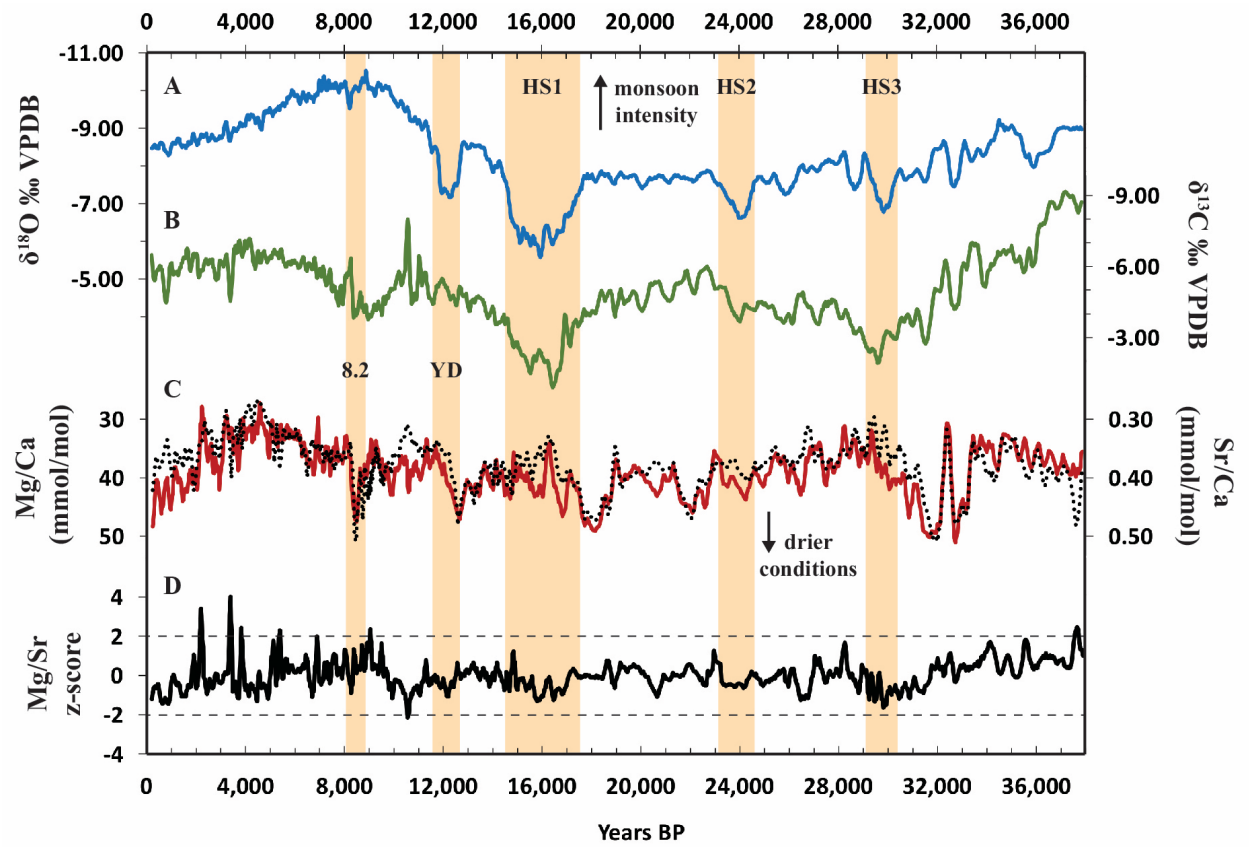

Figure 2.2 – TM-17 proxy time series – "A, B" *-Time series of TM-17 stable isotopes (**A** - $\delta^{18}O$, **B** - $\delta^{13}C$; 5-pt moving averages; data from Johnson et al., in revision). for comparison with "**C" -** trace element ratios (Mg/Ca = solid line, Sr/Ca = dashed line; 5-pt. moving averages). Axes are reversed such that monsoon intensity ($\delta^{18}O$) and/or wetter periods (based on a PCP interpretation of trace elements and/or $\delta^{13}C$) are towards the top of figure. Approximate timings of major events are highlighted in yellow (8.2 – 8.2 ka Event; YD – Younger Dryas; Heinrich Stadials (HS1, HS2, and HS3)). "**D" -** Z-scores of Sr/Mg (bedrock mixing ratio; 5-pt. moving average); dashed lines show 2 standard deviations from mean.*

2.6 Discussion

2.6.1 Controls on speleothem trace element ratios

The dissolution of bedrock by waters in the epikarst is the main source of trace elements often analyzed for speleothem studies (e.g. Mg and Sr), after which trace elements are incorporated in speleothem calcite via drip waters through cation substitution (Fairchild & Treble, 2009). The TM bedrock samples and the TM-17 stalagmite exhibit similar mean Sr/Ca values (0.42 mmol/mol and 0.38 mmol/mol, respectively), though Mg/Ca exhibits wider range in bedrock

samples, which included weathered crusts, potentially containing other minerals, in addition to the bulk limestone (**Table 1.1; Fig. 2.3**). Mg/Ca in TM-17 (mean value of 38.47 mmol/mol, range of 21.22 – 57.44 mmol/mol) falls entirely within the range of bedrock results (mean value of 71.24 mmol/mol, range of 8.98 – 196.96 mmol/mol). Trace elements may also be sourced from soil, aeolian dust, volcanic ash, and sea-salt aerosols (Fairchild & Treble, 2009; Frisia et al., 2005), and increases in Sr and other trace elements can be associated with colloidal input during times of high infiltration (Belli et al., 2017; Borsato et al., 2007; Hartland et al., 2012). Some soil input of trace elements may occur in TM despite the relatively thin depth of karst soils observed above TM, usually <30 cm, compared to the overburden of bedrock of at least 100 m. The soil results show a range on the high end of bedrock Mg/Ca and Sr/Ca (**Table 2.1; Fig. 2.3**), suggesting soil may also provide a source for trace elements in TM-17. Soil leachates are higher in both trace element ratios than bedrock values, with the increase in Mg/Ca more substantial than Sr/Ca (**Table 2.1; Fig. 2.3**). The relatively tight range of TM-17 Mg/Ca and Sr/ Ca (**Fig. 2.3**) reveals a constant sourcing over time, as a changing ratio of bedrock and soil might push values towards the higher ratios found in the soil. The small range of Sr/Ca values and the strong covariation with Mg/Ca (**Fig. 2.2**) in TM-17 suggests that there was no significant or long-term input of Sr from other sources, such as aeolian deposition or colloidal input, which would have caused more variations from Mg/Ca data. We cannot completely rule out some influence from other sources, as Mg/Ca and Sr/Ca are often uncorrelated over shorter time scales and sections of the time series.

Drip water results reveal an enrichment of trace element ratios compared to the bedrock and soil source (**Table 2.1; Fig. 2.3**), after which the final TM-17 calcite returns to values within the

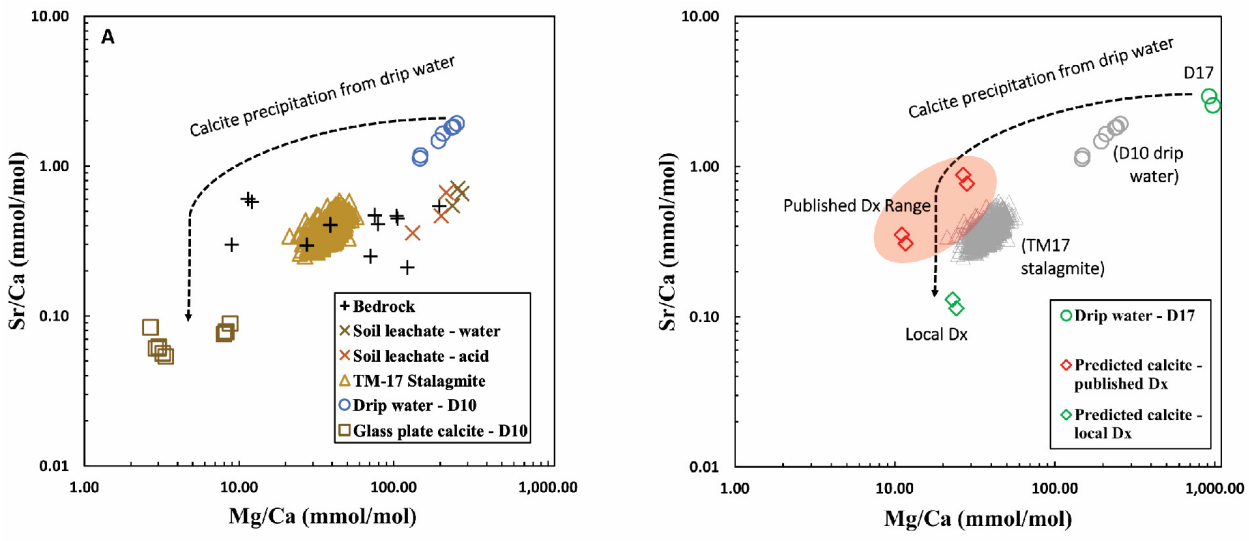

Figure 2.3 – Trace element sampling in Tham Doun Mai - A: *Results from bedrock (+'s); soil leachates (x's); TM-17 stalagmite time series (triangles); site D10 drip waters (o's); and D10 glass plate calcite (squares), which were used to estimate local Dx values, represented by the dashed arrow from drip water to calcite (note log scale on both axes).* ***B:*** *Drip waters from site D17 (o's) with the predicted values for calcite (diamonds) precipitating from the D17 drip based on published and local D_X values. Published Dx value data range (shaded oval: high and low ends plotted as diamonds) is combined from Huang and Fairchild (2001a) and Day and Henderson (2013). See text for full discussion.*

bedrock range. Drip waters near the fossil stalagmite (D-17) and the D-10 drip site are enriched in both Mg/Ca and Sr/Ca relative to the bedrock (and soil), indicating processes beyond simple dissolution of host rock (Fairchild et al., 2000). A distribution coefficient *(D_X,* **eq. 1***,* where X represents the measured trace element) is often used to quantitatively explain the final trace element ratios established during the precipitation of calcite (e.g. Morse & Bender, 1990):

$$D_X = (X/Ca)_{Calcite} / (X/Ca)_{Solution} \qquad \textit{(eq. 1)}$$

As D_{Mg} and D_{Sr} have values <<1 (Day & Henderson, 2013; Huang & Fairchild, 2001a), the fact that TM-17 calcite is within the range of bedrock provides further evidence for an enrichment of the elements in TM drip waters, as bedrock dissolution and secondary precipitation alone would produce values lower than the original bedrock. The drip water enrichment roughly follows the slope of variation in TM-17 values (**Fig. 2.3**), suggesting the drips were enhanced under a similar control to stalagmite variability, likely the PCP mechanism, which is known to affect multiple

trace elements similarly (Fairchild et al., 2000). Previous studies have found that a consistent covariation in Mg/Ca and Sr/Ca ratios in drip water and speleothem calcite, as seen in TM-17, is the best line of evidence for a hydrologic control over trace element ratios, as varying sources or controls between the two elements would cause dissimilar behavior (Fairchild & Treble, 2009; Johnson et al., 2006; Tremaine & Froelich, 2013).

Predicted Mg/Ca and Sr/Ca for calcite precipitated from analyzed drip water, produced by using measurements from TM (D10) and published values for D_{Mg} and D_{Sr}, are used to predict trace element ratios in calcite formed from the D-17 drip site (**Fig. 2.3**). Using **eq. 1** to estimate partition coefficients using local drip sites, D_{Mg} is calculated to be 0.025 (D-10) and 0.041 (D-17), which is comparable to published ranges of 0.012 – 0.031; D_{Sr} is calculated to be 0.045 (D-10) and 0.137 (D-17), comparable to published ranges of 0.057 – 0.300 (Day & Henderson, 2013; Huang & Fairchild, 2001a). The predicted calcite ratios using published D_X are 11.04 – 28.68 mmol/mol for Mg/Ca and 0.31 – 0.88 mmol/mol for Sr/Ca; using the locally estimated D_X, the predicted ratios are 23.00 – 24.27 mmol/mol for Mg/Ca and 0.11 – 0.13 mmol/mol for Sr/Ca (**Fig. 2.3**). The observed TM-17 stalagmite values overlap with these estimates, but are slightly higher on average with a mean Mg/Ca value of 38.47 mmol/mol and a mean Sr/Ca value of 0.38 mmol/mol. The proximity of the predicted calcite values to the TM-17 stalagmite values suggests the D-17 drip site is similar in composition to the drip that could have fed the fossil stalagmite TM-17 (**Fig. 2.3**), though the now-inactive drip likely had even higher Mg/Ca and Sr/Ca than the sampled drips, suggesting PCP and/or WRI enriched TM-17 drip water and stalagmite chemistry to a greater extent than the modern analogue.

Previous studies have provided other methods for identifying hydrology as a trace element control. Sinclair et al. (2012) modeled a specific range of slopes in ln(Mg/Ca) vs. ln(Sr/Ca) for PCP control and the potential effects of calcite-water and water-rock interactions on speleothem trace elements, suggesting that PCP should lead to a distinct slope of ~0.88 (+/- 0.13) for ln(Sr/Ca) v. ln(Mg/Ca). For TM-17, this slope over the full time series equals 0.63 (~30 year resolution; 1,211 data points; $R^2 = 0.44$, $p < 0.001$) (**Fig. S2.1**), which is less steep than the theoretical PCP slope. The slope increases to 0.72 at a ~90 year resolution (3 pt. moving average; $R^2 = 0.53$, $p < 0.001$), 0.81 at ~300 year resolution (9 pt. moving average; $R^2 = 0.61$, $p < 0.001$), and 0.85 at ~900 year resolution (30 pt. moving average; $R^2 = 0.66$, $p < 0.001$) (**Fig. S2.1**), suggesting that PCP is likely a major control on centennial to millennial timescales. Scatter at higher resolution, and the resulting weaker slope, could be the result of selective leaching of elements from bedrock during WRI above the drip (Fairchild et al., 2000) or potentially short-term sourcing changes for the elements (e.g. Belli et al., 2017). When locally estimated D_x values are generated for Mg and Sr (**eq. 1**) from the D-17 or D-10 drip water sites, the resulting slopes are 0.90 (D-17) and 0.98 (D-10) using **eq. 2** (Sinclair et al., 2012), which both fall in the range for PCP control of drip water enhancement (Sinclair et al., 2012; Treble et al., 2015). This suggests a strong modern PCP influence on drip waters in these sampling areas.

$$(D_{Sr} - 1) / (D_{Mg} - 1) = 0.88 \text{ +/- } 0.13 \quad (\textit{eq. 2})$$

The significant correlation between Mg/Ca and Sr/Ca in TM-17 ($R^2 = 0.44$) suggests a broadly similar control on both proxies over the entire record. A constant bedrock mixing ratio (Mg/Sr) is also evidence for hydrologic control on both Mg/Ca and Sr/Ca, and the majority of TM-17 Mg/Sr does not exceed 2 standard deviations from the average (**Fig. 2.2**) (Tremaine & Froelich, 2013). There may be periods when a mix of controls beyond PCP controlled variability, and/or

the drip path and water routing in this relatively deep, matrix-fed drip was not constant, which may explain some of the Mg/Ca vs. Sr/Ca discrepancies on shorter timescales. Temperature and growth rate can also affect trace elements in calcite, but temperatures and growth rates found in most natural cave systems are unlikely to cause significant variation compared to the effects of hydrologic controls (Day & Henderson, 2013). The overall agreement between Mg/Ca and Sr/Ca, along with the monitoring evidence, leads us to conclude that PCP and the local water balance above TM is the major control on TM-17 trace element ratios, whereby increases represent a drier period.

2.6.2 TM-17 trace element hydroclimate record and comparisons to stable isotopes

TM-17 stable isotopes ($\delta^{18}O$ and $\delta^{13}C$) have previously been interpreted alongside another stalagmite from TM (TM-21) that provided replication of TM-17 results and coherence in interpretations (Johnson et al., in revision). Johnson et al. (in revision) interpret $\delta^{18}O$ from these samples as representative of regional monsoon intensity, in this case defined as previous rainout over the Bay of Bengal and ISM regions, and $\delta^{13}C$ is interpreted as representative of the local water balance above TM. In times of weakened monsoon intensity during millennial climate events, such as HS1, HS2, and HS3, $\delta^{13}C$ reveals corresponding drier local conditions. However, the $\delta^{18}O$ and $\delta^{13}C$ records diverge during the Holocene in response to orbital-scale NHSI forcing, suggesting that the local water balance and regional monsoon intensity do not co-vary in MSEA on orbital timescales. The trace element results of this study provide additional hydrologically controlled proxies with which to examine these findings. Assuming PCP is the primary control on the trace elements and has some influence on $\delta^{13}C$, agreement between these proxies is a test for the agreement of regional monsoon intensity and local hydrologic conditions at our site.

The trace element record is not frequently well-matched by variations in stable isotopes during periods prior to the Holocene (>11.7 kyr BP), including the apparent lack of responses above background variability to HS2 and HS3 (**Fig. 2.2**). Large increases in trace elements are apparent around 31-33 kyr BP, but these excursions are not matched by TM-17 stable isotope responses and do not correspond with known climate events. There is more uncertainty in the older parts of the record due to both age uncertainties and the potential for the shorter, growing stalagmite to interact with waters on the slope in addition to the feeding drip, so older portions of the record (>22 kyr BP) are not a focus of this study. Long-term similarities between $\delta^{13}C$ and trace elements during the Holocene, however, point to orbital scale agreement on local hydrologic conditions, while inconsistent responses to abrupt millennial events create a need to examine the active controls on each proxy.

2.6.2.1 Abrupt millennial events in the last deglaciation and Holocene

Trace elements and $\delta^{13}C$ show similarities from the LGM onward outside of discrepancies in and around major climate events (HS1, YD) (**Fig. 2.2**). $\delta^{13}C$ appears to respond more consistently than trace elements to millennial-scale events, especially HS1. A millennial-scale peak of high Mg/Ca and Sr/Ca values is apparent at ~18.5 to 17.5 kyr BP, prior to the start of HS1 (~17.5 kyr BP in TM-17 $\delta^{18}O$) (**Figs. 2, 4**). While displaying high variability, TM-17 trace element ratios do not show the prolonged, systematic response to HS1 as seen in the stable isotope record (Johnson et al., in revision). This pattern is similar for the YD, seen in TM-17 $\delta^{18}O$ as well as $\delta^{18}O$ records from the EASM (e.g. Cheng et al., 2016; Y. Wang et al., 2008), although $\delta^{13}C$ in TM-17 is largely unaffected by the YD (**Fig. 2.4**). At the start of the YD response in $\delta^{18}O$ (~12.5 kyr BP), a sharp peak of increasing trace element ratios (Mg/Ca and Sr/Ca) begins at ~13 kyr BP, which

would match the expected local hydrologic response to a weakened monsoon. The elevated trace element ratios do not continue for the length of the YD, instead decreasing steadily through the event to levels below those prior to the YD (**Fig. 2.2**). We emphasize that the trace elements were analyzed from splits of the same powdered samples as the stable isotopes, thus negating questions of age model uncertainty between these proxies in TM-17. Therefore, the potential differences in controls between $\delta^{13}C$ and trace elements are of interest for interpreting the proxy system.

While PCP may have some control on $\delta^{13}C$ during the entire record, additional controls responsive to other above-cave environmental conditions and climate likely explain the long-term response in $\delta^{13}C$ during HS1 that is unmatched by TM-17 trace elements. Changes in hydrology affecting overall vegetation type, vegetation density, or intensity of soil respiration would affect $\delta^{13}C$ and create such discrepancies. The drier local conditions inferred from $\delta^{13}C$ during HS1 (Johnson et al., in revision) were therefore likely driven by the vegetation and soil zone response to the event as opposed to a PCP control on $\delta^{13}C$. A decrease in vegetation density, increase in the ratio of C3:C4 type vegetation, and/or decreased soil respiration would enrich ^{13}C in the drip water prior to speleothem formation. Long-term changes in hydrology and climate affecting vegetation amounts or types could also take decades or centuries to manifest, so the $\delta^{13}C$ response times in the TM-17 stalagmite could also be lagged compared to a PCP control that would respond more immediately. Therefore, both the length and intensity of climate events could create varying responses in the TM-17 multiproxy system. Although the length of HS1 would encompass any such lag, the relatively short YD (compared to HS1) would affect trace elements more quickly, potentially explaining the sharp peak in trace elements around the start of

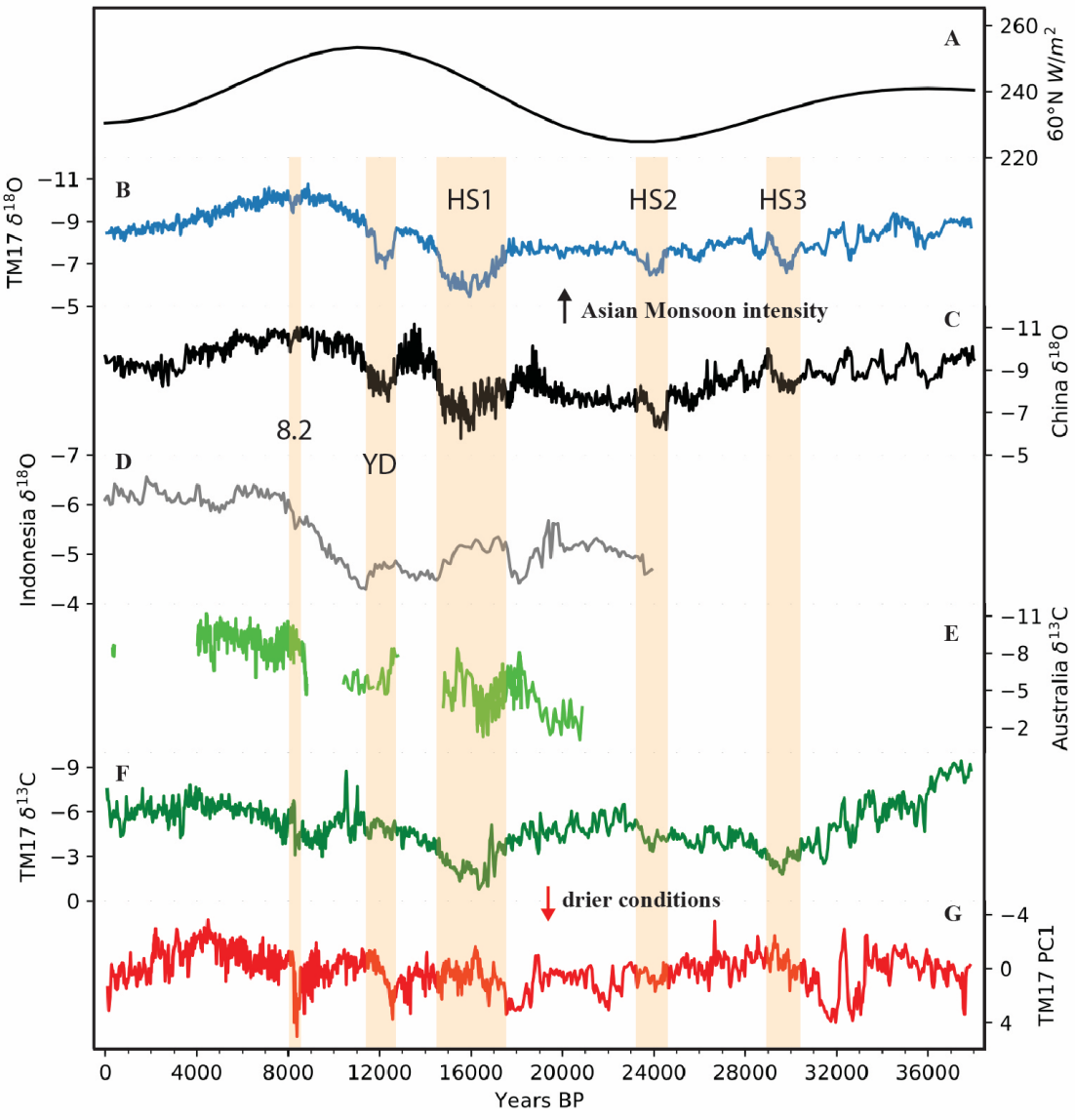

Figure 2.4 – Comparisons to Asian-Australian monsoon records *TM-17 proxy data (**B, F, G**) over the last deglaciation and Holocene compared with other records: **A** – Insolation curve (60° N) in W/m²* (Berger, 1992; Berger & Loutre, 1991)*; **C** - Chinese composite $\delta^{18}O$ record from Hulu, Dongge, and Sanbao caves (Cheng et al., 2016); **D** – Liang Luar, Indonesia $\delta^{18}O$ (Ayliffe et al., 2013); **E** – Overlain stalagmite $\delta^{13}C$ records from KNI-51, Northern Australia (Denniston et al., 2017). TM17 PC1 (**G**) refers to the first principle component of TM-17 Mg/Ca and Sr/Ca analysis ($PC1_{MgSr}$; see text for further details).* Approximate timings of major events are highlighted in yellow (8.2 – 8.2 ka event; YD – Younger Dryas; Heinrich Stadials (HS1, HS2, and HS3)). *TM-17 stable isotope data (**B, F**) from Johnson et al. (in revision).*

this event and the absence of a $\delta^{13}C$ response that is similar to HS1.

The increase of trace element ratios for the ~1,000 years before HS1 suggests the period prior to HS1 is locally drier than the event itself, a conclusion that contrasts with the drier local conditions during HS1 suggested by the $\delta^{13}C$ data (Johnson et al., in revision). Potential non-climatic controls that could affect trace elements while not similarly affecting $\delta^{13}C$ must also be considered. While PCP may dominate the trace element controls on long timescales (**Fig. S2.1**), changes in drip water routing caused by significant or long-term changes in rainfall amounts could affect the trace elements through variations in bedrock contact(s) and residence times. Changes in seepage-flow drip sites, where flow rates are controlled by incoming precipitation amounts, can cause mixing of various water pools, flow paths, and flow rates. While increased WRI times may enrich trace elements in drip waters similar to a PCP control (Belli et al., 2017), incongruent dissolution of Mg from a uniform host rock may also occur due to variable WRI (Baker et al., 2000; Fairchild & Treble, 2009). These types of additional controls on trace elements, potentially active during a millennial-scale climate anomaly such as HS1, could explain the some of the inconsistency between TM-17 $\delta^{13}C$ and trace element ratios during prolonged climate anomalies.

The most abrupt peak and highest individual values in the trace element ratios occur around the 8.2 kyr event (Alley & Ágústsdóttir, 2005) in the Holocene (**Figs. 2, 4**), suggesting more dryness, however short-lived, than at any other time in the deglaciation or Holocene. At ~150 years long, with a prolonged dry period of ~70 years, as seen in the EASM system in China (Y. H. Liu et al., 2013), this event is less lengthy than HS1 and YD, so a sustained response is not

expected in any proxy at our sampling resolution. The 8.2 ka event is seen as a positive anomaly in $\delta^{18}O$, while a negative $\delta^{13}C$ excursion occurs around this event, opposite to the HS1 $\delta^{13}C$ response to a weakened monsoon (**Fig. 2.2**). Assuming some PCP control on $\delta^{13}C$, this would suggest wetter than average conditions during or immediately following the maxima in trace element ratios. As a similar North Atlantic freshwater forcing is likely the cause of a weakened monsoon during HS1, YD, and 8.2 in the AM (McManus et al., 2004), this is surprising. However, the exact timing of the 8.2 responses in our proxies are difficult to pinpoint at our sampling resolution. $\delta^{13}C$ reaches the most positive values around the event at 8,296 yrs BP, directly between the two trace element maxima, and the most negative $\delta^{13}C$ value of the time period is at 8,230 yrs BP, within the resolution of one sampling point to the highest Mg/Ca value. The maxima of trace elements is matched by a smaller, positive peak of $\delta^{13}C$ prior to the larger negative one (**Figs. 2.2, 2.5**). The information taken together suggests prolonged dryness prior to or at the beginning of the event and a drastic change during or after the event, which leads into a new regime of wetter conditions afterwards and into the Mid-Holocene (**Fig. 2.5**). but higher resolution sampling of both speleothem proxies and U-Th dates are needed to fully assess the timing and leads or lags of the proxies for such a relatively brief event.

2.6.2.2 Orbital scale variations and rainfall maxima during the Holocene

The general trends and responses in trace elements and $\delta^{13}C$ are fairly consistent in much of the Holocene (**Fig. 2.5**), suggesting a similar control is active on all three proxies during this period. As Holocene differences between trace elements and $\delta^{13}C$ are less apparent (**Fig. 2.2**), z-scores are utilized in order to examine how uniformly the trace elements and $\delta^{13}C$ responded qualitatively during this period (**Fig. 2.5**), as these proxies are sometimes affected similarly by

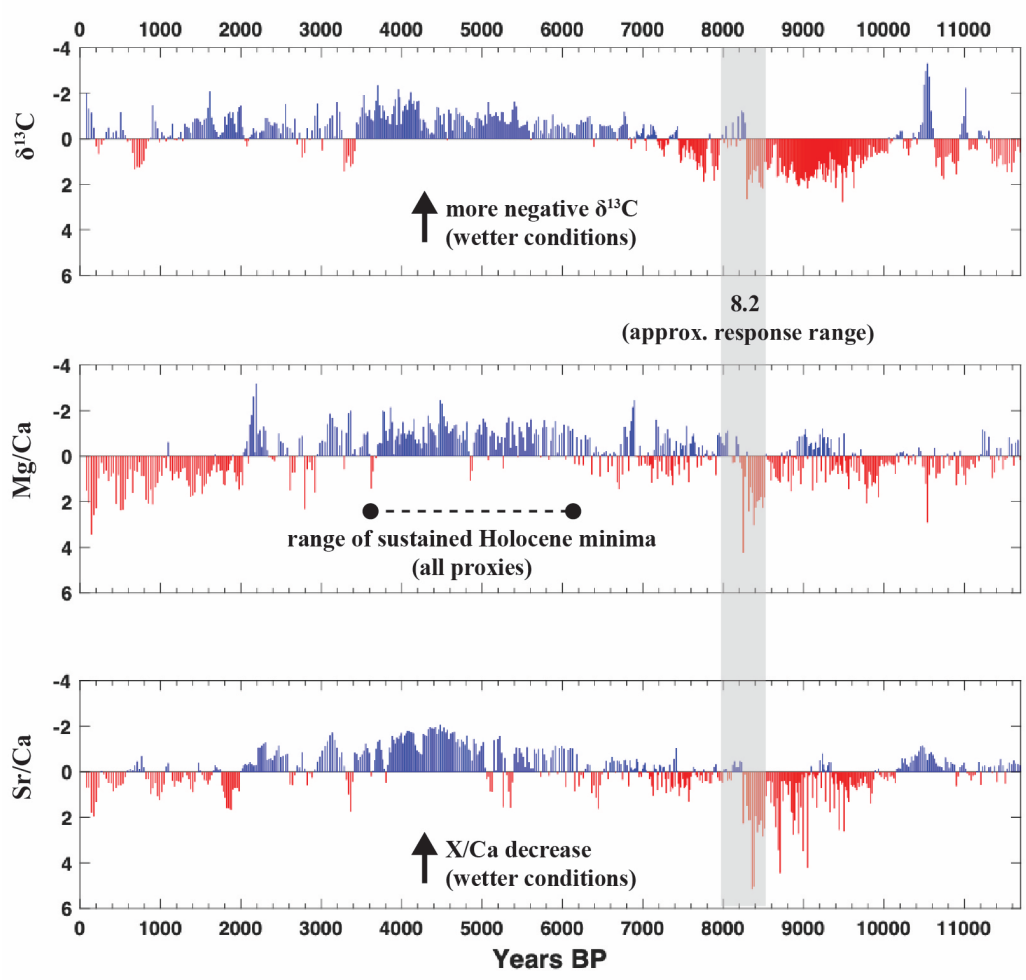

Figure 2.5 – ***Holocene hydrologic reconstruction*** – *Holocene z-scores of $\delta^{13}C$, Mg/Ca, and Sr/Ca show qualitative agreement likely due to PCP control. All proxies show relative dryness in the early Holocene (10.2 – 8.2 kyr BP), an abrupt response around the 8.2 ka event, and maximum sustained wetter period in the Mid-Holocene (between ~4-6 kyr BP) prior to drier conditions towards the modern day.*

local hydrology through the PCP control (Fairchild & Treble, 2009; Johnson et al., 2006). The data shows high trace element ratios and positive $\delta^{13}C$ in the early Holocene (~10.2 – ~8.2 kyr BP) and the abrupt responses in all three proxies around the 8.2 event discussed previously. Following the 8.2 event, there is an apparent long-term shift in hydrology at our site that contrasts with the period of relative dryness in the early Holocene (**Fig. 2.5**). These findings are

similar to sediment core pollen results from Northeastern Cambodia (Maxwell, 2001), which found palynological and other evidence for a climatological regime change and a strengthening monsoon from 8,400 yrs BP until 5,300 yrs BP in MSEA.

TM-17 Mg/Ca, Sr/Ca, and $\delta^{13}C$ show movement to less dry or wetter conditions into the Mid-Holocene with the lowest trace element ratios and most consistently negative $\delta^{13}C$ occurring between ~4 – 6 kyr BP, although the timing of the most sustained values varies by proxy (**Fig. 2.5**). This period of "wet" values in the Holocene is markedly different from TM-17 $\delta^{18}O$, which reaches its most negative values much earlier in the Holocene (~7-9 kyr BP), likely driven by monsoon intensity and upstream rainout increasing in response to a maximum in NHSI (Wanner et al., 2008; Johnson et al., in revision). The timing of Holocene monsoon and rainfall peaks across the EASM is a frequently debated topic (e.g. An et al., 2000; Dykoski et al., 2005; Maher, 2008). Our findings agree with the findings of Johnson et al. (in revision), with $\delta^{13}C$ indicative of local water balance, in that our trace element record provides additional evidence that local rainfall amounts in the SEAM region are decoupled from the peak of Holocene monsoon intensity inferred from speleothem $\delta^{18}O$.

The period of decreased trace element ratios and $\delta^{13}C$ in the mid-Holocene is followed by increases in trace element ratios and more modest and irregular values of $\delta^{13}C$ after 4-5 kyr BP, suggesting a precipitation decrease towards the modern day (**Fig. 2.5**), and this is accompanied by a continued increase in $\delta^{18}O$, suggesting a weakening monsoon (**Figs. 2.2, 2.4**). A drier, potentially more seasonal climate following a previously strengthened monsoon on the Indochina Peninsula was also seen as a possibility by Maxwell (2001) after 5,300 yrs BP. A recent study

utilizing stalagmites closer to the entrance of TM found evidence for drying between ~3-5 kyr BP potentially linked to megadroughts in MSEA, the 4.2 ka event, and the end of the Green Sahara in Africa (Griffiths et al., in revision). This period of drying roughly corresponds to the end of the wetter mid-Holocene evidenced in TM-17 trace elements and $\delta^{13}C$. Differences in the responses are likely due to the samples' varying proximity to the cave entrance and differences in the depth of bedrock overburden, whereas the stalagmites nearer to the entrance are controlled by fracture flow and faster recharge times for drip waters. The deeper areas of the cave, where TM-17 was sampled, may not be as sensitive to the mid- to late-Holocene droughts seen in Griffiths et al. (in revision), potentially because they are fed by multiple reservoirs of stored water in the epikarst (Treble et al., 2013).

2.6.3 Low latitude asymmetry and other records in the Asian-Australian monsoon

In a connected, global monsoon system (e.g. Cheng et al., 2012; Trenberth et al., 2000), an antiphase response between Northern and Southern Hemisphere monsoon regions is sometimes attributed to Intertropical Convergence Zone (ITCZ) shifts (Broccoli et al., 2006; Griffiths et al., 2016; Schneider et al., 2014). Monsoon records show evidence of a hemispheric see-saw effect during both orbitally-induced NHSI changes and shorter-term responses to abrupt climate events, causing a more intense monsoon (or more rainfall) in one hemisphere's tropical or subtropical region coinciding with a decline on the opposite side of the equator (McGee et al., 2014; X. Wang et al., 2006). Slowdowns or cessations in the AMOC, such as those during HS1 (Broecker, 1994; McManus et al., 2004), are tied to Northern Hemisphere cooling and an ITCZ shift to the south due to changes in the hemispheric temperature gradient (McGee et al., 2014; McManus et al., 2004). A more southerly ITCZ weakens the AM system(s) because changes in the Hadley

circulation create increased uplift south of the equator and increased subsidence to the North (Cheng et al., 2012). For example, during HS1, a weak monsoon and lowered precipitation in the Northern Tropics is accompanied by stronger monsoons and more precipitation in Northern Australia and South America, providing global evidence for an ITCZ displaced to the South, although it is unclear whether the mean ITCZ location or length of time spent at a maximum location may have caused the changes (McGee et al., 2014 and refs. within). McGee et al. (2014) show that any global mean shift would be small, while more localized, meridional ITCZ shifts could be much larger. Records are needed in more locations to test this theory and estimate more regional ITCZ responses. It is unlikely any ITCZ reconstruction for the SEAM region could be accurate based on one cave site, as local monsoon heterogeneity in the SEAM region is large (Misra & Dinapoli, 2014). However, evidence for equatorially antiphased behavior in the greater Asian-Australian system is seen when comparing stalagmite records from China and Indonesia during the deglaciation (e.g. Ayliffe et al., 2013). Additional evidence is seen comparing Indonesia and Borneo records during the mid-Holocene (~4-6 kyr BP), with Borneo records showing a $\delta^{18}O$ minima (stronger monsoon) that lines up with an increase of $\delta^{18}O$ in Indonesia (Griffiths et al., 2010a; Griffiths et al., 2010b; Partin et al., 2007). Our trace element record provides support that other regions north of the equator saw increased precipitation during this mid-Holocene interval that may be a response to ITCZ changes in the tropics (**Fig. 2.4**).

The sustained increase in trace element ratios prior to HS1 (~18.5 – 17.5 kyr BP) could potentially be evidence for an asymmetrical cross-equatorial relationship to a Late Glacial Pluvial (LGP) hypothesized by Denniston et al. (2017) in a stalagmite study that found $\delta^{13}C$ evidence for periods of increased rainfall in Northern Australia from ~18.3 – 17.3 kyr BP (**Fig.**

2.4). A potential LGP response is also seen in Indonesia (Ayliffe et al., 2013; note that $\delta^{18}O$ in the Indonesian record was interpreted as a rainfall amount proxy), although the timing difference between the response at this location and the LGP in Northern Australia is large (~1.5 kyr), which Denniston et al. (2017) potentially attribute to the uncertainties in dating methods or the progression of a complex event across two regions. If the events are related, an asymmetrical response above the equator in the SEAM might be expected, which could explain the dry period seen in trace elements at our site prior to HS1. Alternatively, the dry period seen in Indonesia around ~19-18 kyr BP (Ayliffe et al., 2013) could be linked to the response we see in TM-17 trace elements (**Fig. 2.4**), representing a change in monsoon rainfall amounts on both sides of the equator, lessening rainfall in both the SEAM and Indonesia. An extreme southern movement of the ITCZ could explain a drier period in Laos and Indonesia coinciding with increased rainfall in Northern Australia, yet the relative proximity of the southern hemisphere sites (**Fig. 2.1**) make this seem unlikely. The absence of a similar structure over the period prior to HS1 in the EASM region (**Fig. 2.4**) could be due to the increased distance from the tropics, a moisture source independent from the SEAM, and/or the LGP being a more localized event than HS1. Additionally, most records from the EASM have focused on $\delta^{18}O$ over this time period, with an exception being Zhang et al. (2018), which does show a potential peak in dryness around 18.5 kyr BP in the trace element time series. More low latitude records and/or multiproxy records across the greater region are needed to investigate these possibilities.

2.7 Conclusions

Trace element ratios (Mg/Ca and Sr/Ca) from Tham Doun Mai cave in Northern Laos show evidence of hydrologic control over the last 37.8 kyr BP. Hydrologic control is interpreted based

on monitoring evidence of PCP enrichment of trace elements in TM drip waters, a mechanism which increases Mg/Ca and Sr/Ca in the TM-17 stalagmite during drier periods on multi-decadal to millennial timescales. Covariance between Mg/Ca and Sr/Ca in the TM-17 time series (R^2 = 0.44) and a relatively constant bedrock mixing ratio (Mg/Sr) over the length of the record support the interpretation of a shared hydrologic control.

While all proxies in TM-17 display both orbital scale trends and abrupt climate event responses through the last deglaciation and Holocene, comparisons between the new trace element record and previously analyzed $\delta^{13}C$ and $\delta^{18}O$ from the same stalagmite reveal times when proxy controls vary as well as when monsoon strength differs from local rainfall amounts. $\delta^{13}C$, interpreted as a signal of local water balance (Johnson et al., in revision), reveals drying during HS1, HS2, and HS3, when $\delta^{18}O$ also suggests a weakened monsoon. During these millennial-scale events, influence from vegetation and soil respiration changes due to long-term drying likely control the $\delta^{13}C$ signal. The initiation of HS1, YD, and the 8.2 event create sharp increases in trace element ratios, although water routing, mixing, and changing residence times in the epikarst may sometimes affect the dominant signal during longer-term climate anomalies such as HS1.

Agreement among trace element and $\delta^{13}C$ results suggest hydrology (via PCP) was likely a shared control on these proxies during the Holocene. The 8.2 ka event sees the highest individual trace element ratios in the record, and the period immediately following the 8.2 event disrupts a relatively dry period in the Early Holocene. This contrasts with the minimum in $\delta^{18}O$ (strengthened monsoon) that follows the NHSI maximum in the early Holocene. Trace element

ratios (and $\delta^{13}C$) increase into the mid-Holocene, which is interpreted as more local rainfall. The observed differences between $\delta^{18}O$ and trace elements in the early and mid-Holocene agree with previous $\delta^{13}C$ interpretations (Johnson et al., in revision) that suggest local rainfall is decoupled from monsoon intensity on MSEA during the early and mid-Holocene. A weakening monsoon interpretation of $\delta^{18}O$ from the mid-Holocene to the modern day is matched by increases in TM-17 trace elements and $\delta^{13}C$.

The new trace element record from our site in MSEA also provides an opportunity to examine cross-equatorial relationships of past Asian-Australian monsoon responses during the last deglaciation and Holocene using other speleothem studies. More records revealing these types of relationships could provide needed evidence for estimates of the regional extent of past ITCZ shifts or other mechanisms responsible for monsoon and rainfall variability. The multiple environmental controls revealed in TM-17 proxies highlight the ongoing need for obtaining not only more climate records, but for applying multi-proxy analyses to speleothem records. More constraints on each potential control enable more robust interpretations and assist in reconstructing climate in monsoon regions where regional monsoon strength and local rainfall amounts may often diverge.

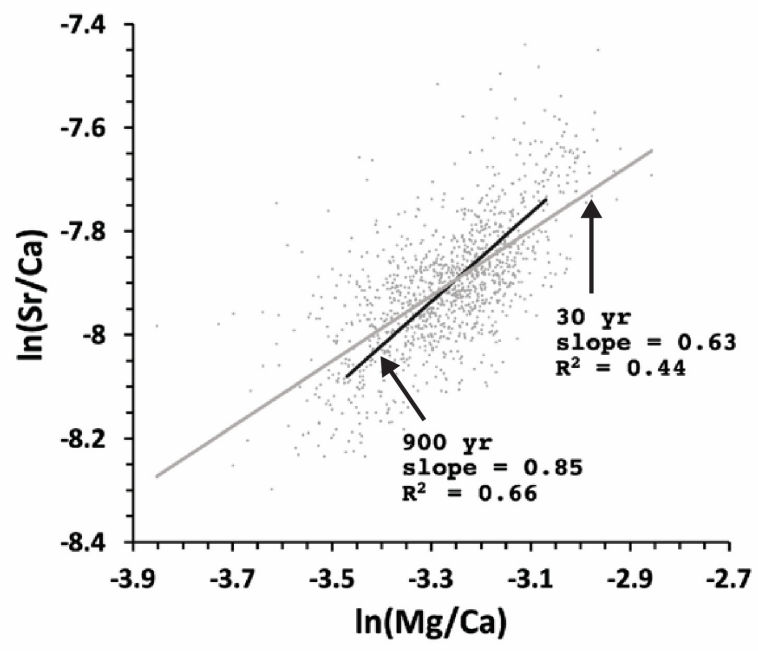

Figure S2.1 – PCP control dominates millennial scale variability *- Plot of the relationship and slope (m) of ln(Mg/Ca) v. ln(Sr/Ca) from all measured samples from stalagmite TM-17 at different time resolutions: lighter grey (m = 0.63, ~30 yr. resolution); black (m = 0.85, ~900 yr. resolution). 30 yr. slope is shallower than predicted for pure PCP control as per Sinclair et al. (2012), but strong correlation (R^2 = 0.44 for Mg/Ca v. Sr/Ca) suggests a similar control. At millennial timescales (30 pt. moving average; ~900 yr. resolution), slope is within predicted range of PCP control. Grey dots are full resolution data.*

Chapter 3

Speleothem radiocarbon evidence for paleohydrologic changes in Mainland Southeast Asia

3.1 Abstract

While the number of speleothem records of paleoclimate continue to grow, the interpretation of some proxies remains elusive and often depends on the specific cave environment. In the greater Asian Monsoon region, the relationship between speleothem $\delta^{18}O$ and past rainfall amount remains a matter of intense debate, enhancing the need for other proxies that are responsive to climate and hydrology. Speleothem ^{14}C measurements, when compared to U-Th dates, indicates the amount of ^{14}C-depleted, or "dead," carbon derived from the carbonate bedrock and/or aged organic matter, both of which are sensitive to climatic conditions. The dead carbon proportion (DCP) of speleothem calcite is often tied to the degree of open vs. closed system dissolution and can function as a proxy of past hydrology. In addition to serving as a hydrologic proxy, DCP data is useful for unraveling of other proxy controls, especially the multiple influences on $\delta^{13}C$. We conducted 52 ^{14}C analyses on a U-series dated stalagmite (TM-17) from Tham Doun Mai cave, Northern Laos spanning the last ~35,000 years. Our results show high and variable DCP of 25.0 – 60.6%, with an average age offset from the U-Th based age model of 4,918 yrs. We present evidence for a dominant bedrock source of dead carbon in TM-17 and hypothesize that the high DCP values are driven by sulfuric acid dissolution in the epikarst. Additionally, we use a recent, karst geochemical model that incorporates cave monitoring data and pyrite oxidation

(sulfuric acid dissolution) to show that the dominant trend of variability in TM-17 DCP is reliant on changes in pCO_2 and the available gas volume in the epikarst, which indicates the open vs. closed system control. A positive correlation between DCP and $\delta^{13}C$ ($R^2 = 0.36$) suggests the bedrock dissolution control is also an active influence on $\delta^{13}C$. DCP variations during the last deglaciation and Holocene confirm the weakened monsoon and drier conditions during abrupt climate events, such as Heinrich Stadial 1 and the 8.2 ka event, consistent with stable isotope and trace element data from the same stalagmite. We utilize a "dissolution-corrected" $\Delta\delta^{13}C$ proxy, based on DCP and monitoring data, to assess non-dissolution controls on $\delta^{13}C$ during specific events. The results reveal multiple non-dissolution controls, likely dominated by soil and/or vegetation changes, during Heinrich Stadial 1 and a strong dissolution-driven response to the briefer 8.2 ka event. This analysis reveals how climate events of varying magnitude and length affected TM-17 proxies in contrasting ways, especially in the carbon isotopic system. The new information presented based on speleothem ^{14}C emphasizes the importance of multiproxy applications in developing speleothem-based climate reconstructions.

3.2 Introduction

3.2.1 Overview

^{14}C-depleted material that is incorporated in a speleothem is sourced from bedrock or aged soil organic matter (SOM) above the cave and creates a measurable offset in the apparent ^{14}C age from ages determined using more robust U-Th dating methods. This input is known as the dead carbon proportion (DCP) (Genty & Massault, 1997). In some speleothems, DCP has been shown to remain remarkably stable over long time periods, and these records have thus proven valuable for improving the radiocarbon calibration curve (Cheng et al., 2018; Reimer et al., 2013; Southon

et al., 2012). More often, speleothem DCP exhibits some variability that may be linked with environmental conditions. For instance, recent studies have utilized DCP variations to estimate the age and turnover time of SOM in the epikarst (Fohlmeister et al., 2011; Genty et al., 1999b; Noronha et al., 2015) and to reconstruct past changes in hydrologic conditions (Genty et al., 2001; Griffiths et al., 2012; Oster et al., 2010). DCP interpretation as a hydrologic proxy relies on the assumption that wetter periods lead to enhanced closed-system bedrock dissolution in the karst system, due to more saturated soil and epikarst conditions. This closed-system dissolution (i.e. dissolution in the presence of a smaller, limited pool of CO_2) increases bedrock C input, and therefore, DCP (Hendy, 1971). Other studies have highlighted that DCP measurements may be useful for improving interpretation of other speleothem proxies, especially stable carbon isotope ($\delta^{13}C$) variations (e.g. Lechleitner et al., 2016b; Rudzka et al., 2011). $\delta^{13}C$ in speleothems responds to a variety of controls, which can vary by site (e.g. Frisia et al., 2011; Wong & Breecker, 2015). Since some of these controls are shared with DCP, the combination of DCP and $\delta^{13}C$ measurements, along with cave monitoring, modeling of subsurface processes, and additional multi-proxy data, provide an opportunity to improve the interpretations of speleothem proxies and create more robust climate reconstructions over many timescales.

The goal of this study is to use numerous lines of evidence to interpret DCP measurements in a new stalagmite data set from Tham Doun Mai cave in Northern Laos and apply the findings to other proxy interpretations of paleoclimatic interest from TM cave. Stalagmite TM-17 reveals a large and variable DCP (25.0 – 60.6%) that we show to be dominantly sourced from bedrock. The DCP results are compared to $\delta^{13}C$ and trace element ratios from the same stalagmite. Trace element ratios (Mg/Ca and Sr/Ca) from stalagmite TM-17 are controlled by local hydrology

through the prior calcite precipitation (PCP) control, and $\delta^{13}C$ from this sample is also affected by the local water balance through various controls (Johnson et al., in revision; Wood et al., in prep., a). The DCP covaries with $\delta^{13}C$ over the last ~35 thousand years (ka), suggesting a significant bedrock dissolution control on both. ^{14}C and $\delta^{13}C$ measurements of the local cave and karst environment are used to evaluate the different controls on $\delta^{13}C$ in the stalagmite, and well documented climate events from the last deglaciation and Holocene create responses in DCP and other TM-17 proxies, including Heinrich stadial 1 (HS1) and the 8.2 ka event. These event responses assist with interpretations of centennial to millennial scale hydrologic changes from our location in Mainland Southeast Asia (MSEA), where terrestrial climate records are relatively scarce.

3.2.2 DCP measurements and interpretations

The calculation of DCP is achieved by comparing the initial stalagmite activity ($a^{14}C_{initial}$), found by correcting the measured activity ($a^{14}C_{measured}$) for decay (***eq. 1***), to the atmospheric activity ($a^{14}C_{atmosphere}$) at the time of deposition (t) (***eq. 2***) (Genty & Massault, 1997). The time of deposition is typically known or estimated from U-Th dating and age modeling of the stalagmite, and $a^{14}C_{atmosphere}$ is estimated using a record of atmospheric ^{14}C activity such as IntCal13 (Reimer et al., 2013).

$$a^{14}C_{initial} = \frac{a^{14}C_{measured}}{\exp\left[\frac{-\ln(2)}{5{,}730} * t\right]} \qquad \textbf{\textit{eq. 1}}$$

$$DCP = \left[1 - \left(\frac{a^{14}C_{initial}}{a^{14}C_{atmosphere}}\right)\right] * 100\% \qquad \textbf{\textit{eq. 2}}$$

^{14}C age model construction is sometimes possible if U-Th methods are not feasible (Hua et al., 2012; Lechleitner et al., 2016a), but ^{14}C is not the preferred dating method for speleothems due to: 1) the more limited age range of ^{14}C dating compared with U-series dating, and 2) the fact that, despite speleothem carbon being sourced locally from in and above the cave setting (Fairchild et al., 2006), both the exact source and age of carbon initially incorporated can be highly variable; therefore, ^{14}C ages require a reservoir age correction, which is often uncertain and/or unstable over time. Once the DCP is assessed, its stability over time may determine the potential use(s) of ^{14}C measurements in a speleothem. If stable, the atmospheric history of ^{14}C, often estimated from marine records with large uncertainties, may be improved by a terrestrial record with a constant offset (Cheng et al., 2018; Southon et al., 2012). Alternatively, significant changes to the DCP are sometimes linked to changes in hydrology that alter conditions in the soil and epikarst zones above a cave. Variation of this nature can be due to changes in the above-cave ecology (Genty et al., 2001), a systematic response of the SOM reservoir to wet or dry periods (Oster et al., 2010), and/or changes to the degree of open or closed system dynamics, also indicative of wet or dry periods, that alter the extent of bedrock dissolution (e.g. Hendy 1971; Griffiths et al. 2012).

An important factor for the open vs. closed system dissolution control is the amount of airspace along the drip water path in the epikarst, which dictates the extent of bedrock dissolution in an above-cave environment. In a fully open system, isotopic exchange with CO_2 in fractures and voids will keep the drip water dissolved inorganic carbon (DIC) in equilibrium with modern ^{14}C values, and DCP will equal 0%. A closed system implies bedrock dissolution occurring in an epikarst zone cut off from the influence of modern CO_2 from the atmosphere or soil zone.

Percolating drip waters previously acidified by soil-zone CO_2 are neutralized with $CaCO_3$ from the ^{14}C-depleted bedrock during dissolution (Hendy, 1971; Noronha et al., 2014). In a fully closed system dominated by CO_2 driven dissolution, the theoretical upper limit of DCP is 50% (Hendy, 1971; Southon et al., 2012). Natural cave systems that display the exact behavior of either end member have not been observed, with most speleothems characterized by a DCP of around 15±5% (Genty et al., 1999b). Recent studies with uncommonly high values of DCP (>50%) have pointed to an additional mechanism for bedrock dissolution in the epikarst that involves sulfuric acid sourced from the oxidation of pyrite or other sulfide minerals (Bajo et al., 2017; Spötl et al., 2016). This sulfuric acid dissolution (SAD), which may act in addition to the typical carbonic acid dissolution (CAD) in karst systems, enhances bedrock carbon inputs into the drip water DIC, thus increasing DCP in the precipitating speleothem. In a karst environment where DCP mainly represents the extent of bedrock dissolution, SAD may enhance the signal of dissolution, creating an unusually reliable proxy for past water infiltration.

3.3 Methods

3.3.1 Field work and sampling

Stalagmite TM-17 was sampled in 2013 from Tham Doun Mai (TM) cave in Northern Laos (N20°45', E102°39'; 352 m asl). Descriptions of the climatic setting and additional cave monitoring information not found in this study can be found in J. K. Wang et al. (2019), Johnson et al. (in revision) and Wood et al. (in prep., a). The stalagmite was previously cut in half, polished, and drilled for U-Th dating, stable isotope ($\delta^{18}O$ and $\delta^{13}C$), and trace elemental (Mg/Ca and Sr/Ca) analysis. Previous studies suspect that the drilling and subsequent heating of dense calcite for powder during ^{14}C sampling may cause contamination from ambient air, especially for

older samples (Hoffmann et al., 2010; Southon et al., 2012). These previous studies used wafers of calcite taken from in-between trenches drilled for U-Th dating in order to avoid the potential modern contamination. As drilling of numerous new trenches would be destructive to TM-17 due to lower resolution U-Th sampling, ^{14}C samples were scraped from the stalagmite using a mineral hardness pick. 52 samples were scraped perpendicular to the growth axis either from trenches previously drilled for U-Th dating or from the surface in-between U-Th trenches. The initial surface layer powder from each sample depth was discarded, and the stalagmite and pick used for scraping were blown with compressed air and wiped clean with ethanol between all samples to avoid cross-contamination.

Cave monitoring samples analyzed for ^{14}C, including cave air, outside air, soil, soil gas, drip waters, and glass plate calcite, were collected on field expeditions to TM cave in 2015 and 2017. Cave air and outside (ambient) air ^{14}C samples were collected in steel traps filled with molecular sieve 13x, which traps CO_2 at ambient temperatures and releases when heated (Bauer et al., 1992; Gaudinski et al., 2000). A sampling system consisting of inert tubing, Drierite desiccant, a steel trap for each sample, a flow meter, and a small air pump was assembled in the field, and flow was set to 0.5 L m^{-1} for 15 minutes. Cave air, sampled from two locations, was collected upon first entry to the cave to minimize contamination with human-respired air. Outside air was sampled above the cave in the general location of the soil gas and soil samples under a heavily forested canopy on a rocky slope. Soil gas was extracted through vertical steel wells installed on site. pCO_2 was measured in each well using a LI-800 CO_2 Gas Analyzer calibrated prior to field deployment. After logging pCO_2 and depth for each well, the tops were sealed and left to accumulate CO_2 prior to sampling. Soil gas samples were collected in either evacuated vials or

molecular sieve 13x traps prepped prior to field deployment. For soil gases collected in glass vials, a syringe was used to pull a known quantity of air from the well, and a needle was used to penetrate the septa of the evacuated vials for soil gas storage. In 2015, 8 locations were sampled. Steel traps were used for wells under 2,000 ppm, and 60 mL vials were used for wells with higher pCO_2 readings. In 2017, 150 mL vials were used for 12 soil gas samples. Ambient pCO_2 was recorded outside the cave near other sampling locations and upon entry to the cave in two different locations using a Vaisala GM70 CO_2 Monitor in both years. Temperature and relative humidity were measured using an Extech probe.

3.3.2 Laboratory methods

Speleothem samples were prepped and analyzed for ^{14}C at the WM Keck Carbon Cycle Accelerator Mass Spectrometry (KCCAMS) laboratory at the University of California, Irvine. Samples were leached (10%) with dilute HCl in order to remove any secondary carbonates (Santos & Xu, 2017) prior to hydrolysis with 85% phosphoric acid. Samples were then graphitized onto a Fe catalyst using a modified hydrogen-reduction method (Beverly et al., 2010; Santos et al., 2004). Scraped powder from a speleothem known to be radiocarbon free from previous work (age >60,000 yrs BP) was utilized during data processing as an additional measurement for blank subtraction, as the typical calcite blanks in the KCCAMS laboratory are not from a comparable speleothem matrix.

Soil samples were collected in 2015 from the area sampled for soil gas. Three samples were acquired from different depth profiles (0-10, 10-20, and 20-30 cm) and stored in whirl-paks. Drip water DIC samples were collected from several locations in the cave and poisoned with $HgCl_2$ in

acid-washed and baked-out glass pyrex bottles. Glass plate calcite was collected from drip site D10 in TM cave (Wood et al., in prep., a) using an ~18 cm diameter watch glass placed on a large, actively growing stalagmite for a two-year period. D10 is a very hydrologically active drip with a rate of 64 drips minute^{-1} when measured in the dry season of 2015. Calcite was gently drilled off of the plate into powder for ^{14}C analysis, as the low-density calcite and low drilling speed should not cause ambient air contamination, and then prepped and analyzed in the same manner as TM-17 samples. Bedrock samples collected from inside and above TM cave were drilled for powder and analyzed for $\delta^{13}C$ using a Thermo Finnigan Kiel VI carbonate device coupled with a Delta V Plus isotope ratio mass spectrometer at the University of California, Irvine.

All ^{14}C monitoring samples were analyzed at the KCCAMS Laboratory. Sample preparation for cave air, outside air, SOM, and soil gas utilized vacuum-line extraction from evacuated vials and/or traps with sample sizes measured manometrically during extraction. Separate aliquots for $\delta^{13}C$ require a minimal manometric sample weight during extraction; some samples contained enough CO_2 for this purpose, but not all ^{14}C gas measurements have a corresponding $\delta^{13}C$ measurement due to low pCO_2 and/or an overall sample size <0.3 mg C. Soil samples were acid washed prior to ^{14}C prep, and sample preparation backgrounds were subtracted based on measurements of ^{14}C-free acid washed coal. CO_2 from all monitoring samples was graphitized in sealed tubes using the zinc reduction method (Xu et al., 2007), pressed into targets and then analyzed by AMS.

Drip waters from multiple field campaigns in TM cave were tested for sulfate (SO_4^{2-}) concentrations using a Dionex ICS 2100 (Dionex IonPac AS-18 Fast 2x 150 mm column) coupled with a Thermo Finnigan TSQ Quantum mass spectrometer. Dilution levels were determined by test runs before final data acquisition. 23 individual drip water samples were tested, although some samples included repeated sites from different field campaigns. Two samples were repeated as duplicates, and the average value of the two runs was used as the final data for these samples.

3.3.3 Data

The U-Th based TM-17 age model (Johnson et al., in revision) was used to assign an estimated age to sample depths without a directly corresponding U-Th analysis for the calculation of DCP. Using data from previous analyses on TM-17 (Johnson et al., in revision; Wood et al., in prep., a), known times and corresponding depths of event responses in other proxies were targeted for higher resolution sampling, including Heinrich stadials, the Younger Dryas, and the 8.2 ka event. All ^{14}C results presented have been corrected for isotopic fractionation, and all units, including fraction modern (FM, or fraction of the modern standard), conventional radiocarbon age (^{14}C age, yrs BP), and $\Delta^{14}C$, are reported following the conventions of Stuiver & Polach (1977). IntCal13 (Reimer et al., 2013) was used for all calculations as the atmospheric ^{14}C value at past dates ($a^{14}C_{atmosphere}$), and the closest individual IntCal13 dates and fraction modern (FM) values for the atmosphere were used with the exception of dates beyond 13,900 yrs BP, which were interpolated to create a consistent 5 year spacing. All correlation coefficients (R^2) and p-values reported for time series data were calculated using the method and code of Macias-Fauria et al.

(2012), which consider the possible effects of autocorrelation of time series data for the Pearson correlation coefficient.

3.4 Results

AMS results of TM-17 samples show $^{14}C_{age}$ offsets from IntCal13 ($^{14}C_{atmosphere}$) of 2,274 – 7,497 years (mean value of 4,918 years), and comparison to U-Th dates, depths, and the TM-17 age model is in **Table 3.1**. The maximum reservoir age (7,497 years) occurred at ~17 kyr BP and the minimum reservoir age (2,274 years) occurred at ~35 kyr BP (**Fig. 3.1**). The reservoir age is consistently several thousand years and frequently stays close to the average value, but anomalous fluctuations are seen in specific periods. The largest reservoir age is accompanied by other high values and large variations between ~14-18 kyr BP, and the largest single-point excursion occurs before and after 8,208 yrs BP (2,774 years differenced from prior point; 1,232 years differenced from following point), although the sampling is not evenly spaced throughout the time series. DCP in TM-17, calculated using **eq. 1**, ranges from 25.0 to 60.6% (**Table 3.1**), with an average value of 45.4 ± 7.2%. The lowest DCP is in the oldest section of the stalagmite, and DCP increases to around the average value of 45.4% by ~30,000 yrs BP. The largest point to point fluctuation is 18.4% over a period of 283 years that corresponds with the highest reservoir age shift (from 8,491 to 8,208 yrs BP).

Results for all TM monitoring samples are presented in **Table 3.2**. Soil gas samples, consisting of 19 samples over two field expeditions, returned an average FM value of 1.03 +/- 0.002. This includes duplicate analyses of two soil well sites using different methods of extraction in the

field (evacuated vials and steel traps), which returned results that display FM differences of 0.009 and 0.021. pCO_2 in soil gas wells displays a linear increase with depth (**Fig. S3.1**),

Table 3.1 - DCP calculation results and TM-17 age model

U-Th ID	14C Sample ID	U-Th age (yrs BP)	TM-17 age model (yrs BP)	(+/-) 2 sigma (yrs BP)	Depth (cm)	Closest age model depth (cm)	Fraction modern (FM)	14C age (BP)	(+/-)	IntCal (yrs BP)	IntCal D14C (per mil)	14C age offset (reservoir age) (yrs)	DCP
TM17_U1	TM17-14C-2	229	229	19	0.27		0.55	4,800	25	230	14.9	4,695	44.3
	TM17-14C-9		680	63	1.04	1.03	0.58	4,445	25	680	-11.20	3,694	36.9
	TM17-14C-13		960	86	1.53	1.53	0.54	4,900	20	960	-15.50	3,842	38.0
	TM17-14C-18		1,199	97	1.99	1.98	0.48	5,900	25	1,200	-14.40	4,617	43.7
TM17-U3	TM17-14C-26	1,560	1,560	47	2.71		0.50	5,610	25	1,560	-19.10	3,939	38.8
	TM17-14C-32		1,862	91	3.41	3.43	0.43	6,760	30	1,860	-10.20	4,870	45.5
	TM17-14C-37		2,075	121	3.96	3.98	0.44	6,535	30	2,075	-11.70	4,424	42.3
	TM17-14C-42		2,259	154	4.42	4.43	0.41	7,180	30	2,260	-0.20	4,982	46.2
TM17-U4	TM17-14C-46	2,403	2,403	85	4.74		0.45	6,350	30	2,400	-10.40	3,934	38.7
TM17_U5	TM17-14C-65	3,417	3,417	28	6.48		0.41	7,130	30	3,420	14.10	3,919	38.6
	TM17-14C-2-76		4,055	80	8	8.03	0.44	6,595	20	4,055	33.50	2,919	30.5
TM17-U6	TM17-14C-88	4,377	4,377	52	8.83		0.36	8,095	35	4,380	47.20	4,209	40.8
TM17-U7	TM17-14C-115	5,572	5,572	40	11.5		0.30	9,670	45	5,570	88.60	4,939	45.9
	TM17-14C-2-128		6,315	481	12.91	12.93	0.30	9,750	25	6,315	74.40	4,190	40.6
TM17_U8	TM17-14C-141	6,917	6,917	419	14.21		0.26	10,960	60	6,920	86.20	4,900	45.7
	TM17-14C-2-156		7,360	336	15.85	15.88	0.24	11,485	25	7,360	94.70	5,060	46.7
TM17-U9	TM17-14C-170	7,696	7,696	56	17.04		0.21	12,610	70	7,695	75.20	5,715	50.9
	TM17-14C-176		7,951	120	17.7	17.73	0.22	12,090	70	7,950	79.20	4,977	46.2
	TM17-14C-183		8,208	109	18.3	18.33	0.25	11,160	60	8,200	71.30	3,745	37.2
	TM17-14C-189		8,491	104	18.95	18.98	0.17	14,240	90	8,490	68.10	6,519	55.6
TM17-U10	TM17-14C-196	8,754	8,754	58	19.65		0.17	14,150	90	8,755	73.90	6,215	53.9
	TM17-14C-2-212		9,288	77	21.46	21.48	0.17	14,110	30	9,290	96.80	5,825	51.6
TM17_U11	TM17-14C-228	9,699	9,699	43	22.84		0.16	14,870	90	9,700	87.90	6,121	53.4
	TM17-14C-2-246		10,434	130	24.7	24.73	0.16	14,545	35	10,435	116.10	5,287	48.2
TM17-U12	TM17-14C-263	11,191	11,191	106	26.39		0.16	14,620	90	11,190	153.00	4,890	45.6
	TM17-14C-270		11,533	180	27.08	27.08	0.14	15,770	140	11,535	158.40	5,742	51.1
	TM17-14C-276		11,804	146	27.57	27.58	0.16	14,840	90	11,805	179.10	4,692	44.3
	TM17-14C-282		12,142	134	28.16	28.18	0.15	15,290	100	12,140	196.30	4,933	45.8
TM17-U13	TM17-14C-289	12,540	12,540	75	28.88		0.14	15,940	110	12,540	228.60	5,408	49.0
	TM17-14C-2-299		13,578	134	30.6	30.63	0.12	17,070	60	13,580	190.60	5,275	48.2
TM17-U14	TM17-14C-312	13,812	13,812	72	31.06		0.11	17,850	150	13,810	190.50	5,831	51.6
	TM17-14C-320		14,274	122	32.01	32.03	0.10	18,170	150	14,270	206.30	5,810	51.5
	TM17-14C-329		14,651	167	32.85	32.88	0.11	17,390	130	14,650	249.60	4,944	46.0
TM17_U15	TM17-14C-337	14,936	14,936	99	33.51		0.10	18,190	150	14,940	275.80	5,629	50.4
	TM17-14C-347		15,374	166	34.54	34.53	0.10	18,320	150	15,370	285.70	5,403	49.0
	TM17-14C-355		15,932	211	35.74	35.73	0.10	18,260	150	15,930	320.30	5,012	46.4
TM17-U16	TM17-14C-363	16,164	16,164	122	36.13		0.08	20,260	190	16,160	328.10	6,836	57.3
	TM17-14C-373		16,983	202	37.23	37.23	0.07	21,470	220	16,980	369.70	7,497	60.6
	TM17-14C-381		17,765	148	38.08	38.08	0.07	20,890	210	17,770	397.40	6,310	54.5
TM17-U17	TM17-14C-390	18,553	18,553	78	38.91		0.09	19,780	180	18,550	410.30	4,516	43.0
	TM17-14C-2-401		19,788	209	40.23	40.23	0.07	21,800	70	19,790	422.50	5,400	49.0
TM17-U18	TM17-14C-415	20,942	20,942	168	41.36		0.06	23,180	280	20,940	450.10	5,817	51.5
	TM17-14C-2-431		23,205	189	43.22	43.23	0.05	23,970	130	23,210	502.10	4,684	44.2
TM17-U19	TM17-14C-442	24,170	24,170	91	44.1		0.04	26,550	430	24,170	522.60	6,440	55.1
TM17_U20	TM17-14C-468	26,304	26,304	197	46.69		0.03	27,190	460	26,480	541.80	4,936	47.1
	TM17-14C-2-480		27,455	324	47.97	47.98	0.04	26,410	170	27,460	546.80	3,230	33.1
TM17-U21	TM17-14C-496	28,666	28,666	198	49.46		0.03	29,220	600	28,660	497.40	4,613	43.6
TM17-U22	TM17-14C-517	29,815	29,815	131	51.55		0.02	30,710	720	29,820	500.00	4,990	46.3
	TM17-14C-2-524		30,224	244	52.21	52.23	0.02	30,980	220	30,220	539.30	5,079	46.8
TM17-U23	TM17-14C-539	31,959	31,959	105	54.19		0.02	31,430	790	31,960	420.40	3,192	32.8
TM17-U24	TM17-14C-544	33,430	33,430	107	55.84		0.02	31,950	850	33,440	518.40	2,810	29.6
TM17-U25	TM17-14C-561	35,055	35,055	162	57.64		0.02	33,500	1,000	35,060	424.70	2,274	25.0
											Average:	**4,918**	**45.4**

although the maximum depth's pCO_2 measurement saturated the instrument (70 cm depth, pCO_2 >20,000 ppm). No relationship is seen between soil gas FM and depth up to 70 cm, and all samples showed FM results that indicate a modern age (FM >1.00; **Table 3.2**). Outside air above the cave site averaged 1.02 +/- 0.002 FM, and cave air averaged 1.00 +/- 0.002 FM, although cave air varied some by year, with 2015 averaging 1.01 FM and 2017 averaging 0.99 FM. DIC drip water samples showed a large range of 0.82 to 1.01 FM (average value 0.96 +/- 0.001 FM). Glass plate calcite, with 0.99 +/- 0.002 FM, had two corresponding drip water DIC measurements (site D10) of 1.00 FM +/- 0.0015 (**Table 3.2**).

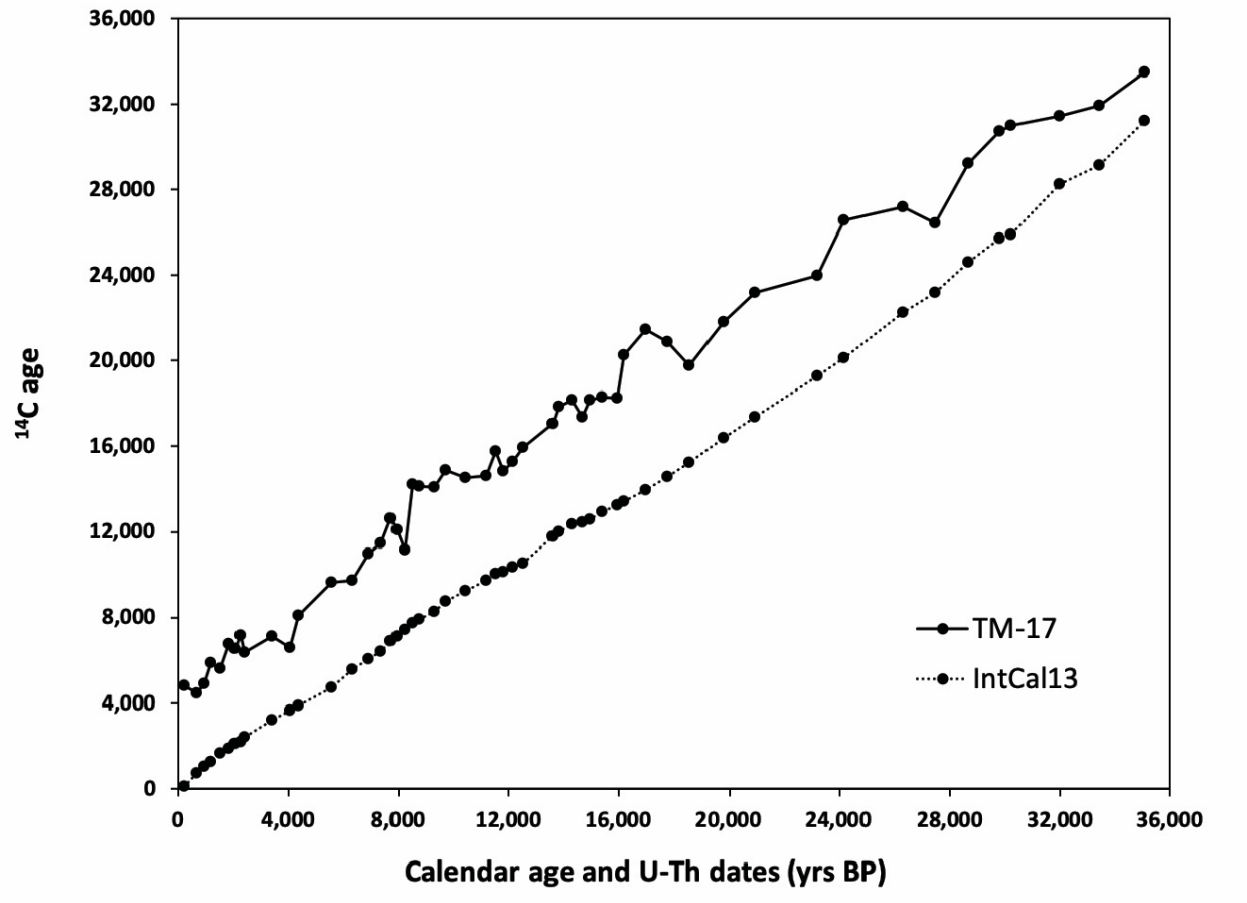

Figure 3.1* – *Reservoir effect in TM-17*. IntCal13 (Reimer et al., 2013) calendar age (x-axis) vs. ^{14}C age (y-axis). TM-17 represents U-Th and TM-17 age model dates (x-axis) vs. ^{14}C age of speleothem carbon (y-axis).*

Bedrock from TM returned an average $\delta^{13}C$ of 4.22‰ V-PDB (+/- 0.07‰ error based on the standard deviation of $\delta^{13}C$ standards during the analysis; n = 8), although there was heterogeneity between samples, creating a standard deviation of 1.28‰. Samples taken inside the cave may represent different periods of mineral deposition and bedrock that potentially did not influence drip waters entering the cave. If samples only from outside of the cave are averaged (n = 5), $\delta^{13}C$ shifts to 4.79‰ V-PDB with a standard deviation of 0.35‰, and this value is used for bedrock $\delta^{13}C$ in this study. This bedrock value ($\delta^{13}C_{BR}$) is within the expected range for carbonates deposited in the Carboniferous and Permian periods, which is the estimated age of TM bedrock (Saltzman & Thomas, 2012; Wood et al., in prep., a).

Soil samples taken at 0-10, 10-20, and 20-30 cm depth above the cave were analyzed for bulk SOM ^{14}C, and results are presented in **Table 3.2**. Up to 20 cm, the soil shows bomb-influenced carbon (FM >1.00) and indicates the near-surface soil contains mostly modern carbon. At 20-30 cm depth, FM <1.00, showing the presence of aged organic matter (OM).

TM drip water [SO_4^{2-}] varied from 2.05 to 5.69 ppm (n = 21) with the exception of two outliers. Two samples elevated in [SO_4^{2-}] included the drip collected closest to the TM-17 sample collection site (38.93 ppm) and one drip site closer to the entrance of the cave (42.64 ppm). These two samples required an extra dilution step (500x) compared to the rest of the samples (50x) to bring them under saturated readings in the instrument.

Table 3.2 - Tham Doun Mai monitoring data: carbon isotopes

Lab ID	Collection year	Sample type	$\delta^{13}C$ (‰)	±	Fraction Modern	±	$\Delta^{14}C$ (‰)	±	^{14}C age (BP)	±
TMOA1_Trap	2015	Outside air - trap	-9.4	0.15	1.0179	0.0020	10.0	2.0	Modern	
TM2017-OA-1	2017	Outside air - trap	-14.6	0.15	1.0177	0.0019	9.5	1.9	Modern	
TM2017-OA-2	2017	Outside air - trap			1.0138	0.0017	5.7	1.7	Modern	
TMCA1_Trap	2015	Cave air - trap	-15.3	0.15	1.0097	0.0017	1.8	1.7	Modern	
TMCA2_Trap	2015	Cave air - trap	-14.3	0.15	1.0162	0.0018	8.2	1.8	Modern	
TM2017-CA-1	2017	Cave air - trap	-16.0	0.15	0.9901	0.0016	-17.9	1.6	80	15
TM2017-CA-2	2017	Cave air - trap	-15.1	0.15	0.9920	0.0015	-16.0	1.5	65	15
TDM-S1	2015	Soil (0-10 cm depth)	-28.8	0.15	1.0616	0.0016	52.8	1.6	Modern	
TDM-S2	2015	Soil (10-20 cm depth)	-26.7	0.15	1.0611	0.0016	52.3	1.6	Modern	
TDM-S3	2015	Soil (20-30 cm depth)	-26.1	0.15	0.9872	0.0015	-21.0	1.5	105	15
TMSG4_Air	2015	Soil gas - evacuated vial	-25.7	0.15	1.0383	0.0017	30.1	1.7	Modern	
TMSG5_Air	2015	Soil gas - evacuated vial			1.0234	0.0017	15.3	1.7	Modern	
TMSG6_Air	2015	Soil gas - evacuated vial	-25.3	0.15	1.0300	0.0020	21.9	2.0	Modern	
TMSG7_Air	2015	Soil gas - evacuated vial	-24.5	0.15	1.0396	0.0016	31.5	1.6	Modern	
TMSG8_Air	2015	Soil gas - evacuated vial			1.0228	0.0017	14.7	1.7	Modern	
TMSG1_Trap	2015	Soil gas - trap			1.0027	0.0022	-5.1	2.2	Modern	
TMSG2_Trap	2015	Soil gas - trap			1.0323	0.0019	24.2	1.9	Modern	
TMSG3_Trap	2015	Soil gas - trap	-21.4	0.15	1.0371	0.0018	29.0	1.8	Modern	
TMSG5_Trap	2015	Soil gas - trap	-20.2	0.15	1.0441	0.0018	35.9	1.8	Modern	
TMSG8_Trap	2015	Soil gas - trap	-19.7	0.15	1.0320	0.0018	23.9	1.8	Modern	
TM2017-SG-01	2017	Soil gas - evacuated vial			1.0345	0.0016	26.1	1.6	Modern	
TM2017-SG-02	2017	Soil gas - evacuated vial			1.0218	0.0024	13.6	2.4	Modern	
TM2017-SG-03	2017	Soil gas - evacuated vial			1.0299	0.0023	21.6	2.3	Modern	
TM2017-SG-04	2017	Soil gas - evacuated vial			1.0231	0.0039	14.8	3.9	Modern	
TM2017-SG-05	2017	Soil gas - evacuated vial			1.0187	0.0016	10.5	1.6	Modern	
TM2017-SG-06	2017	Soil gas - evacuated vial			1.0247	0.0022	16.5	2.2	Modern	
TM2017-SG-10	2017	Soil gas - evacuated vial			1.0285	0.0019	20.2	1.9	Modern	
TM2017-SG-11	2017	Soil gas - evacuated vial	-25.7	0.15	1.0135	0.0016	5.3	1.6	Modern	
TM2017-SG-12	2017	Soil gas - evacuated vial			1.0314	0.0020	23.0	2.0	Modern	
TM-D1-3c_DIC	2015	Drip water DIC	-13.2	0.15	0.8178	0.0012	-188.6	1.2	1615	15
TM-D4c_DIC	2015	Drip water DIC	-9.4	0.15	0.9817	0.0014	-26.0	1.4	150	15
TM-D6-7a_DIC	2015	Drip water DIC	-14.9	0.15	1.0137	0.0016	5.8	1.6	Modern	
TM-D10_DIC	2015	Drip water DIC	-12.9	0.15	1.0008	0.0015	-7.0	1.5	0	15
TM-D1-3d_DIC	2015	Drip water DIC	-16.1	0.15	1.0020	0.0015	-5.8	1.5	Modern	
TM-D6-7b_DIC	2015	Drip water DIC	-14.7	0.15	1.0047	0.0019	-3.1	1.9	Modern	
DIC_TM-D10	2017	Drip water DIC	-15.4	0.1	0.9962	0.0015	-11.9	1.5	30	15
DIC_TM-6-7	2017	Drip water DIC	-15.6	0.1	1.0021	0.0015	-6.0	1.5	Modern	
DIC_TM-4e	2017	Drip water DIC	-15.5	0.1	0.9440	0.0016	-63.7	1.6	465	15
DIC_TM-D4a	2017	Drip water DIC	-9.0	0.1	0.9715	0.0014	-36.4	1.4	235	15
DIC_TM-D4d	2017	Drip water DIC	-12.0	0.1	0.8260	0.0013	-180.7	1.3	1535	15
DIC_TM-D4b	2017	Drip water DIC	-11.0	0.1	0.9511	0.0013	-56.5	1.3	400	15
DIC_TM-D4c	2017	Drip water DIC	-11.1	0.1	0.9473	0.0014	-60.3	1.4	435	15
TMGP-14C-1	2015	Glass plate calcite			0.9925	0.0019	-7.5	1.9	60	20

3.5 Discussion

3.5.1 The source of dead carbon in TM-17

Monitoring samples in and above TM provide data for the examination of local ^{14}C dynamics. Atmospheric air samples taken in 2015 and 2017 (n = 3) averaged 1.02 +/- 0.002 FM, while cave air samples were older, averaging 1.00 +/- 0.011 FM (**Table 3.2**). This offset may reflect the contributions of older CO_2 sourced from the soil zone, bedrock dissolution, and/or deep aged organic matter (Noronha et al., 2015) that enters the cave through fractures and/or via degassing of bedrock-derived C from cave drip waters. DIC samples of TM drip water sites showed high variability, from modern to 1,615 years old (**Table 3.2**), likely driven by site-specific controls on the degree of closed vs. open system dissolution, such as bedrock thickness, fracture vs. matrix flow, intermediate storage pools, and/or other sources of variability. DIC from site D10 averaged 1.00 +/- 0.003 FM (n = 2, samples 2 years apart), and modern calcite from the same drip (n = 1) resulted in 0.99 +/- 0.002 FM, closer to the D10 DIC measurement from the collection year as opposed to the year the glass plate was set (**Table 3.2**). These results suggest the FM of calcite precipitated in the cave is similar to the value of drip water DIC, so we assume FM values of calcite in TM-17 are controlled by the value of drip water at time of formation. No DIC measurement was possible for the TM-17 source drip, as it was a fossil stalagmite, or from drip D17, the closest modern drip (Wood et al., in prep., a), as the drip rate was too slow for the required volume.

As the drip water is the main source of aged or dead carbon for the speleothem, we must examine the potential source(s) of dead carbon to the drip water. In addition to the ancient bedrock in and above a cave environment that is typically "dead," (DCP = 100%), the

contributions of aged SOM (or deeper aged OM in the epikarst) can have significant yet variable effects on aged carbon input. Estimates from speleothem samples and models have shown SOM-sourced effects to be relatively small compared to the bedrock input, with SOM often only altering the DCP by around 1% (Fohlmeister et al., 2011; Genty & Massault, 1999a). A dominant bedrock contribution often leads to an interpretation of DCP being responsive to the amount of precipitation, infiltration, and/or soil moisture, which affect the degree of open vs. closed system dissolution, with relatively small changes in DCP due to SOM turnover rates (Griffiths et al., 2012; Noronha et al., 2014). However, Oster et al. (2010) interpreted DCP changes as a response to similar mechanisms that specifically affected the SOM turnover time, varying DCP by up to 14.08% over a few thousand years. While both mechanisms move DCP in the same direction, changes in climate can alter the bedrock contribution and/or SOM turnover rate, and these competing effects vary by sample and site, as seen in Rudzka et al. (2011).

The atypically high DCP in TM-17 (25.0-60.6%; **Table 3.1**) is a strong indication of bedrock dissolution contributing heavily to the speleothem carbon, as there are no known observations of karst SOM or deeper vadose OM being old enough or contributing large enough amounts of carbon to increase DCP to these levels. The soil zone above TM is rocky, yet observed soil depths, while not frequently greater than 30 cm, sometimes reach 60-70 cm, so an undeveloped, thin, and rocky alpine setting cannot be blamed for a lack of SOM involvement for DCP in TM-17, as in other studies with similarly high DCP (Bajo et al., 2017; Spötl et al., 2016). Additionally, the abundance of tropical vegetation and forest cover indicates a strong possibility for respiration and organic input to the drip water carbon pool. Some studies with estimates of SOM ages up to several centuries old still considered bedrock dissolution to be the dominant

control on DCP (Griffiths et al., 2012; Noronha et al., 2014), and the ~1% change in DCP modeled in Fohlmeister et al. (2011) was calculated with SOM up to 1,000 years old. However, as tropical sites may have an SOM component aged over 6,000 years contributing to the carbon pool (Trumbore, 2000), and considering the previously mentioned studies attributing a larger proportion of changes to DCP via SOM or changing ecology, the potential soil zone contributions cannot always be assumed to be minimal. Additionally, the oxidation of aged OM below the soil zone could also lead to increased DCP, and ancient OM in the vadose zone between the soil and the cave could drive significant variation in sources and ages of carbon (Bergel et al., 2017; Breecker et al., 2012; Noronha et al., 2014). Therefore, as SOM contributions could be significant, the potential effects of SOM to the DCP signal in TM-17 must be estimated in order to assess the extent of bedrock control.

To estimate the age spectrum of SOM in a specific cave, many speleothem studies have used the ^{14}C bomb peak to analyze the response of speleothem DCP to the ^{14}C injected into the atmosphere during nuclear tests in the mid-20th century (Fohlmeister et al., 2011; Genty & Massault, 1999a; Lechleitner et al., 2016b). The amplitude and time lag in the response of the stalagmite ^{14}C is compared to the atmospheric history, and this data is used to estimate the SOM age spectrum, often divided into three age pools with varying contributions. Genty & Massault (1999a) used the idea of total, or apparent, DCP to separate the contributions of SOM and bedrock (equation adapted here):

$$DCP_{APP} = DCP_{BR} + DCP_{SOM} \qquad in\ pMC \qquad \textbf{eq. 3}$$

where DCP_{APP} represents the total measured DCP, and DCP_{BR} is the contribution solely from bedrock, and all are expressed in percent modern carbon (pMC). The SOM contribution (DCP_{SOM}) at any time (t) can be broken down further into respective reservoirs of varying age ($n_{1,2,3}$) and relative contributions ($c_1 + c_2 + c_3 = 1$), which in the case of three reservoirs gives the equation:

$$pMC_{SOM(t)} = c_1 * pMC_{n1} + c_2 * pMC_{n2} + c_3 * pMC_{n3} \qquad \textit{eq. 4}$$

where pMC_{ni} represents the pMC of the SOM pool at the time of inclusion in the speleothem calcite and must be corrected for decay that has occurred since deposition in the soil zone.

As TM-17 was a fossil stalagmite when collected (youngest age model date = 76.4 yrs BP; Johnson et al., in revision), potential SOM age spectrum effects must be estimated in the absence of bomb peak data. Soil results (**Table 3.2**) show that near-surface soils above TM are modern and that the age could increase up to a maximum of ~250 years by 30 cm depth. No data is available from deeper epikarst areas between the soil and cave, and it is possible that much older OM resides in these areas and is available for microbial respiration and incorporation into the drip water and stalagmite carbon pools. Given the lack of observational data for the subsoil zone, SOM spectrums observed in other tropical sites were used to calculate the DCP_{SOM} under two scenarios: an SOM pool with a dominant centennial reservoir and an SOM pool with some contributions from a millennial reservoir. For the centennial reservoir, the SOM age spectrum is based loosely on the age spectrum found in Griffiths et al. (2012), and the modeled SOM consists of 5% with a 1 year turnover rate (assumed to be equal to atmospheric ^{14}C activity at the time of deposition), 15% at a 15 year turnover rate, and 80% at a 300 year turnover rate. For the

millennial pool, the spectrum was loosely based on tropical soil results from Trumbore (2000), with 20% at a 1 year turnover rate, 60% at a 100 year turnover rate, and 20% at a 6,000 year turnover rate. The Trumbore (2000) estimate is not based on a speleothem study or karst region, but the influence of a millennially aged SOM spectrum was chosen to represent a more ancient, yet possible, SOM age spectrum for a tropical site. In this regard, it may also compensate for the possibility of contributions from aged OM below the soil zone.

To estimate the pMC at the time of speleothem formation for each turnover rate (n) of SOM ($pMC_{SOM(n)}$), decay in each contributing reservoir was accounted for at each TM-17 ^{14}C measurement's age (*t*; **Table 3.1**) using the following equation:

$$pMC_{SOM(n)} = \frac{pMC_{atm(t)} + \sum_{i=1}^{\frac{n}{5}} pMC_{atm(t+5i)} * e^{(-\lambda * 5i)}}{\left(\frac{n}{5}\right)+1} \qquad \textbf{\textit{eq. 5}}$$

where λ is the ^{14}C decay constant (ln(2)/5,730), and $pMC_{atm(t)}$ is the $\Delta^{14}C$ value of the atmosphere from IntCal13 (Reimer et al., 2013) converted to pMC. The IntCal13 data set was interpolated beyond 13,900 yrs BP to achieve a 5-year resolution at all time periods, as the Reimer et al. (2013) data set switches to 10-year resolution at 13,900 yrs BP and to 20-year resolution at 24,990 yrs BP. The *n/5* values in ***eq. 5*** account for the 5-year spacing of the interpolated IntCal13 data. As each total turnaround time (n) would potentially involve SOM of all ages up to the total turnaround time, the amount of decay is calculated for every successive age of the SOM pool (*t* + *5i*), starting at the time of speleothem deposition (t) up to the total age of the SOM pool (n). The $pMC_{SOM(n)}$ is then calculated by taking the average value of all states of decay, including the undecayed $pMC_{atm(t)}$ value. For example, with an SOM turnaround time

of 100 years, n = 100, n/5 = 20, and [(n/5)+1] = 21, and ***eq. 5*** returns the value of $pMC_{SOM(100)}$. This is repeated for each age of the three contributing pools of SOM, and then each pMC value and its corresponding contribution (%) is used in ***eq. 4*** to return the estimated average pMC_{SOM} at time *t*.

The resulting $pMC_{SOM(t)}$ is then used to estimate the bedrock contribution to the speleothem by utilizing ***eq.s 3*** and ***4*** to build a two-component mixing model:

$$pMC_{speleothem(t)} = pMC_{SOM(t)} * (1 - DCP_{BR}) + pMC_{BR(t)} * DCP_{BR} \qquad \textit{eq. 6}$$

where $pMC_{speleothem(t)}$ is the result of the TM-17 measurement at time *t*, DCP_{BR} is the unknown contribution of bedrock-sourced carbon, and pMC_{BR} is always equal to 0 pMC (100% DCP). The results of the mixing model show that with a centennial SOM pool, DCP_{BR} is always within 1% of DCP_{APP}, and the millennial pool shifts the DCP_{BR} up to 5% at maximum (**Table S3.1**). With the high DCP_{APP} measured in TM-17, the millennial SOM pool shifts of up to several percent still maintain a majority DCP_{BR} input to DCP_{APP} while maintaining general magnitude and relative shifts throughout the time series.

The DCP_{BR} calculated using **eq. 5**, with inputs into the carbon pool from all SOM ages, is interpreted as a conservatively large estimation of potential SOM effects, as it involves equal inputs from heavily aged SOM that was resistant to decomposition up to that point. Alternatively, once $pMC_{SOM(t)}$ has been calculated (**eq. 4**), the DCP_{SOM} can also be estimated using a simpler method using the following equation adapted from Genty and Massault (1999a):

$$DCP_{SOM} = pMC_{atm(t)} - pMC_{SOM(t)} \qquad \textit{eq. 7}$$

Using **eq. 7** for DCP_{SOM} returns values of DCP_{BR} (**eq. 3**) similar to the previous method for the centennial pool with the average difference between estimates of DCP_{BR} equal to 0.31%; for the millennial pool, the difference between methods increases to an average of ~4.08% over the full time series (**Table S3.1; Fig. S3.2**). The differences between methods increase with age (**Fig. S3.3**), especially with the millennial SOM pool, suggesting **eq. 5** from this study may lead to a more accurate estimate of DCP_{BR} for older time periods, as we assume this is a conservatively large estimate and **eq. 7** returns even larger values (**Table S3.1**).

In summary, bedrock is the dominant source of dead carbon in TM-17, and even applying a large estimate for SOM (or OM) involvement involving carbon aged up to 6,000 years only shifts the DCP by a few percent at maximum (**Table S3.1**). These methods of estimating the DCP_{BR} contribution assume that the SOM age spectrum does not change over time, which is unlikely, given the dramatic climate changes over the late Pleistocene and Holocene. However, given the relatively small changes in total DCP due to SOM involvement (**Figs. 3.2, S3.2**), we focus on the dominant bedrock source of DCP and corresponding interpretations of DCP variability for this study.

3.5.2 Elevated DCP in TM-17

Recent studies involving speleothems with high DCP (in excess of 50%) have examined evidence for disseminated pyrite oxidation (or other sulfide mineral) driving enhanced carbonate dissolution via the addition of SAD to the typical CAD system. Spötl et al. (2016) recorded a

DCP of up to 67% in an aragonitic stalactite from Austria, and reservoir ages from the cave varied from 8,800 to 10,100 years. This study pointed to a thin, undeveloped, and often snow-covered soil zone; the presence of fine, crystalline disseminated pyrite common in Paleozoic limestone; and high values of sulfate in drip waters as evidence for the presence of SAD. In another alpine European cave, Bajo et al. (2017) reported high DCP (44.8 – 68.8%) with large variability in a calcite stalagmite. This study attributed the DCP levels to a combination of SAD and CAD, a nearly closed-system dissolution system highly sensitive to small changes, and a small contribution from aged OM below the soil zone. Both studies provide observational evidence and/or modeling to theorize a contribution of SAD in order to surpass the theoretical CAD limit of 50% DCP originally proposed by Hendy (1971). The DCP in TM-17 (mean 45.4%; max. 60.6%) is similar to the levels seen in these studies, suggesting similar controls could be active.

SO_4^{2-} measurements in TM drip waters provide potential observational evidence for the presence of SAD. Spötl et al. (2016) reported [SO_4^{2-}] of 232 mg/l in cave drip waters as evidence for pyrite (sulfide) oxidation. In Bajo et al. (2017), [SO_4^{2-}] in drip waters near the high-DCP stalagmite were elevated above rainfall and other cave drip waters, and SAD was determined to play a prominent role in the dissolution system after examining possible external sources of SO_4^{2-}. The values for drip water [SO_4^{2-}] referenced in Bajo et al. (2017) are around 34 mg/l (CNR2) and 5.6 mg/l (CNR1) (Piccini et al., 2008), the first of which is comparable to the value of 38.9 mg/l measured in TM closest to the TM-17 sample (drip D17). One other drip site in TM was in this range (42.6 mg/l), while all other tested drips (n = 21) ranged from 2.05 – 5.69 mg/l, suggesting the action of SAD in TM may be limited to, or enhanced at, certain drip sites, and that

the modern drip closest to the TM-17 stalagmite is one of these sites. Additionally, in the model created for a closed system interaction of CAD, SAD, and [SO_4^{2-}] levels (**Fig. 3** in Bajo et al., 2017), the D17 drip measurement of 38.9 mg/l (~0.41 mmol/l) would give a rough estimate of ~60% CAD, ~40% SAD, and a DCP of ~60-65%. This estimate is similar to the maximum DCP of 60.6% recorded in TM-17, providing evidence that SAD in a nearly closed dissolution system was an active influence on dissolution and the large DCP in our sample.

3.5.3 Assessing $\delta^{13}C$ controls via DCP data

In addition to elevated DCP, more positive $\delta^{13}C$ in a speleothem may also indicate a contribution of bedrock dissolution-sourced carbon (Genty et al., 2001). While TM-17 $\delta^{13}C$ values never approach the measured value of TM bedrock samples (4.79‰ V-PDB), they are elevated in sections of the record to anomalously positive values, such as -0.78‰ during HS1 compared to the record's average value of -4.95‰ V-PDB (**Fig. 3.2**). Although the difference in resolution is significant ($\delta^{13}C$ = 1,213 data points vs. DCP = 52 data points over the full TM-17 record), the positive correlation of TM-17 DCP and $\delta^{13}C$ ($R^2 = 0.36$, $p = 0.01$) is evidence that both proxies may have been influenced by a similar control over much of the time series. A dissolution-based control would increase bedrock input when dissolution is intensified, increasing $\delta^{13}C$ and DCP toward the bedrock values of (+) 4.79‰ V-PDB and 100.0%, respectively. However, there are other controls that are known to influence speleothem $\delta^{13}C$ that must be addressed (Johnson et al., in revision; Wood et al., in prep., a).

In addition to the dissolution control, in and above-cave fractionation effects may have also altered TM-17 $\delta^{13}C$. Prior calcite precipitation (PCP), one source of such fractionation, is a

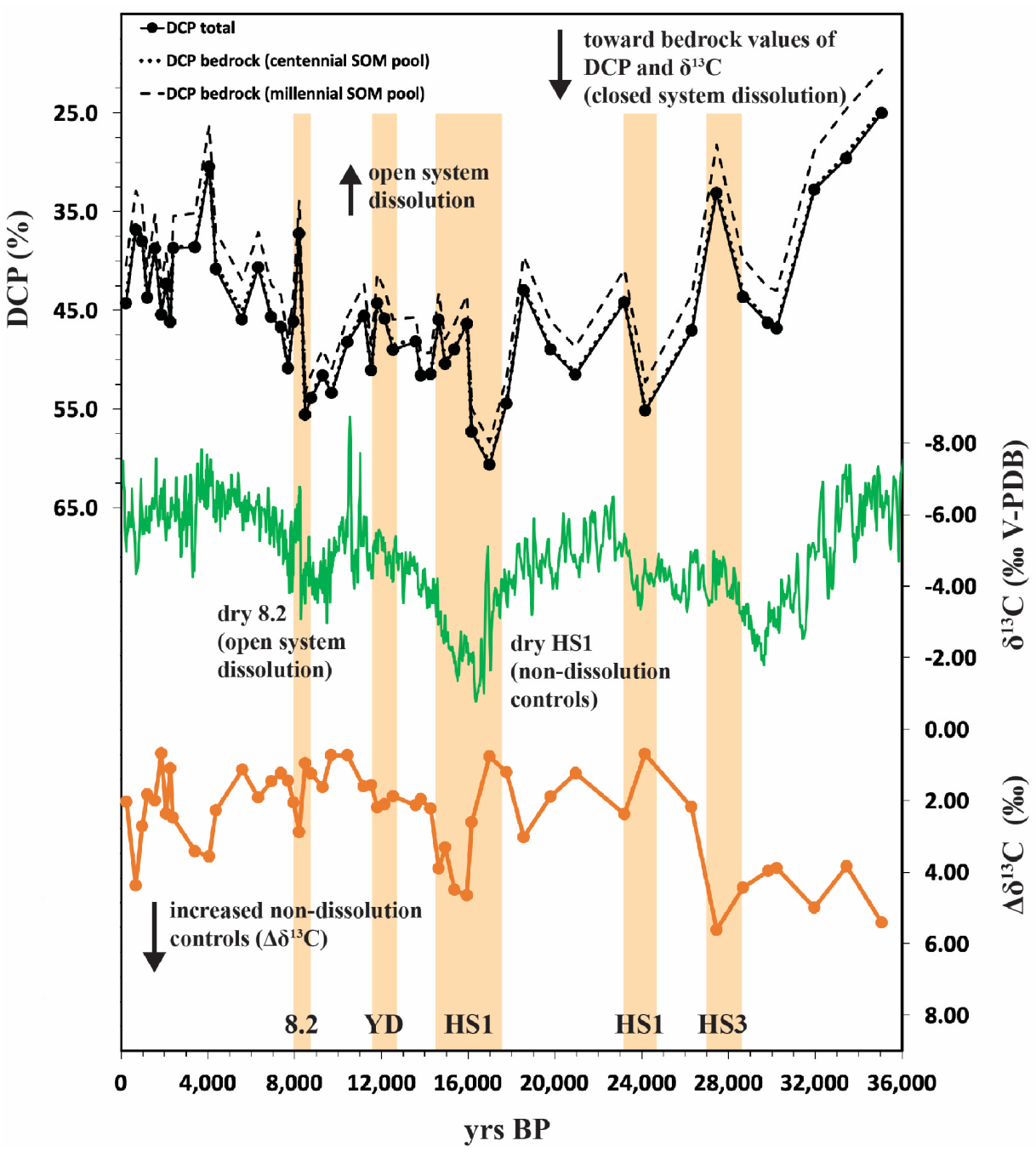

Figure 3.2 – DCP, $\delta^{13}C$, and $\Delta\delta^{13}C$ comparison *– TM-17 DCP, $\delta^{13}C$, and $\Delta\delta^{13}C$ plotted over 36,000 yrs BP to highlight contrasting carbon controls during climate events (see text for details). DCP plotted as DCP total and DCP attributed to bedrock dissolution (DCP bedrock) when adjusted for estimated centennial or millennial SOM pools are calculated. Event labels represent the 8.2 kyr event (8.2), Younger Dryas (YD), and Heinrich Stadials (HS1, HS2, HS3). $\delta^{13}C$ data from Johnson et al. (in review).*

potentially significant control on speleothem $\delta^{13}C$ (Baker et al., 1997; Fairchild et al., 2006; Johnson et al., 2006; Tremaine & Froelich, 2013). PCP has been shown to influence trace elements and influence $\delta^{13}C$ in TM-17, although these proxies do not always respond similarly (Wood et al., in prep., a), indicating additional evidence for multiple active controls on $\delta^{13}C$. Additional fractionation may also occur in the cave due to CO_2 degassing and equilibration with cave air before or during calcite precipitation on the stalagmite, which would move $\delta^{13}C$ in the same direction as PCP and also be prevalent during dry periods (Frisia et al., 2011; Mühlinghaus et al., 2007). Surface and soil-zone changes involving vegetation and/or soil respiration in the local climate and ecosystem can also affect $\delta^{13}C$ values in speleothem calcite. For example, a drier and/or hotter climate with reduced soil moisture could increase the $\delta^{13}C$ value in plants by decreasing the C3:C4 plant ratio and/or decreasing soil respiration, which would allow a greater contribution from atmospheric carbon into the drip water (Dorale, 1998; Genty et al., 2001; Partin et al., 2013; Wong & Breecker, 2015). Temperature and humidity changes could also affect the turnover rate of SOM below ground, although the effects of aged SOM appear to be relatively insignificant in TM-17 (**Fig. 3.2, Table S3.1**). In previous climates and on longer timescales, the controls mentioned above are difficult to distinguish from fractionation effects such as PCP. Therefore, we refer to the combination of all of these influences on $\delta^{13}C$ as *non-dissolution controls* for our purposes. Johnson et al. (in revision) interpret TM-17 as reflecting the local water balance, and it is important to note that the combination of all non-dissolution controls move $\delta^{13}C$ towards more positive values during dry periods (e.g. Johnson et al., in revision; Wong & Breecker, 2015).

Assuming some bedrock dissolution control on TM-17 $\delta^{13}C$, potential conflicting responses to similar environmental changes become apparent. Open system dissolution would result in less bedrock input, lower DCP, and $\delta^{13}C$ values becoming more negative if controlled by dissolution, reflecting more input from CO_2 sources of carbon in the soil zone, where $\delta^{13}C$ is strongly negative (generally -21 to -25‰ if C3 plants are dominant) due to biogenic processes (e.g. Fohlmeister et al. 2011). However, the same open system dissolution, indicative of lowered infiltration, would also favor PCP, which can move $\delta^{13}C$ of the speleothem in the opposite direction, as $\delta^{13}C$ increases in the drip water remaining after calcite precipitation (e.g. Baker et al., 1997). In an attempt to separate the potential effects of dissolution and non-dissolution controls on $\delta^{13}C$ in our record, we apply two techniques: **1)** determining the $\Delta\delta^{13}C$ values through the time series, derived using DCP data as in Griffiths et al. (2012), and **2)** using the CaveCalc geochemical model (R. Owen et al., 2018) to investigate $\delta^{13}C$ and DCP controls.

For the $\Delta\delta^{13}C$ measurement, the $\delta^{13}C$ value of the initial drip water is estimated and compared to the speleothem $\delta^{13}C$. Measurements of soil gas above TM at or below 60 cm give an average value of -25.6‰ (+/- 0.23‰, n = 3) for soil gas (**Table 3.2**), which is used as a starting point for TM drip water $\delta^{13}C$. 8.37‰ is added to account for fractionation during the dissolution of soil gas CO_2 into DIC at the annual mean temperature of 21°C using the temperature-dependent fractionation equation from Mook et al. (1974), which gives $\delta^{13}C_{DIC}$. The $\delta^{13}C$ of initial drip water ($\delta^{13}C_{initial}$) is then estimated with a two-component mixing model that assumes the input of carbon to the drip water is a combination of the distinct soil gas and bedrock inputs (***eq. 8***). The amount of bedrock input is estimated using the DCP (%) as a measure of bedrock dissolution with a $\delta^{13}C$ value of 4.79‰ V-PDB ($\delta^{13}C_{BR}$).

$$\delta^{13}C_{initial(t)} = DCP(t) * \delta^{13}C_{BR} + (1 - DCP(t)) * \delta^{13}C_{DIC} \qquad \textbf{\textit{eq. 8}}$$

Finally, $\Delta\delta^{13}C$ is calculated using $\delta^{13}C_{initial}$ and the $\delta^{13}C$ measured in the stalagmite ($\delta^{13}C_{stal}$) at time *t*:

$$\Delta\delta^{13}C(t) = \delta^{13}C_{initial(t)} - \delta^{13}C_{stal(t)} \qquad \textbf{\textit{eq. 9}}$$

This method assumes a fixed $\delta^{13}C$ of soil gas and a similar cave temperature over time, so the interpretation of $\Delta\delta^{13}C$ must take into account any and all controls beyond dissolution that may have affected $\delta^{13}C$ in addition to fractionation, such as the effects of temperature on fractionation and/or vegetation as well as other climate-related vegetation or soil zone changes that might affect the initial $\delta^{13}C$ of the soil zone.

The geochemical model CaveCalc (Owen et al., 2018) was also applied in order to explore the potential effect of open vs. closed system changes on DCP and speleothem $\delta^{13}C$. Changes in gas volume, i.e. the degree of open vs. closed system dissolution, may arise due to epikarst water infiltration amounts and function as a wet vs. dry proxy. A dissolution system involving SAD, CAD, and high DCP may be very sensitive to small changes in gas volume of the epikarst (Bajo et al., 2017). The CaveCalc model provides an input for pyrite oxidation involvement and the resulting SAD effects on the chemistry of the precipitating speleothem calcite. To explore the system in TM, several CaveCalc parameters involving carbon isotopes in the above and below-ground environment were adjusted to match observed values from TM monitoring efforts (**Table S3.2**), and the remaining settings were left at default values (input from TM monitoring results include cave air and soil gas ^{14}C, soil gas $\delta^{13}C$, soil pCO_2, bedrock $\delta^{13}C$, and cave temperature).

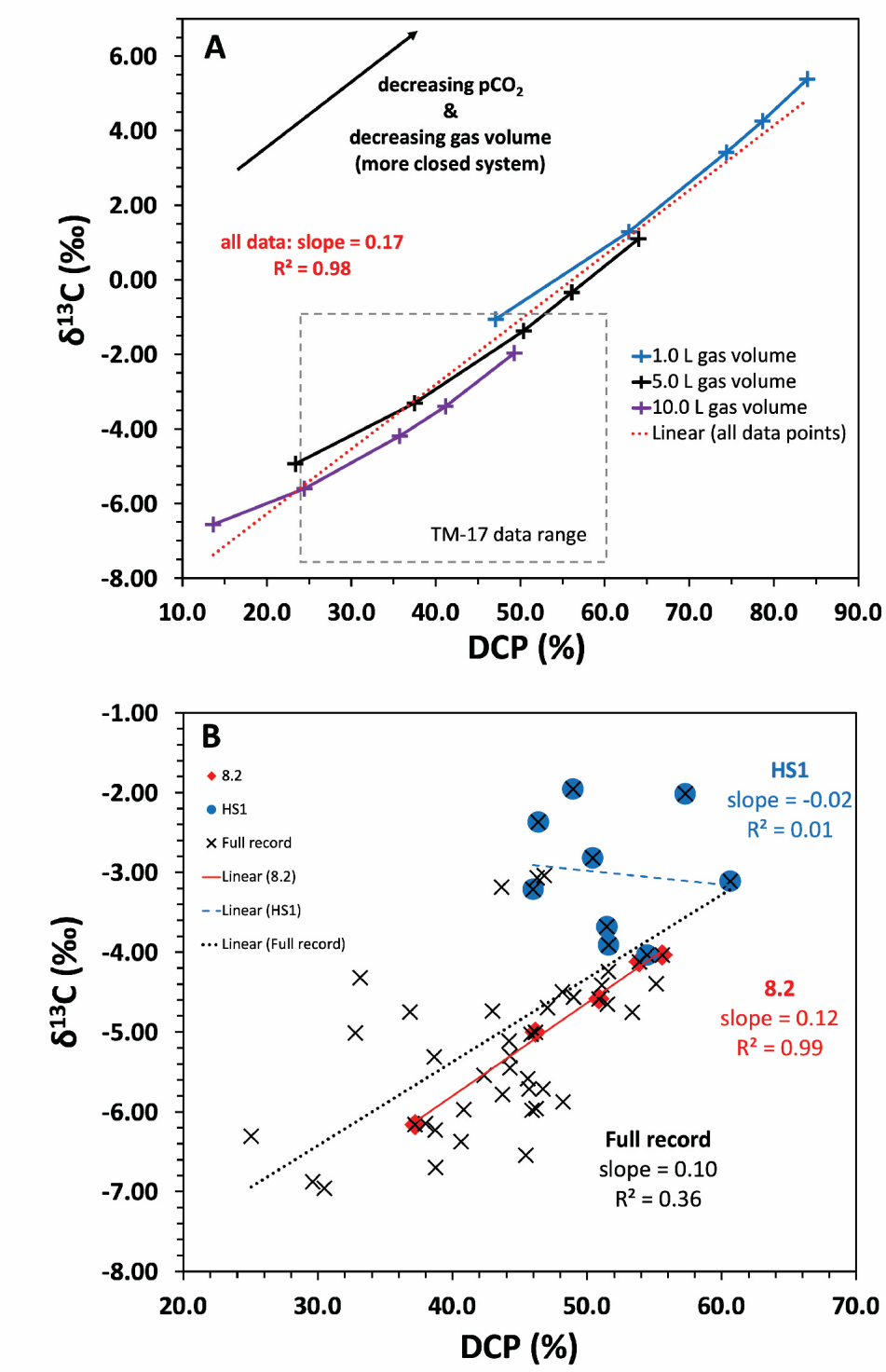

Figure 3.3 – CaveCalc results and TM-17 carbon cross plots ***A)*** *Crossplot of DCP and d13C from CaveCalc modeled results using TDM monitoring values while adjusting parameters associated with closed vs. open system dissolution changes (see text and* ***Table S1****).* ***B)*** *Similar plot using TM-17 DCP and $\delta^{13}C$ results highlighting similarities between the full record (dashed line) and for 8.2 ka event (diamonds) slopes, which contrast with HS1 (circles), where the correlation disappears due to elevated $\delta^{13}C$. Starting and ending points for events chosen from DCP sampling points and corresponding age: Full record (229 – 35,055 yrs BP; n = 52), HS1 (13,812 – 17,765 yrs BP; n = 9), and 8.2 (7,696 to 8,754 yrs BP; n = 5).*

Changes in the final speleothem carbon isotopes were found to be sensitive to two CaveCalc parameters, “Gas Volume (Bedrock Dissolution Conditions)” and “Initial PCO2 (Mixed Gas)” (**Fig. 3.3**). These were both ran at multiple values to provide a range of potential conditions close to those observed in and around TM (**Table S3.2**), especially as the observed pCO_2 in soil wells increased with depth up to 70 cm (**Fig. S3.1**). As the actual gas volume and pCO_2 in the deep epikarst are unobserved, and inputs are relative to the default settings of CaveCalc (e.g. 10 mol bedrock), all modeled gas volume changes are viewed as qualitative relative to other model input results. The level of pyrite in the model runs (0.0005 mol) was adjusted through trial and error to result in final levels of DCP and $\delta^{13}C$ similar to the TM-17 stalagmite. The model runs return a DCP ranging from 13.61 – 83.9% and $\delta^{13}C_{calcite}$ of (-)6.56 – (+)5.38‰ V-PDB, a range covering most the measured results from stalagmite TM-17 (**Fig. 3.3**) ($\delta^{13}C$ reaches more depleted values in the TM-17 record when additional controls for $\delta^{13}C$ are likely active). The CaveCalc modeling results show that high DCP similar to TM-17 can be achieved through known geochemical processes using local monitoring values and an estimate of SAD influence. The major control on variability in these runs is a varying gas volume and pCO_2, parameters representative of changes in open vs. closed system dissolution and ultimately tied to local hydrology and rainfall amounts.

3.5.4 Implications for Regional Hydroclimate over the last 35 ka

DCP measurements, CaveCalc results, and the separation of $\delta^{13}C$ controls utilizing $\Delta\delta^{13}C$, along with the available stable isotope and trace element records from TM (Johnson et al., in revision; Wood et al., in prep. a), allow examination of the climatic implications of the new TM-17 DCP data over the last ~35 ka. Plotting of the $\Delta\delta^{13}C$ reveals that at times of decreased DCP, $\Delta\delta^{13}C$ generally increases, indicating an increase in non-dissolution controls (**Fig. 3.2**). During the

deglaciation, $\Delta\delta^{13}C$ reaches a maximum of 4.65‰ in HS1 and also shows elevated values at other points, such as 2.88‰ at the 8.2 ka event. Therefore, lower DCP, potentially indicating a drier period with more open system dissolution, is accompanied by an increase in non-dissolution controls represented by $\Delta\delta^{13}C$, indicating changes in vegetation, soil moisture, respiration, and/or increased PCP and other fractionation effects. This supports the DCP interpretation, as elevated $\delta^{13}C$ from these controls is expected during dry periods. Differences in the $\Delta\delta^{13}C$ response during certain time periods and abrupt events can also be examined in terms of varying $\delta^{13}C$ controls.

The lowest measurements of DCP in the record are between ~26 – 36 kyr BP and reach 25.0% at the oldest sampling point. These low values occur among large swings in values and are not matched well by patterns in other TM-17 proxies (**Figs. 3.2, S3.4**). Previously, Wood et al. (in prep., a) stated that trace elements in this time period may have been contaminated by cave waters unrelated to the source drips, as the stalagmite was then short and on a wet slope in a hydrologically active section of the cave. Additionally, the DCP sampling resolution prior to the last glacial maximum (LGM, ~22 kyr BP) section is lower, so it is difficult to claim that potential shifts are responses to events or climate outside of normal variability. $\Delta\delta^{13}C$ in this period is elevated, which could imply that either the late Pleistocene, prior to the LGM, was drier at our site, that all carbon isotopes in this section are unreliable due to a climate much unlike the rest of the record, and/or flow waters contaminated proxy signals in this section of the stalagmite.

HS1 and the preceding 1,000 years during the last deglaciation display an interesting interplay of proxies in TM-17. The stable isotopes ($\delta^{18}O$ and $\delta^{13}C$) begin an HS1 response around 17.5 kyr

BP that is interpreted as a weakened monsoon and drying local conditions (Johnson et al., in revision). Trace element data reveals a possible period of aridity prior to HS1 lasting around 1,000 years (Wood et al., in prep., a; **Fig. S3.4)** that is potentially linked to other low latitude monsoon responses in Indonesia and Australia speleothem records, which saw high hydrological variability in similar date ranges (Ayliffe et al., 2013; Denniston et al., 2017). TM-17 shows lower DCP preceding the onset of HS1, representing open system dissolution and dryness, which is in agreement with TM-17 trace element responses (**Fig. S3.4**). These observations may indicate that local conditions on MSEA were drier than the initial centuries of HS1, despite the lower monsoon strength evidenced in TM-17 $\delta^{18}O$ and other Asian monsoon records (Cheng et al., 2016; Dykoski et al., 2005; Y. Wang et al., 2001). The decoupling of $\delta^{18}O$ (and corresponding monsoon strength) from local hydrology at TM is discussed in Johnson et al. (in revision) and Wood et al. (in prep., a) with a focus on the MSEA Holocene rainfall maximum, and the new DCP evidence shows that this decoupling may have been active before and during HS1 as well. While the $\delta^{13}C$ response to HS1 is of similar time range to $\delta^{18}O$ and does not provide evidence for a pre-HS1 period of aridity, the non-dissolution controls outlined previously, which include possible vegetation and soil moisture changes, would be less-directly affected by changes in hydrology alone. A change in rainfall amounts affecting the degree of closed system dissolution or PCP would affect trace elements and DCP more immediately and directly, and the fact that these two controls would have contrasting effects on $\delta^{13}C$, as well as additional vegetation-related controls, may explain the lack of consistency among these proxies prior to, and in early, HS1.

A unifying feature in TM-17 proxy records of HS1 is variability and/or a shift in direction around 16 kyr BP, around the half-way mark of the total HS1 response, most evident in DCP and $\Delta\delta^{13}C$ (**Fig. 3.3**). The high DCP in early HS1 (17.5 – 16 kyr BP), including the highest DCP measurement in the record, shifts from 60.6 to 46.4% in roughly 1,000 years. HS1 also appears to be a dynamic event as evidenced in the $\Delta\delta^{13}C$ proxy, with early HS1 (~17.5 – 16 kyr BP) showing lower $\Delta\delta^{13}C$ than mid-to-late HS1 (~16 – 14.5 kyr BP) (**Fig. 3.3**). The highest $\Delta\delta^{13}C$ value (4.65‰) after the LGM occurs at the mid-HS1 point after one of the lowest values (0.79‰), and this change corresponds with the dates of the large DCP shift. $\delta^{13}C$, while not jumping as significantly, does show movement during mid-HS1 (**Fig. 3.3**), and these shifts can be attributed to the interplay of $\delta^{13}C$ controls evidenced by $\Delta\delta^{13}C$. The total HS1 response, lasting around 3,000 years, is the lengthiest climate anomaly during our record, and it is the longevity that likely causes both the shift in controls and significant, long-term response in $\delta^{13}C$. The non-dissolution controls, especially a potential change in vegetation, biomass, or soil moisture above the cave, have time to take hold during a prolonged weakened monsoon regime.

The 8.2 ka event also shows a large, sudden increase in $\Delta\delta^{13}C$, although the maximum values do not reach the levels of mid-HS1. The 8.2 ka response in $\delta^{13}C$ moves sharply negative, which is at odds with the increase in trace element ratios that indicated a drier climate at 8.2 ka, as well as the positive response of $\delta^{13}C$ over HS1, another weak monsoon / drying event (Johnson et al., in revision; Wood et al., in prep., a; **Figs. 3.2, S3.4**). In contrast to HS1, the 8.2 ka event is relatively brief, and it also takes place in the more modern climate of the (post-deglaciation) Holocene (Alley & Ágústsdóttir, 2005). In the East Asian Summer Monsoon, the event is recorded as a ~150 year event, with a central, drier period of around 70 years (Y. H. Liu et al.,

2013). The 8.2 ka response in MSEA likely did not last long enough for the vegetation or soil zone changes that affected $\delta^{13}C$ during HS1 to take hold. TM-17 trace element ratios reach some of their highest recorded values around the 8.2 ka event, suggesting sudden and extreme relative dryness (Wood et al., in prep., a; **Fig. S3.4**), and the increase of $\Delta\delta^{13}C$ from this study, while not shifting as dramatically as during HS1, also suggests an increase in non-dissolution controls that could include fractionation from PCP, the interpreted driver of trace element responses. However, the sharp, negative $\delta^{13}C$ excursion at the 8.2 ka event is in contrast with the response expected from a strong PCP control. We suggest the bedrock dissolution control on $\delta^{13}C$ in TM-17 dominated the signal during this event. The sharp decrease in DCP around 8.2 ka (**Fig. 3.2**) suggests more open system dissolution caused by less rainfall and more air space in the epikarst. While PCP during a dry period would push $\delta^{13}C$ more positive, a response to the dissolution control, matching the sharp decrease in DCP, would decrease the amount of bedrock input to the carbon pool and push $\delta^{13}C$ towards more negative values.

To address this possibility, CaveCalc results are compared to TM-17 DCP and $\delta^{13}C$ data for evidence of a changing control on $\delta^{13}C$ during HS1 and the 8.2 event. The results of CaveCalc runs with varying gas volume and pCO_2 display a significant covariation between DCP and $\delta^{13}C$ of $R^2 = 0.98$ ($p < 1.0^{-5}$) and form a slope of 0.17 (**Fig. 3.3**). As these modelled results were achieved altering only gas volume and pCO_2, changes in these parameters in the real system would conceivably display a similar slope. TM-17 DCP and $\delta^{13}C$ data for the entire time series covaries at $R^2 = 0.36$ ($p = 0.01$) with a slope of 0.10 (**Fig. 3.3**), and an analysis of data from the approximate timeframes for the climate events of interest reveals when the gas volume and pCO_2 controls may have been more or less dominant. The 8.2 ka event range data (samples from 8,754

– 7,696 yrs BP) correlates more strongly than the full data range ($R^2 = 0.99$, $p = 0.003$) and has a slope (0.12) closer to the modelled CaveCalc relationship (**Fig. 3.3**). HS1 (17,765 – 13,812 yrs BP) is uncorrelated ($R^2 = 0.01$; $p = 0.91$) and does not display a slope resembling the full data series or the CaveCalc results. While DCP is on the higher end of recorded values, including the highest DCP result (60.6%), the elevated $\delta^{13}C$ is the apparent driver of the lack of correlation and unique slope.

As both $\delta^{13}C$ and $\Delta\delta^{13}C$ are elevated during HS1 beyond the typical values of the full record, the enhanced action of non-dissolution controls on $\delta^{13}C$ likely dominate this event (**Figs. 3.2, 3.3**). For the 8.2 ka, the strong dissolution control on $\delta^{13}C$, evidenced by the slope and correlation similar to CaveCalc results, acts in addition to a less dramatic increase of $\Delta\delta^{13}C$. With less bedrock dissolution due to open system conditions, $\delta^{13}C$ would reflect values more typical of soil and vegetation, pushing $\delta^{13}C$ more negative during the 8.2 ka event. Therefore, the dominant control, or set of controls, during these two events differed enough to cause the observed sign change in $\delta^{13}C$ response. This examination of carbon isotopes and $\Delta\delta^{13}C$ data across two events reveals that the differing controls of $\delta^{13}C$ can alter the magnitude and/or sign of total response during events that share similar climate forcings (i.e. a weak monsoon and relatively dry period) (**Figs. 3.2, 3.3**).

With the exception of the anomalous 8.2 ka response in $\delta^{13}C$, trace element and $\delta^{13}C$ data from TM-17 are interpreted by Wood et al. (in prep., a) to both be driven by PCP during much of the Holocene, when agreement between these proxy responses is more robust than during the deglaciation or late Pleistocene. Following the 8.2 ka event, drier conditions in the early

Holocene become consistently wetter towards a peak around ~5 kyr BP, followed by drier conditions up to the end of TM-17 growth near the present day. Lower resolution DCP and the corresponding $\Delta\delta^{13}C$ data from this study show an increase in dry conditions ~4 kyr BP, with DCP decreasing (open system dissolution) and $\Delta\delta^{13}C$ increasing (non-dissolution controls) (**Fig. 3.2**), providing evidence from multiple TM-17 proxies for a trend toward drier conditions relative to the mid-Holocene.

3.6 Conclusions

TM-17 DCP is unusually high, often above 50%, and highly variable. The source of this dead carbon, and therefore a source of a significant portion of the carbon available to the stalagmite, is dominantly bedrock. In our low-latitude, highly vegetated setting, SOM (or deeper OM) could potentially provide additional decayed carbon, yet our estimates of the potential effects of ancient SOM only sway the results by a few percent at maximum and maintain the relative changes over time. The high DCP is likely possible through a combination of SAD and CAD, and the variability of bedrock input and the resulting DCP in TM-17 over time is controlled by hydrology, which affects the degree of open vs. closed system dissolution. We interpret wet periods as increasing the DCP due to a decreased ratio of modern carbon vs. bedrock carbon entering the DIC in drip waters that ultimately precipitated the speleothem (i.e. more closed system dissolution). CaveCalc modelling results show a similar relationship to most TM-17 data when only altering pCO_2 and gas volume, representative of changes in the open vs. closed dissolution system. It is likely that bedrock dissolution also provided some control over $\delta^{13}C$ based on their correlation over the entire time series ($R^2 = 0.36$).

The DCP data, the related $\Delta\delta^{13}C$ proxy, and CaveCalc results provide additional support for previous interpretations of TM-17 proxies, including a weakened monsoon and period of relatively dry climatology on MSEA during HS1, although trace element ratios and DCP suggest the ~1,000 years prior to the event may have also been relatively arid. Around the halfway point of HS1, however, a shift in DCP and $\Delta\delta^{13}C$ suggest more extreme dryness or the effects of long-term dryness taking hold, as non-dissolution controls (increased $\Delta\delta^{13}C$) are very prevalent for $\delta^{13}C$, which is likely affected by long-term changes in vegetation and soil moisture. A contrast in $\delta^{13}C$ control exists at the 8.2 ka event, which affects all TM-17 proxies during the Holocene. In this case, the dissolution control of $\delta^{13}C$ is prevalent, with open system dissolution creating a negative excursion of $\delta^{13}C$ during a sharp decrease in DCP. Trace elements and $\delta^{13}C$ begin to increase from mid-Holocene minima ~5 kyr BP, while DCP and $\Delta\delta^{13}C$ also indicate relative drying following the wetter mid-Holocene period at our site.

The potential sources and the variation in individual cave site dynamics require multiple proxies, cave monitoring, and/or modeling to attempt to distinguish the controls on both radiogenic and stable carbon isotopes, as well as other proxies in speleothems. A large DCP with variations through known climate events, as observed in TM-17, may add valuable data to a multiproxy speleothem study where controls on proxies are not straight-forward. The new DCP record and our interpretations of controls via $\Delta\delta^{13}C$ data and geochemical modeling provide new evidence of the proxy dynamics at work during deglacial and Holocene events at our site, especially the alternate controls at work on $\delta^{13}C$ during 8.2 and HS1, which are both interpreted to be drier than background conditions. Our hydrologically controlled ~35 kyr record of DCP from MSEA corroborates previous proxy interpretations of significant regional responses to past global events

and allows the assignment of varying controls on speleothem $\delta^{13}C$, which is often challenging to interpret.

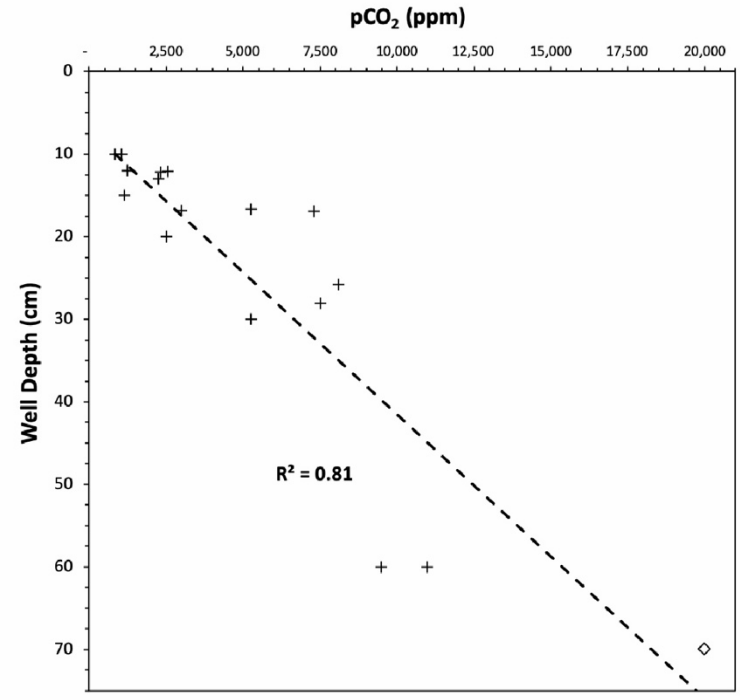

Figure S3.1 – Soil gas measurements of pCO_2 vs. depth of soil well*. Crosses indicate individual samples and diamond indicates saturation of instrument at 20,000 ppm.*

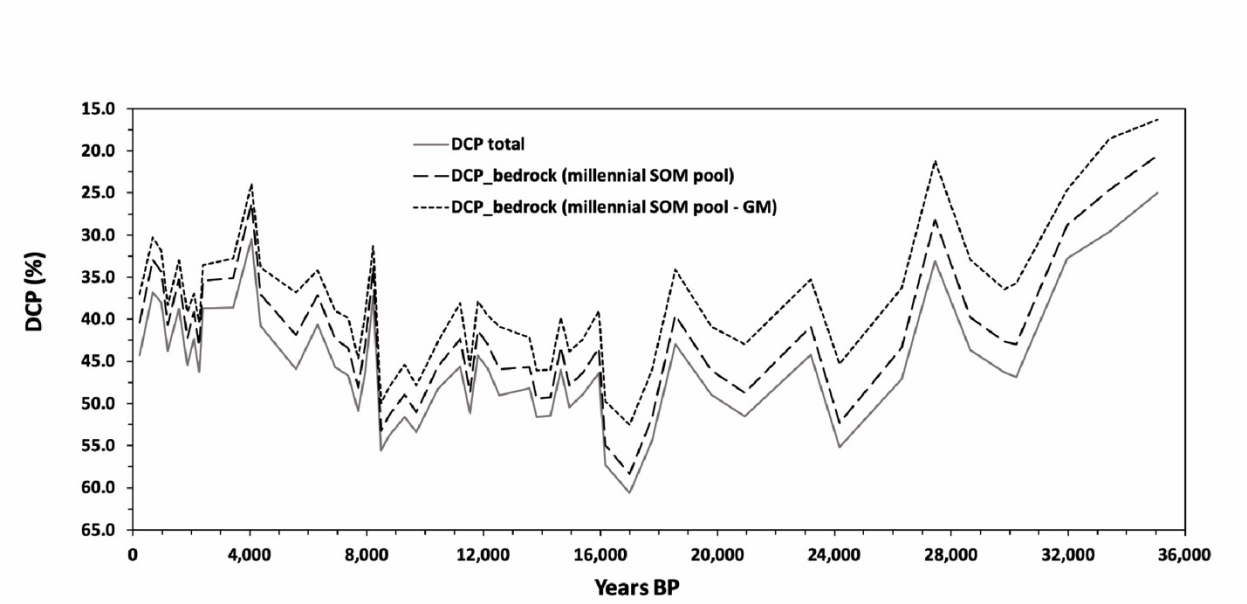

Figure S3.2 – DCP_{BR} estimate method comparison *- SOM effect on the bedrock contribution to DCP estimated for a millennial SOM pool compared to DCP total using method from this study and equation from Genty and Massault (1999a) (GM).*

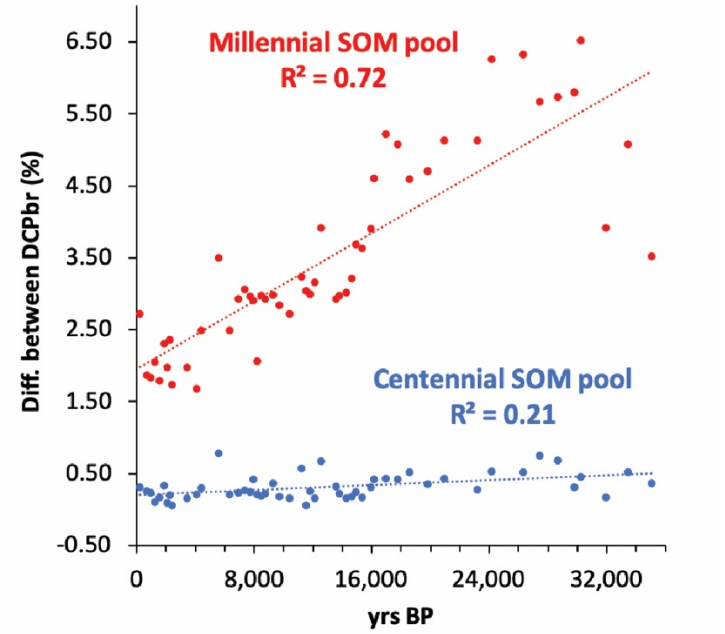

Figure S3.3 – DCP_{BR} calculation method differences – *Difference between the final DCP_{BR} calculated using eq. 6 (this study) and eq. 7 (Genty and Massault, 1999a). The effects of SOM increase the DCP_{BR} difference dramatically with age when a millennial-aged SOM pool is involved, with eq. 6 providing a more uniform contribution through time in this case. For a centennial pool, the differences between methods with age increasing is less pronounced.*

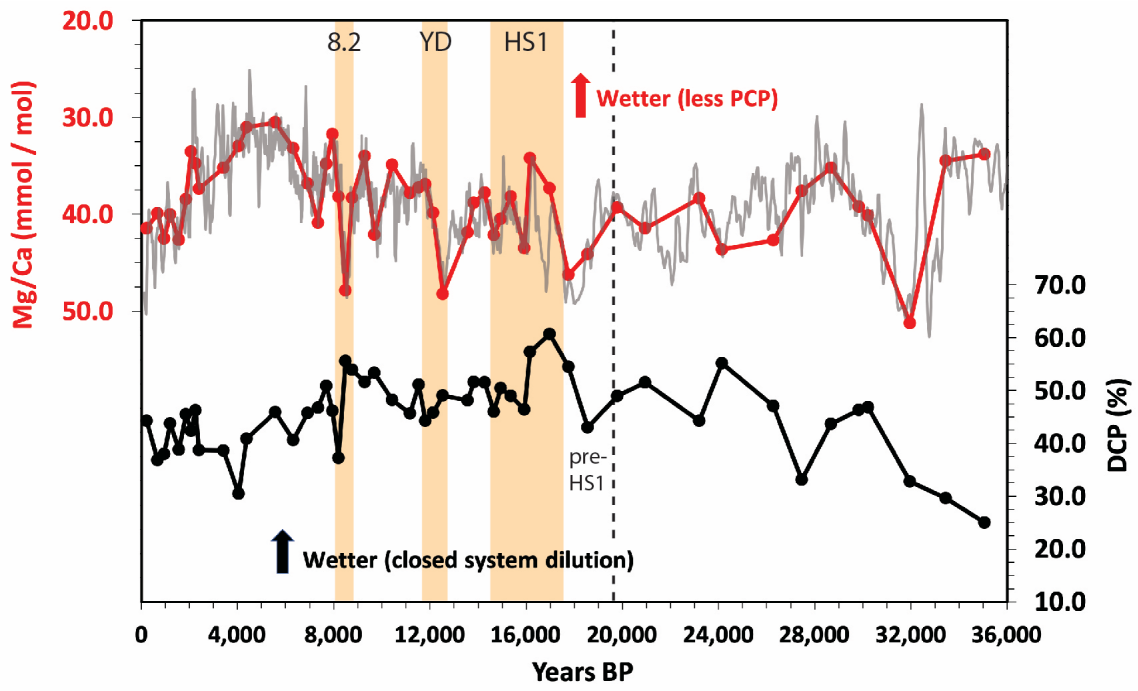

Fig. S3.4 – DCP and Mg/Ca comparison in TM-17 *- DCP (lower black line) and Mg/Ca (upper), with the latter plotted at full resolution (grey line, 3 pt running mean) and low resolution (thicker red line and dots) to match DCP sampling points. Mg/Ca data from Wood et al. (in prep., a).*

Table S3.1 - DCPbr estimate comparison using different methods
(G & M = Genty and Massault, 1999)

	DCPapp	DCPbr (Centennial SOM)			DCPbr (Millennial SOM)		
Sample	%	%	diff. from DCPapp	G & M (1999) diff. from DCPapp	%	diff. from DCPapp	G & M (1999) diff. from DCPapp
TM17-14C-2	44.3	43.9	-0.4	-0.7	40.4	-3.9	-7.3
TM17-14C-9	36.9	36.4	-0.5	-0.7	32.9	-3.9	-6.5
TM17-14C-13	38.0	as	-0.4	-0.6	34.3	-3.7	-6.1
TM17-14C-18	43.7	43.6	-0.1	-0.2	40.6	-3.1	-5.4
TM17-14C-26	38.8	38.5	-0.3	-0.5	35.3	-3.5	-5.7
TM17-14C-32	45.5	45.0	-0.4	-0.7	42.2	-3.2	-6.3
TM17-14C-37	42.3	42.2	-0.1	-0.2	39.2	-3.2	-5.3
TM17-14C-42	46.2	46.0	-0.2	-0.4	43.1	-3.1	-5.9
TM17-14C-46	38.7	38.6	-0.1	-0.1	35.5	-3.3	-5.1
TM17-14C-65	38.6	38.4	-0.2	-0.4	35.1	-3.5	-5.9
TM17-14C-2-76	30.5	30.0	-0.4	-0.7	26.3	-4.2	-6.5
TM17-14C-88	40.8	40.4	-0.4	-0.7	37.1	-3.8	-6.9
TM17-14C-115	45.9	45.1	-0.8	-1.6	41.9	-4.0	-9.1
TM17-14C-2-128	40.6	40.4	-0.3	-0.5	37.1	-3.5	-6.5
TM17-14C-141	45.7	45.5	-0.2	-0.5	42.4	-3.3	-6.7
TM17-14C-2-156	46.7	46.5	-0.3	-0.5	43.4	-3.3	-6.9
TM17-14C-170	50.9	50.7	-0.2	-0.5	48.1	-2.8	-6.2
TM17-14C-176	46.2	45.7	-0.4	-0.8	42.9	-3.3	-7.0
TM17-14C-183	37.2	36.9	-0.3	-0.5	33.9	-3.3	-5.9
TM17-14C-189	55.6	55.5	-0.1	-0.3	53.3	-2.3	-5.6
TM17-14C-196	53.9	53.7	-0.2	-0.4	51.5	-2.4	-5.7
TM17-14C-2-212	51.6	51.3	-0.3	-0.7	49.0	-2.6	-6.2
TM17-14C-228	53.4	53.2	-0.1	-0.3	51.0	-2.3	-5.5
TM17-14C-2-246	48.2	48.1	-0.1	-0.3	45.6	-2.6	-5.6
TM17-14C-263	45.6	45.1	-0.5	-1.1	42.4	-3.2	-7.5
TM17-14C-270 .24mgC	51.1	51.1	0.0	-0.1	48.7	-2.4	-5.5
TM17-14C-276	44.3	44.0	-0.2	-0.5	41.3	-3.0	-6.5
TM17-14C-282	45.8	45.7	-0.1	-0.3	43.0	-2.9	-6.3
TM17-14C-289	49.0	48.5	-0.5	-1.2	45.9	-3.1	-8.2
TM17-14C-2-299	48.2	47.9	-0.3	-0.6	45.7	-2.5	-6.0
TM17-14C-312	51.6	51.4	-0.2	-0.4	49.4	-2.2	-5.6
TM17-14C-320	51.5	51.4	-0.1	-0.3	49.3	-2.2	-5.5
TM17-14C-329	46.0	45.8	-0.1	-0.3	43.3	-2.7	-6.2
TM17-14C-337	50.4	50.3	-0.2	-0.4	47.9	-2.5	-6.6
TM17-14C-347	49.0	48.8	-0.1	-0.3	46.4	-2.6	-6.5
TM17-14C-355	46.4	46.2	-0.2	-0.5	43.4	-2.9	-7.4
TM17-14C-363	57.3	57.1	-0.2	-0.6	54.9	-2.4	-7.6
TM17-14C-373	60.6	60.5	-0.2	-0.6	58.4	-2.3	-8.1
TM17-14C-381	54.5	54.3	-0.2	-0.6	51.8	-2.7	-8.4
TM17-14C-390	43.0	42.6	-0.4	-0.9	39.5	-3.4	-8.9
TM17-14C-2-401	49.0	48.8	-0.2	-0.6	46.1	-2.9	-8.1
TM17-14C-415	51.5	51.3	-0.2	-0.6	48.7	-2.8	-8.6
TM17-14C-2-431	44.2	44.0	-0.2	-0.4	40.9	-3.3	-8.9
TM17-14C-442	55.1	54.9	-0.2	-0.7	52.3	-2.9	-9.9
TM17-14C-468	47.1	46.8	-0.3	-0.8	43.4	-3.7	-10.8
TM17-14C-2-480	33.1	32.6	-0.6	-1.3	28.2	-4.9	-11.9
TM17-14C-496	43.6	43.2	-0.4	-1.1	39.8	-3.9	-10.7
TM17-14C-517	46.3	46.1	-0.2	-0.5	42.7	-3.6	-9.9
TM17-14C-2-524	46.8	46.6	-0.2	-0.7	43.0	-3.8	-11.1
TM17-14C-539	32.8	32.6	-0.2	-0.3	28.9	-3.9	-8.2
TM17-14C-544	29.6	29.1	-0.5	-1.0	24.6	-5.0	-11.1
mean	45.4	45.2	-0.3	-0.6	42.2	-3.2	-7.3

Table S3.2 *– CaveCalc (Owen et al., 2018) settings adjusted from default.*

Sub-section	Input	Value	Unit	Measured/Observed Value?
Mixed Gas	Initial R14C	102.8	pMC	yes
	Initial d13C	-25.6	‰ V-PDB	yes
	Initial pCO2	5000	ppm	in observed range
		7500	ppm	in observed range
		10000	ppm	in observed range
		20000	ppm	saturated reading (70 cm depth)
		50000	ppm	no - possible deep subsurface value
Cave Air	Cave Air R14C	100.2	pMC	yes
	Cave Air d13C	-15.2	‰ V-PDB	yes
	Cave Air pCO2	630	ppm	yes
Bedrock Chemistry	d13C	4.79	‰ V-PDB	yes
Bedrock Dissolution Conditions	Pyrite	0.0005	mol	no - fit to data
	Gas Volume	1	L	[no - relative to 10 mol bedrock
		5	L	and 1 kg soil-H20 in CaveCalc]
		10	L	
General	Temp	21	℃	yes

Chapter 4

High Resolution, multiproxy speleothem record of the 8.2 ka event from Mainland Southeast Asia

4.1 Abstract

The 8.2 ka event, an abrupt Holocene climate anomaly with global extent lasting ~160-170 years, is evidenced by century-scale shifts in numerous climate proxy records from many continents. A temporarily weakened Asian Monsoon likely coincides with well-documented drops in temperature across the Northern Hemisphere, but a lack of records from Mainland Southeast Asia (MSEA) currently limit knowledge of the spatial extent of the regional response. High resolution proxy records from stalagmite TM-17 from Tham Doun Mai, Northern Laos reveal that the extent of the monsoon weakening, and the associated drier climate during the event, extend into MSEA. A newly developed U-Th age model covering the 8.2 ka range is combined with new proxy data sets ($\delta^{18}O$, $\delta^{13}C$, Mg, and Sr) that reveal abrupt and significant drying at the initiation of the event. A more positive shift (2σ) from the pre-event period in $\delta^{18}O$ provides evidence for a weakened monsoon state that begins ~8,289 yrs BP and lasts for a minimum of ~173 years. $\delta^{13}C$ and Mg, more responsive to local hydrologic conditions, display statistically significant shifts due to local drying ~67 years prior to the start of the $\delta^{18}O$ anomaly. The interpretation of 8.2 ka drying in MSEA agrees with the pattern of change in climate model simulations in which the event is triggered by an abrupt North Atlantic freshwater forcing, while

the event length in TM-17 (~173 + years) agrees with proxy records that estimate global climate responses of at least 150 years. $\delta^{13}C$ and Mg remain outside of pre-event averages up to ~200 years longer than the event as recorded in $\delta^{18}O$. The multi-proxy approach enhances estimates of the 8.2 ka event initiation in the TM-17 age model (~8,355 yrs BP) and local response length by showing that regional drying in MSEA continued beyond the boundaries of a weakened monsoon state.

4.2 Introduction

The abrupt global climate event that initiated around 8.2 thousand years ago (ka), or '8.2 ka event,' is represented in numerous paleoclimate records from around the world and is thought to be the most significant climate anomaly of the Holocene epoch (Alley et al., 1997; Kobashi et al., 2007). The root cause of the event is most often attributed to a freshwater input into the North Atlantic, likely from a glacial outburst flood or ice sheet saddle collapse (Alley & Ágústsdóttir, 2005; Cheng et al., 2009b; Matero et al., 2017). Effects in the North Atlantic and surrounding areas are well studied, but the extent of climatic effects in other areas of the world continue to be discovered and refined. While some records of the event are well-dated with robust age models, including temperature anomalies interpreted from Greenland ice cores (e.g. Thomas et al., 2007) and monsoon strength changes in Asia and South America interpreted from stalagmite records (Cheng et al., 2009b; Y. H. Liu et al., 2013), evidence of pre-existing trends in climate and age uncertainties in other records leave open the possibility that some global climate responses around this time period could be unrelated to the specific North Atlantic trigger (Rohling & Pälike, 2005). While nearly coinciding climatic responses in the North Atlantic and East Asian Summer Monsoon (EASM) are likely related by an atmospheric teleconnection with

a near-annual response time (Y. H. Liu et al., 2013), no high resolution record of the event exists from Mainland Southeast Asia (MSEA) to corroborate the EASM response or to examine the potential for regionally variable hydroclimatic changes. To this end, we present new high-resolution proxy records over the 8.2 ka event period from stalagmite TM-17 from Tham Doun Mai cave, Northern Laos, which has been previously analyzed over the last ~38 kyr BP (Johnson et al., in revision; Wood et al., in prep., a, b). Using a refined age model based on additional U-Th dates, higher resolution stable isotope ($\delta^{18}O$ and $\delta^{13}C$) data, and new laser ablation inductively-coupled plasma (LA-ICP-MS) analysis of trace elements (Mg and Sr), we combine previous proxy interpretations from this sample and the local cave environment with new data sets in order to outline the response of MSEA hydroclimate to the 8.2 ka event. The signal of drying, timing, and length of the 8.2 ka event response in MSEA is comparable to other records and model simulations of the 8.2 event and surrounding centuries, and multi-proxy information suggests the relatively dry conditions persisted in MSEA beyond the length of the monsoon weakening.

4.3 Materials and Methods

Stalagmite TM-17, from Tham Doun Mai (TM) cave, Northern Laos (N20°45', E102°39'; 352 m asl), has been analyzed previously at lower resolutions for stable isotopes (Johnson et al., in revision), trace elements (Wood et al., in prep., a), and radiocarbon (Wood et al., in prep., b), as well as a high-resolution stable isotope analysis of the last 2 ka (J. K. Wang et al., 2019). Details about the sample, cave, and previous age model(s) may be found in these studies. For higher resolution analysis, a ~7.40 cm vertical slab of TM-17 was cut from the half previously used for stable isotope and trace element analyses and sawed in half along the growth axis. New analyses

were performed on the surface perpendicular to the original cut. The central 3.133 cm section of this piece was used for the micro-milling of calcite powder ($\delta^{18}O$ and $\delta^{13}C$) and laser ablation lines (Mg and Sr) in this study (depth from top = 16.790 – 19.924 cm), while the stalagmite half used for the U-Th age model in Johnson et al. (in revision) was utilized for drilling additional U-Th samples at corresponding depths. As the amount of calcite powder needed for U-Th dates is relatively large, the smaller slab used for new high-resolution drilling and laser ablation was not used for dating in order to avoid destruction of the sampling surface. Sample depths (distance from top of the stalagmite) were measured on the edge of the new slab closest to the growth axis and previous low-resolution sampling, and depths were kept constant along visible growth layers away from the edge.

Seven new U-Th dates were analyzed at the University of Oxford, UK and used in conjunction with two previously analyzed dates on the outside boundaries of new samples. These 9 samples were used in the construction of a new age model for this section of the stalagmite using COPRA (Breitenbach et al., 2012), which calculates depth to age relationships between U-Th sampling points based on a Monte Carlo modeling approach. 700 stable isotope ($\delta^{18}O$ and $\delta^{13}C$) samples were micro-milled at a resolution of 45 μm over the 3.133 cm section utilizing a New Wave Instruments Micromill fitted with a diamond drill bit. 513 samples were analyzed for stable isotope composition on a Thermo Finnigan Kiel IV carbonate device coupled with a Delta V Plus isotope ratio mass spectrometer at the University of California, Irvine (every sample was analyzed in the central portion of the section between depths 17.501 – 19.021 cm, while every 2nd drilled sample was analyzed from depths 16.79 – 17.501 and 19.021 – 19.915, resulting in the 513-pt. sample set). Stable isotope results are presented relative to the V-PDB standard and

expressed using conventional δ notation (‰). 15 standards were analyzed with each batch of 31 stalagmite powders (IAEA-CO-1, NBS-18, and OX, an in-house quality control standard). Trace elements were analyzed by laser ablation inductively coupled mass spectrometry (LA-ICPMS) at the University of Rutgers using a Thermo Scientific Neptune Plus MC-ICPMS. Depth resolution of individual data points during the laser ablation (LA) process was ~ 0.75 μm. The LA-ICPMS analyses were conducted along a line on the inside of the trench created during high-resolution micro-milling for stable isotopes.

4.4 Results

4.4.1 TM-17 U-Th and Proxy results

The new U-Th results (n = 7) display uncertainties of +/- 24-32 yrs (corrected age), while the previously reported samples (n = 2) have uncertainty of +/- 56-58 yrs (**Table 4.1**). The new age model, utilizing all 9 dates and developed using COPRA (Breitenbach et al., 2012), displays depth to age relationships built using the sampling resolution of new $\delta^{18}O$ data, resulting in a 513-pt. age model spanning 8910.9 - 7574.6 years before 1950 (yrs BP) (**Fig. 4.1**). While growth rate varies between all dates (~10 – 40 μm/yr), a slowdown in growth rate is apparent due to a shallower slope between the dating points of 8373 – 8131 yrs BP (**Figs. 4.1, S4.1**).

$\delta^{18}O$ varies from -10.52 to -8.84‰ V-PDB with a mean value of -9.84‰, and $\delta^{13}C$ varies from -7.39 to -3.64‰ V-PDB with a mean value of -5.33‰ (**Fig. 4.2**). Long-term standard deviation (1σ) for stable isotopes in standards were 0.07‰ for $\delta^{18}O$ and 0.05‰ for $\delta^{13}C$. By applying the new age model to stable isotope sampling depths, the mean sample resolution for $\delta^{18}O$ and $\delta^{13}C$

Table 4.1 U-Th concentrations, isotope ratios, and calculated ages for the analyzed portion of stalagmite TM-17

Sample ID	Depth from top (cm)	^{238}U (ppm)	^{232}Th (ppb)	$(^{234}U/^{238}U)$	$(^{230}Th/^{232}Th)$	$(^{230}Th/^{238}U)$	$(^{234}U/^{238}U)_{initial}$	Raw Age (yrs BP)	Corr. Age (yrs BP)
TM-17-U9[2]	17.04	3.35	1.00	1.6488 ± 0.0053	1170.7 ± 18.8	0.1138 ± 0.0008	1.6630 ± 0.0054	7703 ± 56	7696 ± 56
TM17_8.2_U2	17.48	3.91	0.83	1.6636 ± 0.0056	1670.7 ± 11.3	0.1158 ± 0.0003	1.6781 ± 0.0054	7763 ± 23	7758 ± 23
TM17_8.2_U3	17.81	3.30	1.58	1.6455 ± 0.0054	744.3 ± 4.2	0.1165 ± 0.0003	1.6599 ± 0.0054	7901 ± 23	7890 ± 26
TM17_8.2_U4	18.08	3.75	0.83	1.6539 ± 0.0055	1636.6 ± 11.2	0.1187 ± 0.0003	1.6686 ± 0.0054	8016 ± 24	8011 ± 24
TM17_8.2_U5	18.35	3.07	3.21	1.6647 ± 0.0056	355.5 ± 1.8	0.1215 ± 0.0003	1.6800 ± 0.0054	8154 ± 23	8131 ± 32
TM17_8.2_U6	18.66	4.19	0.54	1.5988 ± 0.0054	2855.4 ± 23.0	0.1197 ± 0.0003	1.6130 ± 0.0053	8376 ± 23	8373 ± 24
TM17_8.2_U7	19.01	4.05	2.14	1.5884 ± 0.0055	700.9 ± 3.4	0.1212 ± 0.0003	1.6026 ± 0.0052	8550 ± 24	8537 ± 27
TM17_8.2_U8	19.26	3.47	2.52	1.5857 ± 0.0053	513.5 ± 2.8	0.1221 ± 0.0003	1.5999 ± 0.0052	8626 ± 22	8609 ± 28
TM-17-U10[2]	19.65	4.11	0.83	1.5804 ± 0.0050	1868.0 ± 32.9	0.1234 ± 0.0008	1.5949 ± 0.0051	8759 ± 57	8754 ± 58

[1]Uncertainties are 2σ. Half lives are those of Cheng et al. (2013). All ages are relative to 1950. Corrected ages assume an initial $^{230}Th/^{232}Th$ atomic ratio of 5.38 +5.38/-4.84 ppm. [2]Samples originally analyzed and reported in full (~38 kyr) TM-17 age model (Johnson et al., in revision).

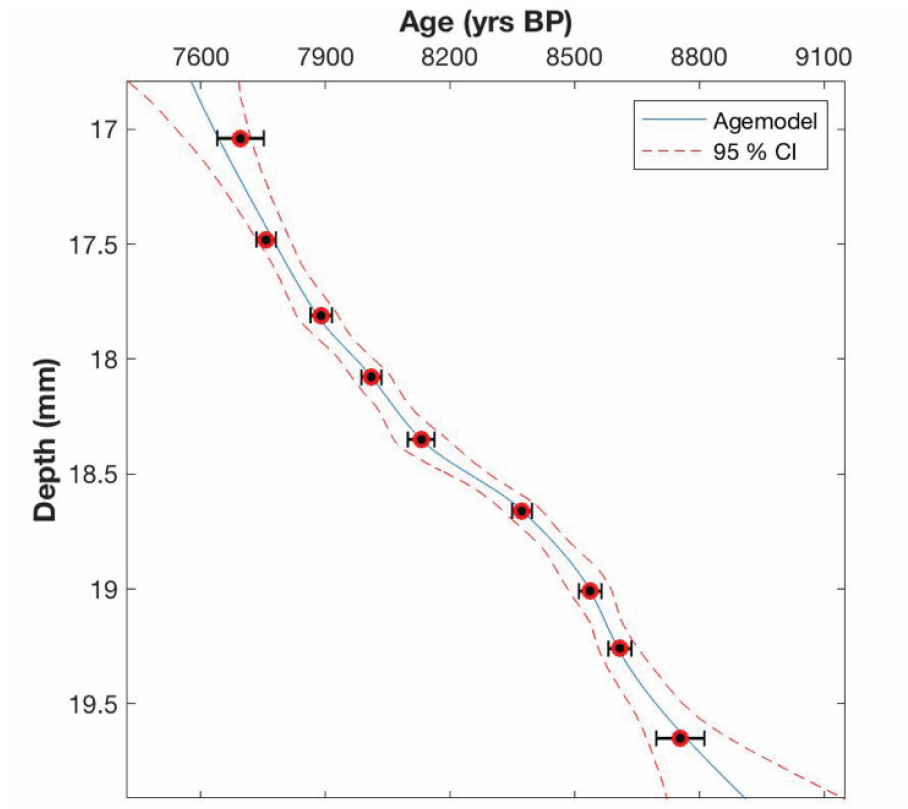

Figure 4.1 – **COPRA age model results** – *Age model for the 8.2 section of TM-17 used in this study developed using COPRA (Breitenbach et al., 2012). Circles represent mean modeled values for U-Th samping depths bracketed by errors. Upper and lower ages were originally reported in Johnson et al. (in revision), and seven new samples were drilled in-between to increase the confidence of age modeling for new high-resolution proxies.*

over the full record is ~2.61 years with a minimum of 1.11 years. For the central portion of the record (17.501 – 19.021 cm; 7,781.6 – 8,541.7 yrs BP), the mean resolution is ~2.25 years. LA-ICP-MS for trace elements resulted in mean values of 12,104 ppm for Mg and 357 ppm for Sr over the full time series (**Fig. 4.2**). The 513-pt. age model used for stable isotopes was interpolated to the trace element LA-ICP-MS data depths (41,765 points), and a 100 pt. running mean was applied to data to reduce noise and outlier effects, resulting in an approximate 3.27 year average resolution for Mg and Sr data.

4.4.2 Defining the 8.2 ka event in new proxy records

To determine the timing and length of the 8.2 ka event in the new TM-17 proxy records, a pre-event average is calculated; 8,400.5 - 8,910.9 yrs BP ($\delta^{18}O$ and $\delta^{13}C$) and 8,400.0 - 8,942.7 yrs BP (Mg and Sr). For $\delta^{18}O$, the pre-event average is -9.96‰ V-PDB, and the beginning of a continuous increase greater than 1σ appears at 8,292.5 yrs BP, and the end of the continuous anomaly occurs at 8,085.2 yrs BP (**Fig. 4.2**), which results in an anomaly of 207.3 years. At 2σ, the range shrinks to 8,288.6 – 8,115.6 yrs BP for a length of 173.0 years. The maximum value of $\delta^{18}O$ during the event is -8.84‰ for a difference of of 1.12‰ from the pre-event average, and the mean value during the anomaly is -9.20‰. Anomalous points (2σ) outside of the continuous range (interrupted by values within 1σ) occur on both sides of the 2σ range; if these are included, the anomaly in $\delta^{18}O$ can be extended to a range of 8,336.2 – 8,045.8 yrs BP, for a maximum event response estimate of 290.4 years in $\delta^{18}O$ data. A more concise estimate of the event in $\delta^{18}O$ results emerges using proxy output from COPRA, which uses depths, U-Th dates, U-Th uncertainties, and proxy values to assign uncertainty to the proxy by assuming fixed dates along the age model (**Fig. 4.3**) (Breitenbach et al., 2012). Using the median of the range of possible

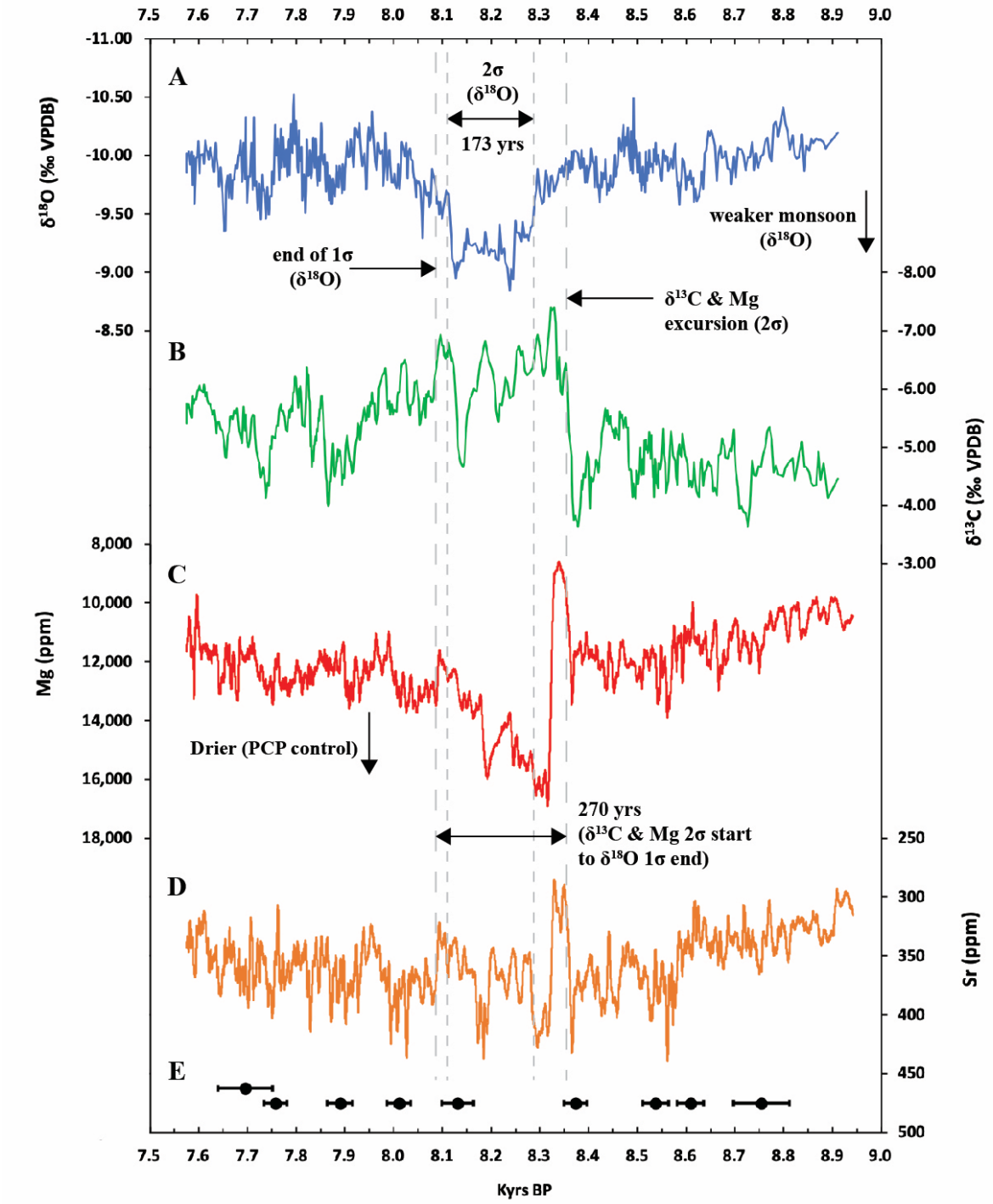

***Figure 4.2** – **TM-17 multiproxy analysis of the 8.2 ka event – A** and **B** – 513 pt. stable isotope records ($\delta^{18}O$ and $\delta^{13}C$); **C** and **D** – LA-ICP-MS trace element records as labeled on y-axes (100 pt running mean from original data). **E** – U-Th results used for age model construction with associated error bars. Proxy standard deviations (σ) were calculated compared to a pre-event average (8910 – 8400 yrs BP).*

$\delta^{18}O$ values at each sampling point and adjusting the pre-event average to COPRA output values, the continuous 1σ excursion occurs from 8322.3 – 8042.0 yrs BP (280.3 years), and the continuous 2σ range is extended to 8315.0 – 8053.4 yrs BP (261.6 years) (**Fig. 4.3**). The 2σ mean (-9.41‰) is 0.54‰ more positive than the pre-event average in COPRA output (-9.95‰).

In $\delta^{13}C$, a sharp decrease (more negative values) occurs prior to the statistically significant $\delta^{18}O$ anomaly (**Figs. 4.2, 4.3**). In both the instrumental measurements and COPRA proxy output, this increase reaches 2σ from the pre-event average at ~8,356 yrs BP (we note that running COPRA with $\delta^{13}C$ requires a second Monte Carlo-driven age model to be produced, resulting in slight differences from the age model built with $\delta^{18}O$; the mean of the two modeled ages for $\delta^{13}C$ is 8,356.4 yrs BP with a difference of 1.5 years). The pre-event average in $\delta^{13}C$ is -4.76‰ V-PDB, and the most negative value(s) during the event is -7.39‰ (reached twice), a difference of 2.63‰ from the pre-event average. Large variations occur in the instrumental $\delta^{13}C$ data around the central and late stages of the event as defined by $\delta^{18}O$, so there is not a continuous anomaly in $\delta^{13}C$ that approaches the length of the anomaly in $\delta^{18}O$. $\delta^{13}C$ even exceeds the pre-event average during the event as defined by $\delta^{18}O$ with a maximum of -4.67‰ at ~8,143 yrs BP. However, a discontinuous instrumental data anomaly (2σ) occurs from 8,355.6 – 7,938.0 yrs BP (417.6 years) (**Fig. 4.2**). The modeled COPRA data for $\delta^{13}C$ produces a continuous anomaly from 8,357.1 – 7,926.0 yrs BP (431.1 years) (**Fig. 4.3**). The average value of the COPRA anomaly is -6.00‰, which is 1.22‰ more negative than the pre-event average in COPRA output (-4.78‰).

Mg data display a sharp decrease around the timing of the initial decrease of $\delta^{13}C$, which reaches 2σ from the pre-event average in alignment with the $\delta^{13}C$ anomaly at 8,354.8 yrs BP (**Fig. 4.2**).

This increase reverses in a smooth arc and becomes a positive anomaly from the pre-event average at 8,322.5 yrs BP, and the final continuously positive value above 2σ occurs at 8,178.2 yrs BP, which would place the length of the event response at 144.3 years. However, this range ends inside of the $\delta^{18}O$ anomaly, and a discontinuous sequence of anomalous values in Mg results in a range of up to 8,133.7 yrs BP, for an event response length of 221.1 years. Positive anomalies after longer breaks in continuity occur for the rest of the Mg record, suggesting there is no complete return to pre-event values in Mg. Discontinuous anomalies can be mapped to the full range of the discontinuous $\delta^{13}C$ response (>400 years) (**Fig. 4.2**).

Sr data is noisier than Mg and appears to have long-term (event-length) anomalies similar to those seen in the Mg sequence. However, a peak of decreased values in Sr matches the initial decrease in Mg at the onset of the anomalous period at ~8,355 yrs BP (**Fig. 4.2**). Additionally, TM-17 results from the Australian Synchrotron (Paterson et al., 2011) contain a similar double peak at the same stalagmite distance from top (**Fig. S4.2**), providing confidence in our depth measurements as well as the alignment of the Sr and Mg anomalies. The synchrotron Sr results (see **Supplementary Methods**), which were performed on a separate section of TM-17 (at the same depth range) are more visually similar to the LA-ICP-MS Mg results, which increase sharply following the peak of minimum values (**Figs. 4.2, S4.1**). Therefore, while the LA-ICP-MS Sr data is not useful in defining the event response, the data adds confidence to the Mg results when compared with both the Mg data and synchrotron Sr results.

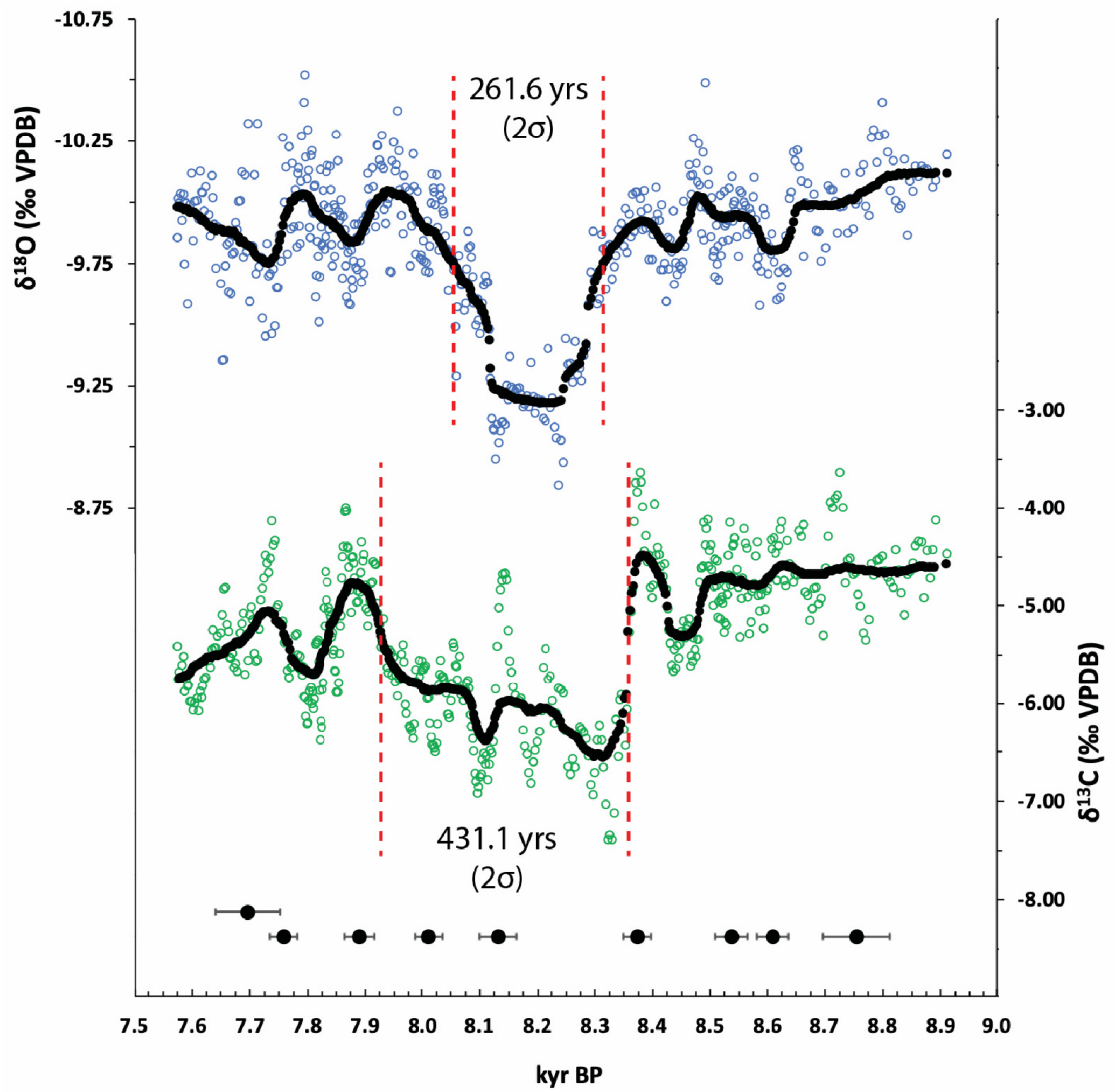

Figure 4.3 – COPRA proxy results and event lengths *– TM-17 stable isotope results ($\delta^{18}O$ and $\delta^{13}C$) from median COPRA output (solid black dots) and proxy response length (dashed vertical lines) to the 8.2 ka event as defined by a 2σ anomaly from the pre-event average (event responses here as defined only by COPRA proxy output). Instrumental results are displayed in open circles, and U-Th ages with uncertainties are above x-axis.*

4.5 Discussion

4.5.1 TM-17 proxy interpretations at the 8.2 ka event

In previous TM studies covering the 8.2 ka event range at lower resolution (Johnson et al., in revision; Wood et al., in prep., a, b), anomalies in all proxies are present around 8.2 kyr BP, and their individual interpretations reveal abrupt drying at the study site visible on multi-decadal

timescales. $\delta^{18}O$ results, interpreted as a proxy for regional monsoon intensity, display a peak of more positive values that represent a weaker regional monsoon at ~8.2 kyr BP (Johnson et al., in revision). This response matches the direction of change in TM-17 $\delta^{18}O$ during millennial-scale Northern Hemisphere cooling events such as Heinrich stadials and the Younger Dryas, which are thought to have a similar climatic forcings to the 8.2 ka event, namely a North Atlantic freshening causing a weakening or cessation of the Atlantic meridional overturning circulation (AMOC) (Alley & Ágústsdóttir, 2005; McManus et al., 2004). More positive values of speleothem $\delta^{18}O$ are also seen at the 8.2 ka event in other records in the EASM, such as Dongge and Heshang Caves (Cheng et al., 2009b; Dykoski et al., 2005; Hu et al., 2008; Y. H. Liu et al., 2013), indicating that the response of a weakened monsoon state across much of East Asia is large in spatial scale.

$\delta^{13}C$ and trace elements (Mg/Ca and Sr/Ca) in TM-17 have been interpreted to be more responsive to the local hydrology above the cave, which is sometimes decoupled from the regional monsoon intensity signal from $\delta^{18}O$. $\delta^{13}C$ from Johnson et al. (in revision), interpreted as a proxy for local water balance, also shows a response to the 8.2 event, although the shift to more negative values is opposite to that of more positive $\delta^{13}C$ during Heinrich stadials. The opposite direction of change for a weaker monsoon / drying event is explained by the varying controls on $\delta^{13}C$ (Wood et al., in prep., b). During the 8.2 ka event, more open system bedrock dissolution, leading to less bedrock input to the carbon pool, directs the $\delta^{13}C$ signal, as biologically controlled inputs to the drip water carbon pool are depleted relative to bedrock. This is in contrast to the non-dissolution controls active during Heinrich stadial 1 (HS1), such as potential changes in above-cave vegetation types, soil moisture, soil respiration rates, and/or

fractionation that create a longer-term positive response in $\delta^{13}C$. These conclusions are supported by a sudden decrease in the dead carbon proportion (DCP) signifying open system bedrock dissolution during the dry period (Wood et al., in prep., b). The lowered input of positive $\delta^{13}C$ sourced from bedrock pushes $\delta^{13}C$ toward more negative values. Prior calcite precipitation (PCP), which fractionates $\delta^{13}C$ and can also act as a non-dissolution control, is interpreted as the dominant driver of TM-17 trace element ratios (Mg/Ca, Sr/Ca) (Wood et al., in prep., a). Mg/Ca and Sr/Ca show some of the highest values in ~38 kyr in an abrupt increase around the 8.2 event due to drying at the study site, as PCP increases trace element ratios during dry periods (Wood et al., in prep., a). However, the resolution of these studies (~30 yrs.), as well as the much lower resolution DCP data, previously prevented a more exact estimate of the onset and length of the event as well as an assessment of any potential leads or lags between the various proxy responses that could further bolster interpretations.

New data from this study provide increased chronological accuracy and sampling resolution for TM-17 stable isotopes and trace elements across the 8.2 ka event, and previous proxy interpretations are applied for a breakdown of the event response. Despite ongoing controversy about the exact interpretation of $\delta^{18}O$ in the Asian Monsoon region (e.g. Chiang et al., 2015; Dayem et al., 2010; Johnson, 2011; Pausata et al., 2011), a more positive $\delta^{18}O$ anomaly is generally indicative of a weak monsoon and/or lowered local rainfall amounts at TM cave (Yang et al., 2016). In regard to the 8.2 ka event in TM-17, the less-negative anomaly at the event seen in this study most likely represents a weakened regional monsoon intensity as supported in Johnson et al. (in revision), similar to the longer-lived events (HS1, The Younger Dryas) that display more extreme responses in the same direction. Additionally, $\delta^{18}O$ in the Asian Monsoon

region responds similarly to the event in regions to the North and East (Cheng et al., 2009b; Hu et al., 2008; Y. H. Liu et al., 2013), and their interpretations are in agreement with a weakened monsoon and/or relatively dry 8.2 response. The maximum value of $\delta^{18}O$ at Heshang Cave is 2.15‰ more positive than the pre-event average (Y. H. Liu et al., 2013), while Dongge Cave and this study report excursions closer to ~1.00‰ during the event (TM-17 $\delta^{18}O$ maximizes at 1.12‰ from the pre-event average, and the range of results from stalagmite D4 in Dongge is 1.31‰) (Cheng et al., 2009b). This difference in magnitude may be due to Y. H. Liu et al., (2013) defining a pre-event average (low resolution data from 9-5 kyr BP) and/or regional differences in the $\delta^{18}O$ of precipitation over large spatial areas.

Multiple controls on $\delta^{13}C$ are potentially active, and interpretations of this proxy often vary in different cave environments. As previously mentioned, TM-17 $\delta^{13}C$ rapidly becomes more negative at the 8.2 event (**Fig. 4.2**), likely due to more open system dissolution during a drier period, allowing more carbon input from biologically controlled values in the soil zone and epikarst (as opposed to the relatively positive values in TM bedrock). However, during a dry period, PCP could also increase. PCP would enrich ^{13}C and contrast with the direction of change created by more open system dissolution. If the event is interpreted as dry throughout, these opposing controls likely explain the high variability in the instrumental $\delta^{13}C$ data during the event (**Fig. 4.2**). The increased length of the event response in $\delta^{13}C$ (relative to $\delta^{18}O$), while discontinuous in the instrumental data, is potentially attributable to changes in vegetation and soil moisture that take longer to recover to pre-event levels. However, the ambiguity of which controls are active on $\delta^{13}C$, and for how long, makes the end of the event difficult to pinpoint with this proxy.

Mg levels depart from the pre-event average in alignment with $\delta^{13}C$, supporting the evidence that the response at TM begins at ~8,355 yrs BP in our age model (**Fig. 4.2**). The previous interpretation of trace element variability being controlled by PCP in TM-17 involves a significant increase in Mg/Ca and Sr/Ca at the 8.2 ka event (Wood et al., in prep., a). In the new high-resolution data set, Mg first decreases significantly before increasing for the majority of the response (**Fig. 4.2).** The initial decrease may be connected to the bedrock dissolution response in $\delta^{13}C$ that begins at the same date. More open system dissolution, or less bedrock dissolution in general, during an abrupt shift to dryness may decrease the concentration of Mg entering the drip water (and speleothem calcite), as bedrock and soil are the major sources of Mg in TM-17 (Wood et al., in prep., a). When the decrease maximizes, ~16.9 years after the initial significant shift in Mg, Mg levels begin to increase rapidly. We suggest PCP then begins to dominate the control of Mg towards the Mg maximum at 8,315.4 yrs BP, ~39.4 years from the event initiation. The short-lived Mg decrease was missed at lower resolutions, but a general interpretation of drying and increasing Mg via PCP is still applicable for the majority of the event response. Additionally, despite the lack of a significant response in LA-ICP-MS Sr data, the Mg and Sr 100 pt. running means used for analysis and plotting in this study covary ($R^2 = 0.41$) at a similar level as lower-resolution ICP-MS data from Wood et al. (in prep., a) ($R^2 = 0.44$ over ~38 kyr), supporting the PCP interpretation for control of trace elements in this sequence (Fairchild & Treble, 2009b; Johnson et al., 2006; Tremaine & Froelich, 2013).

In summary, TM-17 proxy interpretations suggest an abrupt and significant drying at the 8.2 ka event in MSEA. Additionally, the growth rate for TM-17, estimated using the COPRA age model output, reveals the slowest average growth rates (<20 μm/yr) between the two U-Th dates

bordering the event (**Fig. S4.1**). While growth rate is not always a reliable proxy for drip rates and the associated precipitation amounts, low growth rates during this interval are consistent with drying, cooler air temperatures, or a change in Ca^{2+} concentrations (e.g. Y. H. Liu et al., 2013), which could all be signs for the onset of the 8.2 response in TM-17 chemistry.

4.5.2 Comparison with other records and models of the 8.2 ka event

While the age resolution in this study is higher and the age model more well-developed than previous records analyzed from TM-17, other records of the 8.2 ka event have utilized yearly layer counting and likely have a more accurate age model, such as those from Greenland (Thomas et al., 2007) or the EASM region (Y. H. Liu et al., 2013). An onset of 8.25 +/- 0.10 kyr BP is predicted in Y. H. Liu et al. (2013), a stalagmite study from Heshang Cave, China (N30°27', E110°25'; 294 m asl) in which the relatively high growth rate of the sample (annual layers of ~50 – 500 μm) allowed annual layer counting that enhances confidence in the age model. Greenland ice core age models also utilizing annual layer counting leading to lower uncertainty (+/- 50 yrs) display a similar start date (Y. H. Liu et al., 2013; Thomas et al., 2007), and stalagmites from multiple locations in the Asian and South American monsoons record $\delta^{18}O$ anomalies that also suggest the event response begins at a similar time, 8.21 +/- 0.02 kyr BP (Cheng et al., 2009b). The initiation of the event response in TM-17 occurs at 8.35 +/- 0.03 kyr BP (using the largest uncertainty in the two U-Th dates bordering the event) (**Fig. 4.2**), which is within the upper error of the Y. H. Liu et al. (2013) estimate from Heshang Cave. Using only the TM-17 $\delta^{18}O$ data, the statistically significant anomaly begins later, at ~8.29 kyr BP, although a visible increase in $\delta^{18}O$ that is not yet statistically significant begins at the time of the Mg and $\delta^{13}C$ excursions (**Fig. 4.2**). While Mg/Ca data was used as evidence for proxy interpretations in

Y. H. Liu et al. (2013), the event timing estimate is limited to the shifts in $\delta^{18}O$. In the case of TM-17, the multi-proxy information available may be used to estimate a response initiation that would be missed using only $\delta^{18}O$ criteria. However, assigning an exact date may not be as reliable, as the age model in this study contains no supplemental annual layer counting data due to slower growth rates in TM-17 (~10-40 μm/yr; **Fig. S4.1**).

Depending on the proxy and criteria applied, the length of the 8.2 ka event response in TM-17 proxies is similar to or longer than the estimates of prior studies, which have the event length at ~150-160 years (Cheng et al., 2009b; Y. H. Liu et al., 2013; Thomas et al., 2007). The 2σ anomaly in instrumental $\delta^{18}O$ data that lasts 174 years is the most similar (**Fig. 4.4**). A 1σ $\delta^{18}O$ anomaly from the pre-event average reaches 207.3 years in TM-17 instrumental data and up to 261.6 years in $\delta^{18}O$ COPRA results (**Figs. 4.2, 4.3**), suggesting that even the event response as described only by $\delta^{18}O$ could be extended in our study region. Assuming a regional monsoon intensity interpretation of $\delta^{18}O$, the event may have only affected the greater monsoon for a time range similar to the mentioned studies, while the proxies more indicative of local water balance reveal a longer response.

However, the exact timing of the event's start and end is less clear among the other TM-17 proxies. The significant (2σ) response in $\delta^{18}O$ occurs up to 68.5 years later than the 2σ shift in both $\delta^{13}C$ and Mg, suggesting that the event starts earlier than suggested by $\delta^{18}O$ (**Fig. 4.2**). As $\delta^{13}C$ and Mg have both been interpreted to be more responsive to local hydrologic factors, the start of the local climate response is likely more well-defined by $\delta^{13}C$ and Mg. Both of these proxies suggest the statistically significant (2σ) response begins at ~8,356 yrs BP, but the end of the event is more difficult to pinpoint. There is no clear endpoint to the discontinuous anomalies

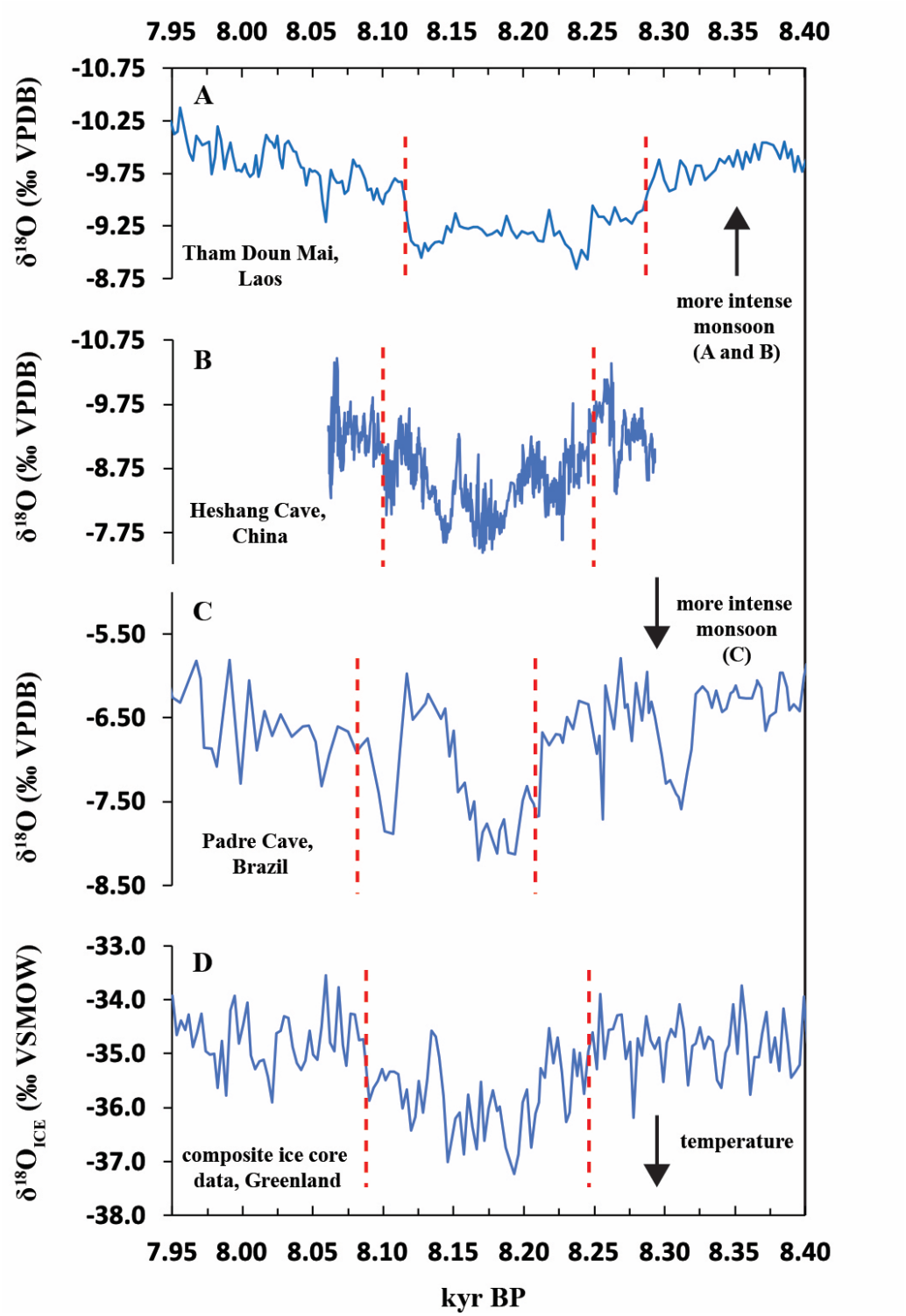

Figure 4.4 – Comparisons of 8.2 ka event responses around the globe *– Dashed vertical lines approximate the event beginning and end as according to the criteria of each study.* ***A*** *– Stalagmite TM-17 from Tham Doun Mai, Northern Laos (this study);* ***B*** *– HS4 stalagmite from Heshang Cave, China (Y. H. Liu et al., 2013);* ***C*** *– PAD07 stalagmite from Padre Cave, Brazil (Cheng et al., 2009b);* ***D*** *– a composite, normalized record of isotopic data from four ice cores in Greenland, details of which can be found in Thomas et al. (2007).*

in Mg, and the relatively slow recovery of $\delta^{13}C$ continues for many decades beyond the end of the $\delta^{18}O$ anomaly (**Fig. 4.2**). When using COPRA proxy outputs and a 2σ criteria, the $\delta^{13}C$ anomaly lasts for an additional 169.5 years, which would double the total event length. It is possible that the dry conditions (relative to the pre-event average) continued at our site for many years after the event influenced the greater monsoon system, creating the extended and ambiguous event recovery in $\delta^{13}C$ and Mg. The much longer event response of $\delta^{13}C$ at 2σ (417.6 or 431.1 years using a discontinuous instrumental anomaly or the COPRA outputs, respectively) is either a result of the specific controls on $\delta^{13}C$, such as vegetation and soil zone changes, that may take much longer to recover to pre-event values after a significant drying event, or a result of locally dry conditions that continue for decades or centuries after the event.

To summarize the event length as defined by TM-17 proxy data, the response range could last from 173 years ($\delta^{18}O$ instrumental data using 2σ anomaly range; **Fig. 4.2**) to a maximum of 431.1 years ($\delta^{13}C$ COPRA data; **Fig. 4.3**). Using $\delta^{13}C$ and Mg data for the initiation of the event and the 2σ anomaly in $\delta^{18}O$ instrumental data as the end of the event (earlier than the cessation of the anomaly in COPRA data), the event response in TM-17 proxies lasts for 240 years (~8,356 – 8,116 yrs BP). Using a 1σ criteria in instrumental $\delta^{18}O$ as the endpoint, the length increases to 270 years (**Fig. 4.2**). These estimates may be a conservative minimum length for the MSEA hydrological response based on the additional proxy information presented. These observations may also be local to MSEA or the result of a lack of multi-proxy data used to investigate the event length in previous studies.

Model simulations have been successful in reproducing the 8.2 ka event in some respects, such as the overall pattern of global precipitation and temperature change. Climate models simulating the event often use freshwater forcing in the North Atlantic (via Hudson Bay) as the catalyst, as the draining of the ice age lakes Agassiz and Ojibway from the Laurentide ice sheet remnant is hypothesized to be the root cause of the event (e.g. Barber et al., 1999; Morrill et al., 2013a). In a comparison of four simulations using three earth system models (CCSM v. 3, GISS ModelE-R, and LOVECLIM v. 1.2; references in Morrill et al. (2013a)), Morrill et al. (2013a) used a meltwater pulse (MWP) of 2.5 Sv (Sverdrup = 10^6 m^3 s^{-1}) over 1 year to simulate the event, an estimate of the rate of freshwater release based on the work of Clarke et al., (2004). Comparing these simulations to spatially widespread proxy records of the 8.2 event, the authors find that the patterns of global change often match in the direction of temperature and precipitation anomalies, yet the duration is typically too short, and the magnitudes are not well-matched. In simulations run with the HADCM3 GCM, Tindall & Valdes (2011) reach similar conclusions, as a 5 Sv input of freshwater caused global patterns similar to proxy records but unable to match the longevity. Timing the freshwater release to a relatively weak AMOC period or the addition of background ice sheet melt could be necessary to increase the intensity and longevity of the event to match proxy records (Tindall & Valdes, 2011).

In reference to MSEA, simulations show modest but irregularly-spaced drying, while proxy records from the EASM display a consistent dry response (**Fig. 4.5**; (Morrill et al., 2013a; Morrill et al., 2013b). TM-17 proxy data extend the available record of 8.2 responses farther south, from the EASM domain into MSEA, and give evidence for the modeled drying response on MSEA to be robust. The length of the anomalies in TM-17 proxies also support conclusions

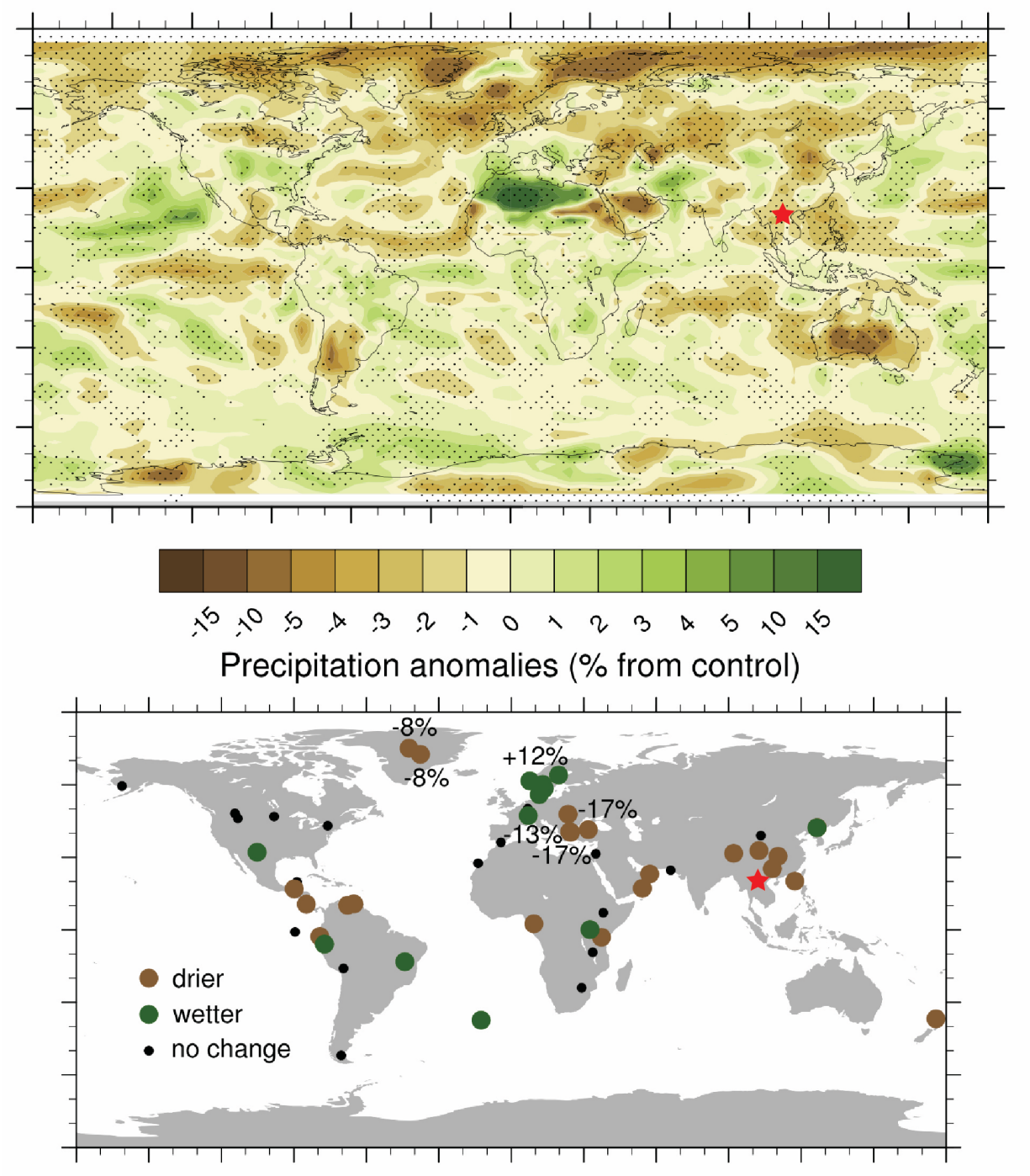

Figure 4.5 – Model and proxy comparisons – *Figure from Morrill et al. (2013a). Upper panel shows simulation results for a N. Atlantic freshwater-forced 8.2 ka event precipitation anomaly (% change from control). Lower panel displays the wet or dry response (and/or % change from quantified records) of proxy records (references in Morrill et al., 2013a). Red stars indicate approximate location of Tham Doun Mai (not in original figure).*

that the event was longer lived (at least 173 years) than most simulation results, suggesting that proposed changes to model simulations may be necessary, such as a larger freshwater forcing, higher sensitivity of climate to freshwater inputs in the North Atlantic, and/or a weakened AMOC background state (Morrill et al., 2013a; Tindall & Valdes, 2011).

Outside of the question of proxy response length, the initial timing and expected direction of response (i.e. weakened monsoon) in TM-17 $\delta^{18}O$ is in agreement (within errors) with previous studies and published records of the 8.2 ka event around the world, including other speleothem records from Asia, Oman, and Brazil, as well as Greenland temperature proxy records from ice cores (**Fig. 4.4**) (Cheng et al., 2009b; Y. H. Liu et al., 2013; Thomas et al., 2007). A weakened Asian monsoon coincides with a strengthened South American summer monsoon in reaction to the 8.2 ka event, which all occur around the time of abrupt temperature drops in Greenland, revealing the global extent of climate anomalies (Cheng et al., 2009b). Some proxy records of the 8.2 event display evidence for a multi-stage event, which could potentially be caused by separate drainage events from the glacial lakes into the North Atlantic (Alley et al., 1997; Ellison et al., 2006; LeGrande & Schmidt, 2008; Teller et al., 2002). In the EASM domain, as well as monsoon records from Brazil that display an anti-phase response, previously reported proxy records sometimes display a "double-plunging" structure that may indicate multiple stages of the event (**Fig. 4.4**) (Cheng et al., 2009b). However, LeGrande & Schmidt (2008) find, using ensemble isotope-enabled coupled atmosphere ocean climate model (GISS ModelE-R), that multiple meltwater stages are not required to create a multi-stage climate event, although they also cannot rule out the possibility. TM-17 instrumental $\delta^{18}O$ contains a comparable double-plunging structure as well a similar end-date (~8.12 kyr BP) to the event response estimated in

Cheng et al., 2009b utilizing several records (8.08 kyr BP) (**Fig. 4.4**). However, other TM-17 proxies, as well as COPRA $\delta^{18}O$ output, do not mirror the exact timing or structure of the instrumental TM-17 $\delta^{18}O$ data. These mismatches may provide evidence that the instrumental $\delta^{18}O$ data is the most appropriate data to compare with previous 8.2 ka event proxy studies, but the extended response in $\delta^{13}C$ and Mg also suggest that the period of aridity attributable to the event is extended in MSEA relative to other regions. However, the multiple controls likely active on $\delta^{13}C$ and the irregular and ongoing shifts in Mg data after the event are potentially to blame for a less-conclusive event length and structures that differ from the $\delta^{18}O$ response.

4.6 Conclusions

Multiple proxies in stalagmite TM-17 from Tham Doun Mai cave, Laos provide evidence for a MSEA response to the 8.2 ka event comparable to well-constrained proxy records of the event around the globe. The response indicates abrupt dryness in response to a weakened monsoon, which is in agreement with the results of both proxy studies and models of global change during the event. New U-Th dates provide improved age modeling and enhanced resolution compared to previous TM-17 analyses that covered the last ~38 kyr, while the longevity of previous studies enhances confidence in the interpretations of involved proxies. Compared to the pre-event average calculated from new high-resolution data, the positive excursion of $\delta^{18}O$ (2σ) around 8.2 ka (~8289 – 8,116 yrs BP in our age model) indicates a weakened monsoon state in MSEA with a minimum length of 173 years. The length of the response as defined by the 2σ anomaly in $\delta^{18}O$ is extended by ~66 years (~239 years total) if the event initiation is defined by significant (2σ) excursions in $\delta^{13}C$ and Mg, which display an abrupt start to the local hydrologic response (~8,355 yrs BP) and an extended period of discontinuous excursions from the pre-event average

that lasts ~200-400 years. Based on these proxies, which are more responsive to the local water balance, the local MSEA drying may last longer than the regional monsoon weakening, and the importance of the inclusion of multiple speleothem proxies when developing event records is evident.

The minimum length for the TM-17 response (173 years in $\delta^{18}O$) aligns with estimated lengths of the event from Greenland, the EASM, Brazil, and Oman proxy records (~150-160 years), suggesting TM-17 $\delta^{18}O$, representing widespread monsoon weakening, may be the most appropriate proxy for estimating a climate anomaly with global significance. While previous 8.2 studies with age models supplemented by annual layer counting may provide a more confident estimate for the exact dates involved, this study provides a similar estimate of the event initiation and new event length estimates in a region lacking highly resolved records. The minimum TM-17 proxy response length agrees with the assessments of modeling studies that find simulations of the event are typically too short-lived and may require a higher overall input of North Atlantic freshwater, faster rates of input, higher climate sensitivity to freshwater forcing, and/or a weakened AMOC state prior to the freshwater release. Our results are the first high-resolution proxy study from MSEA that record how the 8.2 ka event affected the monsoon intensity and local hydrology in this region, confirming the expected dryness predicted by models and relatively close regions in East Asia.

4.7 Supplementary Methods

Synchrotron radiation X-ray fluorescence - from (J. K. Wang et al., 2019)

Synchrotron radiation X-ray fluorescence (XRF) microscopy was performed on the XFM beamline at the Australian Synchrotron (Paterson et al., 2011) using the Kirkpatrick-Baez mirror microprobe end-station. A 12 mm-thick polished slab was analyzed with a monochromatic 2 μm beam spot size and energy at 18.5 keV. A 45 x 2 mm map was acquired in the axial part of the stalagmite at 2 μm pixel size resolution on both axis and a dwell time of 1.2 ms/pixel, yielding a detection limit for Sr of ~ 2 ppm. Single element foils Mn, Fe and Pt (Micromatter, Canada) were utilized as references to calibrate the final elemental spectra. The Maia XRF spectral data were analyzed using the GeoPIXE software suite which uses a fundamental parameters approach, with spectral deconvolution and imaging using the dynamic analysis method. Spectra were fitted using X-ray line relative intensities that reflect integration of yields and X-ray self-absorption effects for the calcite matrix and the contrasting efficiency characteristics across the detector array (Ryan et al., 2010).

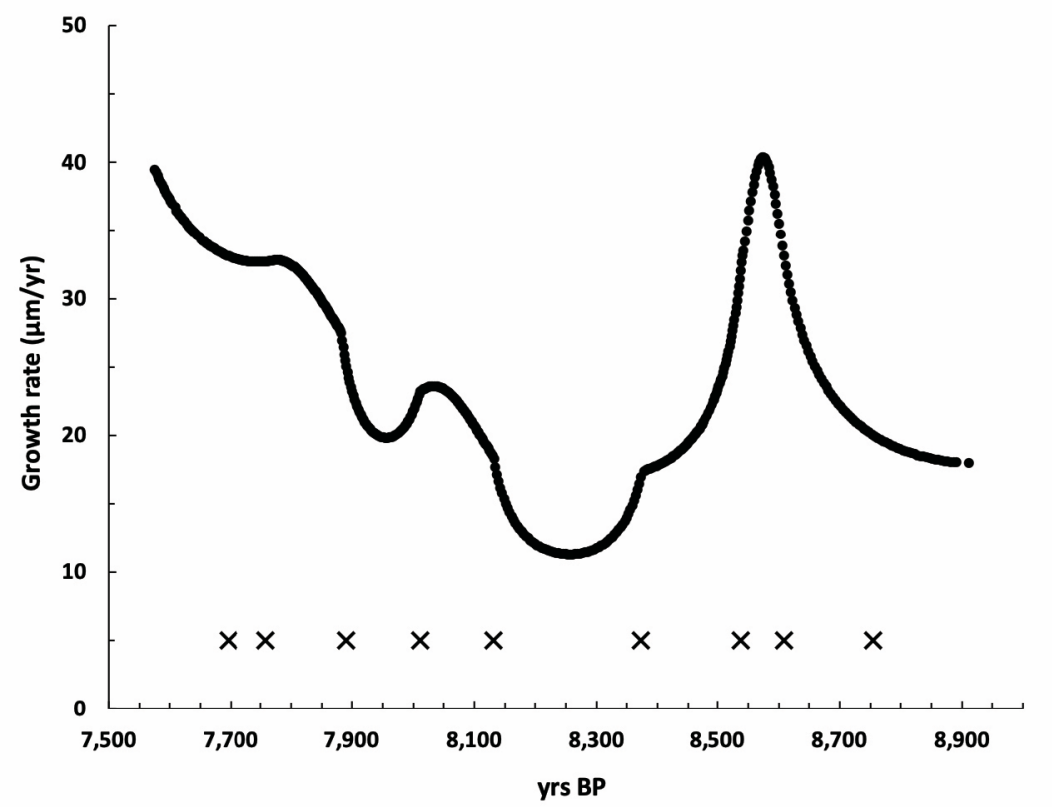

Figure S4.1 – TM-17 estimated growth rates – *Growth rates (black dots) for the section of TM-17 used in this study in µm/yr, which is calculated using the COPRA age model output (513 pts.). Points of inflection in growth rate occur at the location of U-Th dates (x's) and reveal the modeled connectivity between sections as average growth rate changes. The lowest average growth rates are estimated during the approximate timing of the 8.2 ka event response (~8,373 – 8,131 yrs BP).*

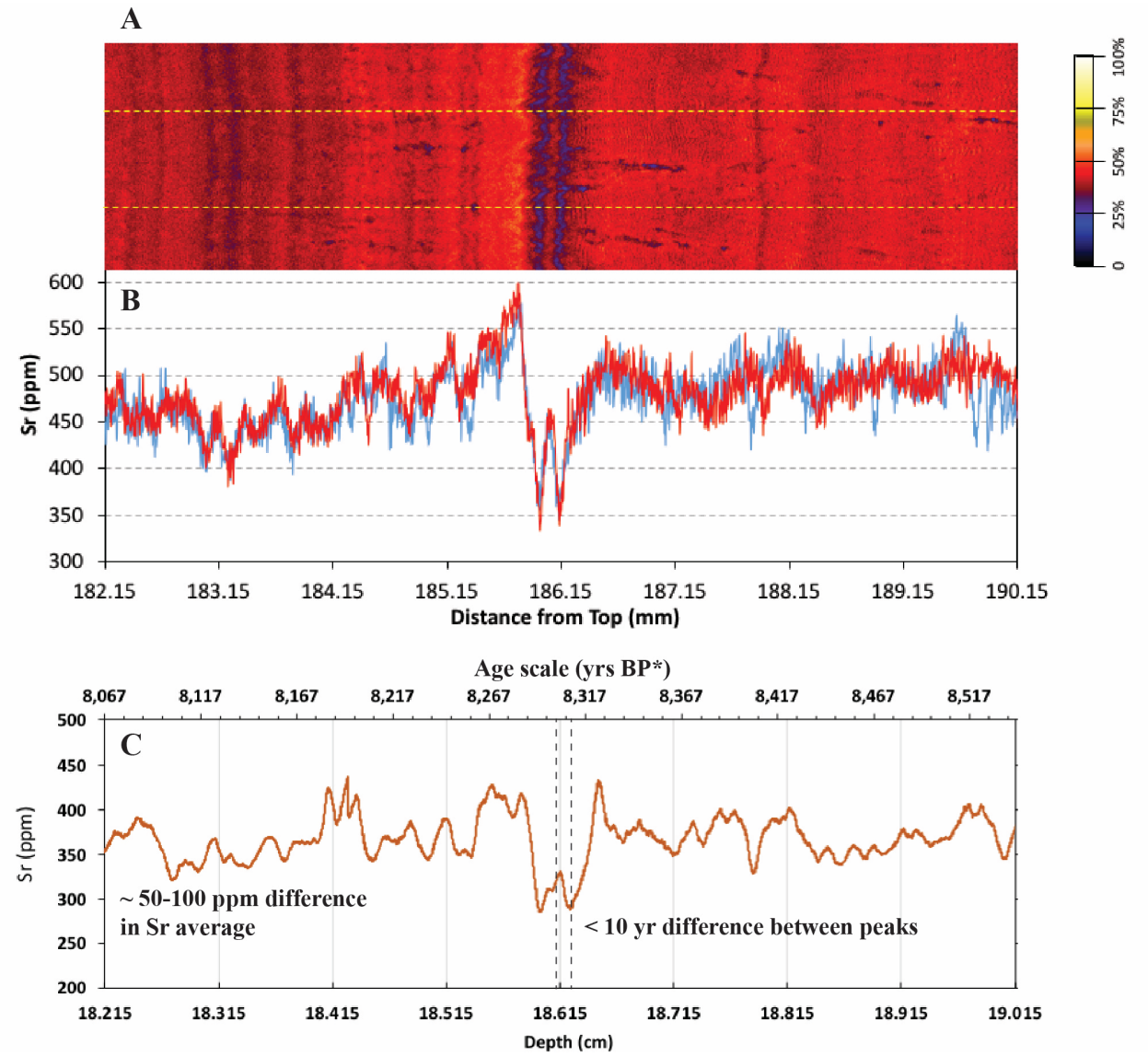

Figure S4.2 – Comparison between Synchrotron and LA-ICP-MS Sr analyses – *A: Visual results of synchrotron Sr data; B: Synchrotron Sr measurements plotted with distance from top of TM17; C: LA-ICP-MS analysis of Sr (100 pt running mean) with depth (distance from top) on bottom axis and age scale on top axis (*age model (growth rate) not accounted for in depth to age matching, so ages are not exact with age model plots vs. depth). There is less than ~10 yr difference in location of double peak in Sr near the beginning of 8.2 ka event between instruments, despite using separate pieces of TM17 and independent depth estimates. Range of Sr varies by roughly 50-100 ppm.*

Chapter 5

Conclusions

In the presented studies, speleothem trace element (Mg and Sr) ratios and concentrations, along with both radiogenic (^{14}C) and stable carbon ($\delta^{13}C$) isotopes are examined to reconstruct hydrologic changes in the Late Pleistocene and Holocene periods on Mainland Southeast Asia (MSEA), where terrestrial climate records are scarce. Using a well-dated stalagmite (TM-17), new records of Mg/Ca, Sr/Ca and the dead carbon proportion (DCP, based on ^{14}C measurements) are interpreted to describe past hydrological changes at Tham Doun Mai cave (TM), Laos over a ~38,000-year time period. In addition to examining long term trends in relative rainfall amounts, a key focus is on how global climate events since the last deglaciation, which are already well-documented in the East Asian Monsoon and other locations around the globe, may have affected local hydrology in MSEA. The results provide evidence that MSEA rainfall was decreased during the abrupt, millennial to centennial scale climate events that weakened the Asian Monsoon during the deglaciation and Holocene, including Heinrich Stadial 1 (HS1), the Younger Dryas (YD), and the 8.2 ka event. Additionally, the results show that the regional monsoon strength signal interpreted using $\delta^{18}O$ from TM does not always reflect the corresponding local hydrologic history at our study site, an observation most prominent in the early to mid-Holocene, where Northern Hemisphere summer insolation maxima and $\delta^{18}O$ minima suggest a more intense monsoon occurs several thousand years before a peak in rainfall seen in Mg/Ca, Sr/Ca, and $\delta^{13}C$.

The higher resolution records of TM-17 proxies during the 8.2 ka event also reveal key differences in the timing and length of proxy responses during this relatively recent climate anomaly: while the overall response time of TM-17 in $\delta^{18}O$ is comparable with other regional and global records of the 8.2 ka event, the addition of proxies more tied to local hydrology show that rainfall was significantly altered decades prior to the significant change in $\delta^{18}O$, and the local hydrologic disruption at TM may last much longer than apparent using only $\delta^{18}O$ data.

A lack of numerous paleoclimate proxy records from MSEA is one of the main drivers of this research, and other proxy records from this and associated regions could improve confidence in the conclusions. The uncertainties present in speleothem age models and proxy measurements, as well as the complicated interpretations due to numerous controls, create a strong need for replication. More speleothem analyses from TM, other caves in the same karst region, and/or an extension of the research locations into other areas of MSEA could provide robust comparisons for the findings of this work. The Johnson Lab at the University of California, Irvine (Department of Earth System Science) has already begun sampling and monitoring caves in Southern Laos, where analyses of future samples may provide verification of TM records and/or reveal differences in the precipitation history from two regions of MSEA. Additionally, work has begun in Vietnam on the opposite side of the Annamite Mountains in a karst region that experiences an alternative wet season and receives moisture from a distinctly different source of water vapor (the South China Sea as opposed to the Bay of Bengal). Future samples from this region in Vietnam may assist the Johnson Lab's research by further breaking down $\delta^{18}O$ controls in the Southeast Asian Monsoon as well as developing hydrologic histories from the new area.

Many of the major climate events studied in this dissertation (HS1, YD, 8.2) likely involve past meridional shifts in the intertropical convergence zone (ITCZ), so additional speleothem records of the tropics and subtropics from MSEA to Northern Australia could provide new evidence of the extent of ITCZ shifts and how they affected the monsoon strength and hydrology of each region. The early deglacial period prior to HS1, when TM-17 trace elements and DCP suggest a dry period, would be an exciting time period to study in new samples from low-latitude regions, as hints of large hydrologic changes are seen in TM-17, Indonesia, and Northern Australia, which could be corroborated and further developed by samples from new sites.

A distinct opportunity for the refinement of our speleothem interpretations from MSEA could arise with a sample containing annual growth layers for some or all of the time periods in question. While seasonal changes may sometimes affect speleothem proxies, the resolution of the records from TM typically only reveal multi-decadal changes. Even the high-resolution work during the 8.2 period never exceeds 1-2 years per sampling point. Determining if some of the hydrological changes seen in our proxies were brought about by differences in summer vs. winter rainfall amounts or seasonally changing rainfall sources could provide valuable information and assist in interpretations of the climatic changes during dramatic events. For example, some studies of the 8.2 ka event from some regions determine that changes in climate during the Northern Hemisphere winter months control the proxy responses. If the ratio of summer to winter precipitation changed in MSEA during this event or at other times in our record, interpretations of $\delta^{18}O$ and other proxies might need to be refined. Additionally, annual layers can create an age model with lower uncertainties, which assists in all interpretations and claims made from proxy records.

Other than developing existing and novel speleothem proxies mentioned in Chapter 1, the addition of more data from other archives, such as tree rings or lake sediment cores, would provide independent analyses of climate and hydrology at any sites within the low-latitude region of the Asian-Australian monsoon. Tree ring records of rainfall could be used for comparison with more recent speleothem growth in order to investigate interpretations, and this type of work is already in progress in the Johnson Lab and with collaborators. Currently, there are not a great number of pollen records over the desired time frames, potentially because karst regions do not often contain stable, above-ground bodies of water. More pollen records from lake sediment cores could provide evidence of vegetation changes over long timescales, and as $\delta^{13}C$ from TM-17 is likely influenced by vegetation changes, more records of pollen from MSEA within the appropriate time periods could add robust evidence for the $\delta^{13}C$ interpretations and associated climatic changes.

The multiproxy speleothem methods used in this study could be applied to other caves and samples for further refinement of the controls and chemical relationships at play. For example, similar work with existing or new data sets could determine whether the relationship between DCP and $\delta^{13}C$ seen in TM-17 is typical in a stalagmite with a high and variable DCP. Bedrock dissolution is not commonly attributed to $\delta^{13}C$ variability in climate reconstructions, and the level of DCP may be a reliable test for when this control is significant. The relationship between Mg/Ca and Sr/Ca is often examined in stalagmite studies, and the hydrologic control revealed by investigating their ratios and covariance established in previous studies could be refined with future analysis of multiple stalagmites and drip sites. The dissolution signal seen in TM-17 DCP could potentially be applied to trace element data, as they are heavily bedrock sourced, and

relationships between Mg/Ca, Sr/Ca, and DCP may reveal more clues about each proxy's relationship to open vs. closed system bedrock dissolution as a sign of past rainfall change.

There are also many opportunities to examine speleothem proxy relationships in the laboratory. As a postdoctoral scholar at the University of Waikato, New Zealand, I plan to utilize newly developed laboratory instrumentation that precipitates calcite in cave-analogue conditions. I see bedrock dissolution input and the DCP and a potential focus for this work, as development of this proxy in stalagmites with significant DCP could be coupled with high-resolution sampling of ^{14}C to create robust hydrologic records. The sulfuric acid dissolution (SAD) control on DCP is a relatively new area of focus in speleothem research, and I believe that this and similar mechanisms active during dissolution may have significant and as-of-yet unknown effects on the trace element and isotopic chemistry of drip waters and stalagmites. These ideas could potentially be explored by seeding drip waters with ^{14}C-dead $CaCO_3$ and discrete amounts of sulfate and/or sulfuric acid to mimic SAD. The resulting precipitate could provide new information on the DCP in existing and new stalagmite records. Additionally, by mixing ^{14}C-dead and modern sources of $CaCO_3$, the precipitation of DCP in calcite from known drip water concentrations could refine hypotheses about how DCP and modern carbon sources are partitioned in stalagmite calcite. Refinements to these hypotheses would then, in turn, assist in interpretations of $\delta^{13}C$, which may always involve a unique mix of controls in any cave setting.

While future work is an exciting prospect, it is important to fully develop the new records and data sets presented in this research. Perhaps the most exciting results in this dissertation are the sharp proxy responses in Mg, Sr, and $\delta^{13}C$ at the 8.2 ka event in TM-17. As there is ongoing

interest in this relatively modern, abrupt, and significant climate disruption, developing a method for determining a quantifiable amount of rainfall change from the multi-proxy system would be a major goal for this or other 8.2 records from the Asian Monsoon region. Through future data analysis, collaborations with climate modelers, and/or analyzing additional samples from the region, we may eventually provide estimates on the amount of rainfall change during this event, which would assist in establishing the sensitivity of hydrology on MSEA to global changes.

As the overarching goal of paleoclimate study is to better understand the Earth system and more confidently project future climate change, applying the findings of monsoon region paleoclimate records to future change should be an ultimate goal of any speleothem scientist. While the current anthropogenic CO_2 forcing of our modern climate is not likely to be duplicated in a speleothem record of the past, the sensitivity of the monsoon to past temperature change and sea level rise can be used to help predict future changes in rainfall. While future research projects may sometimes focus on geochemistry, laboratory experiments, and a better understanding of speleothem and karst region paleoclimate proxies, a clearer picture of future climate will be a goal when developing final records of past climate enhanced by the more specific studies. In this way, the knowledge gained about the past environments via cave samples will improve the knowledge of our climate future, the study of which may be the most impactful field for scientific study in the coming decades and centuries.

The research results presented and discussed in this dissertation provide new paleoclimate records in a region lacking in records of similar length and quality. While the broad assumptions of past rainfall in MSEA based on speleothem proxies and cave-karst hydrology could be

improved by future work and/or replication, the signals of climatic and hydrologic change seen at our study site add to a growing network of proxy records in the region. The weakened monsoon periods during climate events of last deglaciation and Holocene can now be confidently extended from the East Asian Summer Monsoon into MSEA, and the proxy records presented here provide evidence that a weakened monsoon also reduces rainfall amounts in the MSEA region. However, we observe that the monsoon intensity signal is not always coupled with rainfall amounts in MSEA, especially in regard to the early and mid-Holocene discrepancies, suggesting a multiproxy approach in this region may be necessary when constructing climate records of past hydrologic change. Additionally, multiple proxies in our sample are needed to fully define the extent of the 8.2 ka event response, showing that important changes in past climate should not be left to the interpretations or timing of one proxy response. Speleothems are often unique in their chemistry and relationships to the local environment, and a well-dated sample over the desired time periods and in the desired location is not always available. Thus, a multiproxy approach allows the maximum amount of data to be extracted from a well-dated and useful sample. The new records presented here will provide comparisons for future proxy investigations and modeling studies looking into the past climate of MSEA, and they will give insight into global changes over the last deglaciation and Holocene, which will in turn assist in projecting future changes of the hydroclimate of Southeast Asia.

References

Alley, R. B., Mayewski, P. A., Sowers, T., Stuiver, M., Taylor, K. C., & Clark, P. U. (1997). Holocene climatic instability: A prominent, widespread event 8200 yr ago. *Geology*, *25*(6), 483–486. https://doi.org/10.1130/0091-7613(1997)025<0483:HCIAPW>2.3.CO;2

Alley, R. B. (2003). Palaeoclimatic insights into future climate challenges. *Philosophical Transactions of the Royal Society of London. Series A: Mathematical, Physical and Engineering Sciences*, *361*(1810), 1831–1849. https://doi.org/10.1098/rsta.2003.1236

Alley, R. B., & Ágústsdóttir, A. M. (2005). The 8k event: Cause and consequences of a major Holocene abrupt climate change. *Quaternary Science Reviews*, *24*(10–11), 1123–1149. https://doi.org/10.1016/j.quascirev.2004.12.004

An, Z., Porter, S. C., Kutzbach, J., Xihao, W., Suming, W., Xiaodong, L., et al. (2000). Asychrnous Holocene optimum of the East Asian monsoon. *Quaternary Science Reviews*, *19*, 743–762.

Ayliffe, L. K., Gagan, M. K., Zhao, J. X., Drysdale, R. N., Hellstrom, J. C., Hantoro, W. S., et al. (2013). Rapid interhemispheric climate links via the Australasian monsoon during the last deglaciation. *Nature Communications*, *4*(May), 1–6. https://doi.org/10.1038/ncomms3908

Bajo, P., Borsato, A., Drysdale, R., Hua, Q., Frisia, S., Zanchetta, G., et al. (2017). Stalagmite carbon isotopes and dead carbon proportion (DCP) in a near-closed-system situation: An interplay between sulphuric and carbonic acid dissolution. *Geochimica et Cosmochimica Acta*, *210*, 208–227. https://doi.org/10.1016/j.gca.2017.04.038

Baker, A., Genty, D., & Fairchild, I. J. (2000). Hydrological characterisation of stalagmite dripwaters at Grotte de Villars, Dordogne, by the analysis of inorganic species and luminescent organic matter. *Hydrology and Earth System Sciences*, *4*(3), 439–449. https://doi.org/10.5194/hess-4-439-2000

Baker, A., Ito, E., Smart, P. L., & McEwan, R. F. (1997). Elevated and variable values of 13C in speleothems in a British cave system. *Chemical Geology*, *136*(3–4), 263–270. https://doi.org/10.1016/S0009-2541(96)00129-5

Banner, J. L., Musgrove, M., Asmerom, Y., Edwards, R. L., & Hoff, J. A. (1996). High-resolution temporal record of Holocene ground-water chemistry: Tracing links between climate and hydrology. *Geology*, *24*(11), 1049. https://doi.org/10.1130/0091-7613(1996)024<1049:HRTROH>2.3.CO;2

Barber, D. C., Dyke, A., Hillaire-Marcel, C., Jennings, A. E., Andrews, J. T., Kerwin, M. W., et al. (1999). Forcing of the cold event of 8,200 years ago by catastrophic drainage of Laurentide lakes. *Nature*, *400*(6742), 344–348. https://doi.org/10.1038/22504

Bauer, J. E., Williams, P. M., & Druffel, E. R. M. (1992). 14C activity of dissolved organic carbon fractions in the north-central Pacific and Sargasso Sea. *Nature*, *357*(6380), 667–670. https://doi.org/10.1038/357667a0

Beck, J. W., Zhou, W., Li, C., Wu, Z., White, L., Xian, F., et al. (2018). A 550,000-year record of East Asian monsoon rainfall from 10Be in loess. *Science (New York, N.Y.)*, *360*(6391), 877–881. https://doi.org/10.1126/science.aam5825

Belli, R., Borsato, A., Frisia, S., Drysdale, R., Maas, R., & Greig, A. (2017). Investigating the hydrological significance of stalagmite geochemistry (Mg, Sr) using Sr isotope and particulate element records across the Late Glacial-to-Holocene transition. *Geochimica et Cosmochimica Acta*, *199*, 247–263. https://doi.org/10.1016/j.gca.2016.10.024

Bergel, S. J., Carlson, P. E., Larson, T. E., Wood, C. T., Johnson, K. R., Banner, J. L., & Breecker, D. O. (2017). Constraining the subsoil carbon source to cave-air CO2and speleothem calcite in central Texas. *Geochimica et Cosmochimica Acta*, *217*, 112–127. https://doi.org/10.1016/j.gca.2017.08.017

Berger, A. (1992). Orbital variations and insolation database. IGBP PAGES/World Data. Center-A for Paleoclimatology Data Contribution Series #92-007. NOAA/NCDC. Paleoclimatology Program. *Ftp://Ftp.Ncdc.Noaa.Gov/Pub/Data/Paleo/Insolation/Orbit91*. Retrieved from https://ci.nii.ac.jp/naid/10023994571/

Berger, A., & Loutre, M. F. (1991). Insolation values for the climate of the last 10 million years. *Quaternary Science Reviews*, *10*(4), 297–317. https://doi.org/10.1016/0277-3791(91)90033-Q

Beverly, R. K., Beaumont, W., Tauz, D., Ormsby, K. M., von Reden, K. F., Santos, G. M., & Southon, J. R. (2010). The Keck Carbon Cycle AMS Laboratory, University of California, Irvine: Status Report. *Radiocarbon*, *52*(2), 301–309. https://doi.org/10.1017/S0033822200045343

Bond, G., Heinrich, H., Broecker, W., Labeyrie, L., McManus, J., Andrews, J., et al. (1992). Evidence for massive discharges of icebergs into the North Atlantic ocean during the last glacial period. *Nature*, *360*(6401), 245–249. https://doi.org/10.1038/360245a0

Borsato, A., Frisia, S., Fairchild, I. J., Somogyi, A., & Susini, J. (2007). Trace element distribution in annual stalagmite laminae mapped by micrometer-resolution X-ray fluorescence: Implications for incorporation of environmentally significant species. *Geochimica et Cosmochimica Acta*, *71*(6), 1494–1512. https://doi.org/10.1016/j.gca.2006.12.016

Breecker, D. O., Payne, A. E., Quade, J., Banner, J. L., Ball, C. E., Meyer, K. W., & Cowan, B. D. (2012). The sources and sinks of CO 2 in caves under mixed woodland and grassland vegetation. *Geochimica et Cosmochimica Acta*, *96*, 230–246. https://doi.org/10.1016/j.gca.2012.08.023

Breitenbach, S. F. M., Rehfeld, K., Goswami, B., Baldini, J. U. L., Ridley, H. E., Kennett, D. J., et al. (2012). Constructing proxy records from age models (COPRA). *Climate of the Past*, *8*(5), 1765–1779. https://doi.org/10.5194/cp-8-1765-2012

Broccoli, A. J., Dahl, K. A., & Stouffer, R. J. (2006). Response of the ITCZ to Northern Hemisphere cooling. *Geophysical Research Letters*, *33*(1), 1–4. https://doi.org/10.1029/2005GL024546

Broecker, W., Bond, G., Klas, M., Clark, E., & McManus, J. (1992). Origin of the northern Atlantic's Heinrich events. *Climate Dynamics*, *6*(3–4), 265–273. https://doi.org/10.1007/BF00193540

Broecker, W. S. (1994). Massive iceberg discharges as triggers for global climate change. *Nature*, *372*(6505), 421–424. https://doi.org/10.1038/372421a0

Cheng, H., Edwards, R. L., Broecker, W. S., Denton, G. H., Kong, X., Wang, Y., et al. (2009a). Ice Age Terminations. *Science*, *326*(5950), 248–252. https://doi.org/10.1126/science.1177840

Cheng, H., Fleitmann, D., Edwards, R. L., Wang, X., Cruz, F. W., Auler, A. S., et al. (2009b). Timing and structure of the 8.2. kyr B.P. event inferred from δ 18O records of stalagmites from China, Oman, and Brazil. *Geology*, *37*(11), 1007–1010. https://doi.org/10.1130/G30126A.1

Cheng, H., Sinha, A., Wang, X., Cruz, F. W., & Edwards, R. L. (2012). The Global Paleomonsoon as seen through speleothem records from Asia and the Americas. *Climate Dynamics*, *39*(5), 1045–1062. https://doi.org/10.1007/s00382-012-1363-7

Cheng, H., Lawrence Edwards, R., Shen, C. C., Polyak, V. J., Asmerom, Y., Woodhead, J., et al. (2013). Improvements in230Th dating,230Th and234U half-life values, and U-Th isotopic measurements by multi-collector inductively coupled plasma mass spectrometry. *Earth and Planetary Science Letters*, *371–372*, 82–91. https://doi.org/10.1016/j.epsl.2013.04.006

Cheng, H., Edwards, R. L., Sinha, A., Spötl, C., Yi, L., Chen, S., et al. (2016). The Asian monsoon over the past 640,000 years and ice age terminations. *Nature*, *534*(7609), 640–646. https://doi.org/10.1038/nature18591

Cheng, H., Lawrence Edwards, R., Southon, J., Matsumoto, K., Feinberg, J. M., Sinha, A., et al. (2018). Atmospheric 14C/12C changes during the last glacial period from hulu cave. *Science*, *362*(6420), 1293–1297. https://doi.org/10.1126/science.aau0747

Chiang, J. C. H., & Bitz, C. M. (2005). Influence of high latitude ice cover on the marine Intertropical Convergence Zone. *Climate Dynamics*, *25*(5), 477–496. https://doi.org/10.1007/s00382-005-0040-5

Chiang, J. C. H., Fung, I. Y., Wu, C. H., Cai, Y., Edman, J. P., Liu, Y., et al. (2015). Role of seasonal transitions and westerly jets in East Asian paleoclimate. *Quaternary Science Reviews*, *108*, 111–129. https://doi.org/10.1016/j.quascirev.2014.11.009

Clark, P. U., Dyke, A. S., Shakun, J. D., Carlson, A. E., Clark, J., Wohlfarth, B., et al. (2009). The Last Glacial Maximum. *Science*, *325*(5941), 710–714. https://doi.org/10.1126/science.1172873

Clarke, G. K. C., Leverington, D. W., Teller, J. T., & Dyke, A. S. (2004). Paleohydraulics of the last outburst flood from glacial Lake Agassiz and the 8200 BP cold event. *Quaternary Science Reviews*, *23*(3–4), 389–407. https://doi.org/10.1016/j.quascirev.2003.06.004

Clemens, S. C., Prell, W. L., & Sun, Y. (2010). Orbital-scale timing and mechanisms driving Late Pleistocene Indo-Asian summer monsoons: Reinterpreting cave speleothem $\delta^{18}O$. *Paleoceanography*, *25*(4), 1–19. https://doi.org/10.1029/2010PA001926

Dansgaard, W. (1964). Stable isotopes in precipitation. *Tellus*, *16*(4), 436–468. https://doi.org/10.3402/tellusa.v16i4.8993

Day, C. C., & Henderson, G. M. (2013). Controls on trace-element partitioning in cave-analogue calcite. *Geochimica et Cosmochimica Acta*, *120*, 612–627. https://doi.org/10.1016/j.gca.2013.05.044

Dayem, K. E., Molnar, P., Battisti, D. S., & Roe, G. H. (2010). Lessons learned from oxygen isotopes in modern precipitation applied to interpretation of speleothem records of paleoclimate from eastern Asia. *Earth and Planetary Science Letters*, *295*(1–2), 219–230. https://doi.org/10.1016/j.epsl.2010.04.003

Denniston, R. F., Asmerom, Y., Polyak, V. J., Wanamaker, A. D., Ummenhofer, C. C., Humphreys, W. F., et al. (2017). Decoupling of monsoon activity across the northern and southern Indo-Pacific during the Late Glacial. *Quaternary Science Reviews*, *176*, 101–105. https://doi.org/10.1016/j.quascirev.2017.09.014

Dorale, J. A. (1998). Climate and Vegetation History of the Midcontinent from 75 to 25 ka: A Speleothem Record from Crevice Cave, Missouri, USA. *Science*, *282*(5395), 1871–1874. https://doi.org/10.1126/science.282.5395.1871

Dreybrodt, J., Laumanns, M., and Steiner, H., (2013a). Ten years of exploration and over 100km of caves surveyed in Northern Laos, UIS Congress Brno, 2013, 68–70.

Dreybrodt, J., and Laumanns, M. (eds), (2013b). The unknown north of Laos. (Part 5 – 2012–2013: Karst and caves of the provinces Luang Nam Tha, Luang Prabang and Houaphan). Berliner Hoehlenkundliche Berichte, Vol.49, 5–148.

Dykoski, C. A., Edwards, R. L., Cheng, H., Yuan, D., Cai, Y., Zhang, M., et al. (2005). A high-resolution, absolute-dated Holocene and deglacial Asian monsoon record from Dongge Cave, China. *Earth and Planetary Science Letters*, *233*(1–2), 71–86. https://doi.org/10.1016/j.epsl.2005.01.036

Edwards, R., Chen, J. H., & Wasserburg, G. J. (1987). 238U234U230Th232Th systematics and the precise measurement of time over the past 500,000 years. *Earth and Planetary Science Letters*, *81*(2–3), 175–192. https://doi.org/10.1016/0012-821X(87)90154-3

Ellison, C. R. W., Chapman, M. R., & Hall, I. R. (2006). Surface and deep ocean interactions during the cold climate event 8200 years ago. *Science*, *312*(5782), 1929–1932. https://doi.org/10.1126/science.1127213

Fairchild, I. J., & Baker, A. (2012). *Speleothem Science: From Process to Past Environments*. Wiley-Blackwell.

Fairchild, I. J., & Treble, P. C. (2009). Trace elements in speleothems as recorders of environmental change. *Quaternary Science Reviews*, *28*(5–6), 449–468. https://doi.org/10.1016/j.quascirev.2008.11.007

Fairchild, I. J., Borsato, A., Tooth, A. F., Frisia, S., Hawkesworth, C. J., Huang, Y., et al. (2000). Controls on trace element (Sr-Mg) compositions of carbonate cave waters: Implications for speleothem climatic records. *Chemical Geology*, *166*(3–4), 255–269. https://doi.org/10.1016/S0009-2541(99)00216-8

Fairchild, I. J., Smith, C. L., Baker, A., Fuller, L., Spötl, C., Mattey, D., & McDermott, F. (2006). Modification and preservation of environmental signals in speleothems. *Earth-Science Reviews*, *75*(1–4), 105–153. https://doi.org/10.1016/j.earscirev.2005.08.003

Fleitmann, D., Burns, S. J., Neff, U., Mudelsee, M., Mangini, A., & Matter, A. (2004). Palaeoclimatic interpretation of high-resolution oxygen isotope profiles derived from annually laminated speleothems from Southern Oman. *Quaternary Science Reviews*, *23*(7–8), 935–945. https://doi.org/10.1016/j.quascirev.2003.06.019

Fohlmeister, J., Kromer, B., & Mangini, A. (2011). The influence of soil organic matter age spectrum on the reconstruction of atmospheric 14C levels via stalagmites. *Radiocarbon*, *53*(1), 99–115.

Ford, D. C., & Williams, P. (2013). *Karst hydrogeology and geomorphology*. Wiley.

Frisia, S., Borsato, A., Fairchild, I. J., & Susini, J. (2005). Variations in atmospheric sulphate recorded in stalagmites by synchrotron micro-XRF and XANES analyses. *Earth and Planetary Science Letters*, *235*(3–4), 729–740. https://doi.org/10.1016/j.epsl.2005.03.026

Frisia, S., Fairchild, I. J., Fohlmeister, J., Miorandi, R., Spötl, C., & Borsato, A. (2011). Carbon mass-balance modelling and carbon isotope exchange processes in dynamic caves. *Geochimica et Cosmochimica Acta*, *75*(2), 380–400. https://doi.org/10.1016/j.gca.2010.10.021

Frumkin, A., & Stein, M. (2004). The Sahara-East Mediterranean dust and climate connection revealed by strontium and uranium isotopes in a Jerusalem speleothem. *Earth and Planetary Science Letters*, *217*(3–4), 451–464. https://doi.org/10.1016/S0012-821X(03)00589-2

Gaudinski, J. B., Trumbore, S. E., Davidson, E. A., & Zheng, S. (2000). Soil carbon cycling in a temperate forest: radiocarbon-based estimates of residence times, sequestration rates and partitioning of fluxes. *Biogeochemistry*, *51*(1), 33–69. https://doi.org/10.1023/A:1006301010014

Genty, D., & Massault, M. (1997). Bomb 14C recorded in laminated speleothems: calculation of dead carbon proportion. *Radiocarbon*, *39*(1), 33–48.

Genty, D., & Massault, M. (1999a). Carbon transfer dynamics from bomb- 14C and δ13C time series of a laminated stalagmite from SW France-Modelling and comparison with other stalagmite records. *Geochimica et Cosmochimica Acta*, *63*(10), 1537–1548. https://doi.org/10.1016/S0016-7037(99)00122-2

Genty, D., Massault, M., Gilmour, M., Baker, A., Verheyden, S., & Kepens, E. (1999b). Calculation of Past Dead Carbon Proportion and Variability by the Comparison of AMS ^{14}C and Tims U/TH Ages on Two Holocene Stalagmites. *Radiocarbon*, *41*(3), 251–270. https://doi.org/10.1017/S003382220005712X

Genty, D., Baker, A., Massault, M., Proctor, C., Gilmour, M., Pons-Branchu, E., & Hamelin, B. (2001). Dead carbon in stalagmites: Carbonate bedrock paleodissolution vs. ageing of soil organic matter. Implications for 13C variations in speleotherms. *Geochimica et Cosmochimica Acta*, *65*(20), 3443–3457. https://doi.org/10.1016/S0016-7037(01)00697-4

Griffiths, M. L., Fohlmeister, J., Drysdale, R. N., Hua, Q., Johnson, K. R., Hellstrom, J. C., et al. (2012). Hydrological control of the dead carbon fraction in a Holocene tropical speleothem. *Quaternary Geochronology*, *14*, 81–93. https://doi.org/10.1016/j.quageo.2012.04.001

Griffiths, M. L., Drysdale, R. N., Gagan, M. K., Frisia, S., Zhao, J. X., Ayliffe, L. K., et al. (2010a). Evidence for Holocene changes in Australian-Indonesian monsoon rainfall from stalagmite trace element and stable isotope ratios. *Earth and Planetary Science Letters*, *292*(1–2), 27–38. https://doi.org/10.1016/j.epsl.2010.01.002

Griffiths, M. L., Drysdale, R. N., Vonhof, H. B., Gagan, M. K., Zhao, J. X., Ayliffe, L. K., et al. (2010b). Younger Dryas-Holocene temperature and rainfall history of southern Indonesia from d18O in speleothem calcite and fluid inclusions. *Earth and Planetary Science Letters*, *295*(1–2), 30–36. https://doi.org/10.1016/j.epsl.2010.03.018

Griffiths, M. L., Johnson, K. R., Pausata, F. S. R., White, J. C., Henderson, G. M., Wood, C. T., Yang, H., Ersek, V., Conrad, C., Sekhon, N. (in revision). Holocene megadroughts in the middle Mekong basin linked to global climate changes. (in revision for submission to *Science Advances*)

Griffiths, M. L., Kimbrough, A. K., Gagan, M. K., Drysdale, R. N., Cole, J. E., Johnson, K. R., et al. (2016). Western Pacific hydroclimate linked to global climate variability over the past two millennia. *Nature Communications*, *7*, 11719. https://doi.org/10.1038/ncomms11719

Gupta, A. K., Anderson, D. M., & Overpeck, J. T. (2003). Abrupt changes in the Asian southwest monsoon during the Holocene and their links to the North Atlantic Ocean. *Nature*, *421*(6921n), 354–357. https://doi.org/10.1038/nature01340

Hartland, A., Fairchild, I. J., Lead, J. R., Borsato, A., Baker, A., Frisia, S., & Baalousha, M. (2012). From soil to cave: Transport of trace metals by natural organic matter in karst dripwaters. *Chemical Geology*, *304–305*, 68–82. https://doi.org/10.1016/j.chemgeo.2012.01.032

Heinrich, H. (1988). Origin and Consequences of Cyclic Ice Rafting in the Northeast Atlantic Ocean During the Past 130,000 Years. *Quaternary Research*, *29*(2), 142–152. https://doi.org/10.1016/0033-5894(88)90057-9

Hellstrom, J. (2006). U-Th dating of speleothems with high initial 230Th using stratigraphical constraint. *Quaternary Geochronology*, *1*(4), 289–295. https://doi.org/10.1016/j.quageo.2007.01.004

Hendy, C. (1971). The isotopic geochemistry of speleothems—I. The calculation of the effects of different modes of formation on the isotopic composition of speleothems and their applicability as palaeoclimatic indicators. *Geochimica et Cosmochimica Acta*, *35*(8), 801–824. https://doi.org/10.1016/0016-7037(71)90127-X

Hoffmann, D. L., Beck, J. W., Richards, D. A., Smart, P. L., Singarayer, J. S., Ketchmark, T., & Hawkesworth, C. J. (2010). Towards radiocarbon calibration beyond 28 ka using speleothems from the Bahamas. *Earth and Planetary Science Letters*, *289*(1–2), 1–10. https://doi.org/10.1016/J.EPSL.2009.10.004

Hu, C., Henderson, G. M., Huang, J., Xie, S., Sun, Y., & Johnson, K. R. (2008). Quantification of Holocene Asian monsoon rainfall from spatially separated cave records. *Earth and Planetary Science Letters*, *266*(3–4), 221–232. https://doi.org/10.1016/j.epsl.2007.10.015

Hua, Q., McDonald, J., Redwood, D., Drysdale, R., Lee, S., Fallon, S., & Hellstrom, J. (2012). Robust chronological reconstruction for young speleothems using radiocarbon. *Quaternary Geochronology*, *14*, 67–80. https://doi.org/10.1016/j.quageo.2012.04.017

Huang, Y., & Fairchild, I. J. (2001a). Partitioning of Sr2+ and Mg2+ into calcite under karst-analogue experimental conditions. *Geochimica et Cosmochimica Acta*, *65*(1), 47–62. https://doi.org/10.1016/S0016-7037(00)00513-5

Huang, Y., Fairchild, I. J., Borsato, A., Frisia, S., Cassidy, N. J., McDermott, F., & Hawkesworth, C. J. (2001b). Seasonal variations in Sr, Mg and P in modern speleothems (Grotta di Ernesto, Italy). *Chemical Geology*, *175*(3–4), 429–448. https://doi.org/10.1016/S0009-2541(00)00337-5

Johnson, K. R. (2011). Palaeoclimate: Long-distance relationship. *Nature Geoscience*, *4*(7), 426–427. https://doi.org/10.1038/ngeo1190

Johnson, K. R., Griffiths, M., Bhattacharya, T., Borsato, A., Wood, C. T., Frisia, S., Henderson, G., LeGrande, A., Lewis, M., Mason, A., Syed, S., Tierney, J., Wang, J. K., Yang, H. (in revision). Orbital and millennial variability of Southeast Asian hydroclimate over the past 38,000 years. (in revision for submission to *Nature Geoscience*)

Johnson, K. R., & Ingram, B. L. (2004). Spatial and temporal variability in the stable isotope systematics of modern precipitation in China: Implications for paleoclimate reconstructions. *Earth and Planetary Science Letters*, *220*(3–4), 365–377. https://doi.org/10.1016/S0012-821X(04)00036-6

Johnson, K. R., Hu, C., Belshaw, N. S., & Henderson, G. M. (2006). Seasonal trace-element and stable-isotope variations in a Chinese speleothem: The potential for high-resolution paleomonsoon reconstruction. *Earth and Planetary Science Letters*, *244*(1–2), 394–407. https://doi.org/10.1016/j.epsl.2006.01.064

Kiernan, K. (2015). Karst geomorphology along the Nam Ou, northern Lao PDR. *Cave and Karst Science*, *42*(2), 86–94.

Kobashi, T., Severinghaus, J. P., Brook, E. J., Barnola, J.-M., & Grachev, A. M. (2007). Precise timing and characterization of abrupt climate change 8200 years ago from air trapped in polar ice. *Quaternary Science Reviews*, *26*(9–10), 1212–1222. https://doi.org/10.1016/J.QUASCIREV.2007.01.009

Lau, K. M., & Yang, S. (1997). Climatology and interannual variability of the southeast asian summer monsoon. *Advances in Atmospheric Sciences*, *14*(2), 141–162. https://doi.org/10.1007/s00376-997-0016-y

Lechleitner, F. A., Fohlmeister, J., McIntyre, C., Baldini, L. M., Jamieson, R. A., Hercman, H., et al. (2016a). A novel approach for construction of radiocarbon-based chronologies for speleothems. *Quaternary Geochronology*, *35*, 54–66. https://doi.org/10.1016/j.quageo.2016.05.006

Lechleitner, F. A., Baldini, J. U. L., Breitenbach, S. F. M., Fohlmeister, J., McIntyre, C., Goswami, B., et al. (2016b). Hydrological and climatological controls on radiocarbon concentrations in a tropical stalagmite. *Geochimica et Cosmochimica Acta*, *194*, 233–252. https://doi.org/10.1016/j.gca.2016.08.039

Lechleitner, F. A., Breitenbach, S. F. M., Cheng, H., Plessen, B., Rehfeld, K., Goswami, B., et al. (2017). Climatic and in-cave influences on δ18O and δ13C in a stalagmite from northeastern India through the last deglaciation. *Quaternary Research*, (2017), 1–14. https://doi.org/10.1017/qua.2017.72

LeGrande, A. N., & Schmidt, G. A. (2008). Ensemble, water isotope-enabled, coupled general circulation modeling insights into the 8.2 ka event. *Paleoceanography*, *23*(3), n/a-n/a. https://doi.org/10.1029/2008PA001610

Liu, J., Chen, J., Zhang, X., Li, Y., Rao, Z., & Chen, F. (2015). Holocene East Asian summer monsoon records in northern China and their inconsistency with Chinese stalagmite $\delta^{18}O$ records. *Earth-Science Reviews*, *148*, 194–208. https://doi.org/10.1016/j.earscirev.2015.06.004

Liu, Y. H., Henderson, G. M., Hu, C. Y., Mason, A. J., Charnley, N., Johnson, K. R., & Xie, S. C. (2013). Links between the East Asian monsoon and North Atlantic climate during the 8,200 year event. *Nature Geoscience*, *6*(2), 117–120. https://doi.org/10.1038/ngeo1708

Macias-Fauria, M., Grinsted, A., Helama, S., & Holopainen, J. (2012). Persistence matters: Estimation of the statistical significance of paleoclimatic reconstruction statistics from autocorrelated time series. *Dendrochronologia*, *30*(2), 179–187. https://doi.org/10.1016/j.dendro.2011.08.003

Maher, B. A. (2008). Holocene variability of the East Asian summer monsoon from Chinese cave records: a re-assessment. *The Holocene*, *18*(6), 861–866. https://doi.org/10.1177/0959683608095569

Matero, I. S. O., Gregoire, L. J., Ivanovic, R. F., Tindall, J. C., & Haywood, A. M. (2017). The 8.2 ka cooling event caused by Laurentide ice saddle collapse. *Earth and Planetary Science Letters*, *473*, 205–214. https://doi.org/10.1016/J.EPSL.2017.06.011

Mattey, D. P., Fairchild, I. J., Atkinson, T. C., Latin, J.-P., Ainsworth, M., & Durell, R. (2010). Seasonal microclimate control of calcite fabrics, stable isotopes and trace elements in modern speleothem from St Michaels Cave, Gibraltar. *Geological Society, London, Special Publications*, *336*(1), 323 LP – 344. Retrieved from http://sp.lyellcollection.org/content/336/1/323.abstract

Maxwell, A. L. (2001). Holocene Monsoon Changes Inferred from Lake Sediment Pollen and Carbonate Records, Northeastern Cambodia. *Quaternary Research*, *56*(3), 390–400. https://doi.org/10.1006/qres.2001.2271

McGee, D., Donohoe, A., Marshall, J., & Ferreira, D. (2014). Changes in ITCZ location and cross-equatorial heat transport at the Last Glacial Maximum, Heinrich Stadial 1, and the mid-Holocene. *Earth and Planetary Science Letters*, *390*, 69–79. https://doi.org/10.1016/j.epsl.2013.12.043

McManus, J. F., Francois, R., Gheraradi, J. M., Keigwin, L. D., & Brown-Leger, S. (2004). Collapse and rapid resumption of Atlantic meridional circulation linked to glacial climate changes. *Nature*, *428*(April), 834–837.

Medina-Elizalde, M., Burns, S. J., Lea, D. W., Asmerom, Y., von Gunten, L., Polyak, V., et al. (2010). High resolution stalagmite climate record from the Yucatán Peninsula spanning the Maya terminal classic period. *Earth and Planetary Science Letters*, *298*(1–2), 255–262. https://doi.org/10.1016/j.epsl.2010.08.016

Misra, V., & Dinapoli, S. (2014). The variability of the Southeast Asian summer monsoon. *International Journal of Climatology*, *34*(3), 893–901. https://doi.org/10.1002/joc.3735

Mook, W. G., Bommerson, J. C., & Staverman, W. H. (1974). Carbon isotope fractionation between dissolved bicarbonate and gaseous carbon dioxide. *Earth and Planetary Science Letters*, *22*(2), 169–176. https://doi.org/10.1016/0012-821X(74)90078-8

Moore, G. W. (1952). Speleothem - a new cave term. *Natl Speleol Soc News*, *10*(2).

Morrill, C., Legrande, A. N., Renssen, H., Bakker, P., & Otto-Bliesner, B. L. (2013a). Model sensitivity to North Atlantic freshwater forcing at 8.2 ka. *Clim. Past*, *9*, 955–968. https://doi.org/10.5194/cp-9-955-2013

Morrill, C., Anderson, D. M., Bauer, B. A., Buckner, R., Gille, E. P., Gross, W. S., et al. (2013b). Proxy benchmarks for intercomparison of 8.2 ka simulations. *Climate of the Past*, *9*(1), 423–432. https://doi.org/10.5194/cp-9-423-2013

Morse, J. W., & Bender, M. L. (1990). Partition coefficients in calcite: Examination of factors influencing the validity of experimental results and their application to natural systems. *Chemical Geology*, *82*(C), 265–277. https://doi.org/10.1016/0009-2541(90)90085-L

Mühlinghaus, C., Scholz, D., & Mangini, A. (2007). Modelling stalagmite growth and δ13C as a function of drip interval and temperature>. *Geochimica et Cosmochimica Acta*, *71*(11), 2780–2790. https://doi.org/10.1016/j.gca.2007.03.018

Noronha, A. L., Johnson, K. R., Hu, C., Ruan, J., Southon, J. R., & Ferguson, J. E. (2014). Assessing influences on speleothem dead carbon variability over the Holocene: Implications for speleothem-based radiocarbon calibration. *Earth and Planetary Science Letters*, *394*, 20–29. https://doi.org/10.1016/j.epsl.2014.03.015

Noronha, A. L., Johnson, K. R., Southon, J. R., Hu, C., Ruan, J., & McCabe-Glynn, S. (2015). Radiocarbon evidence for decomposition of aged organic matter in the vadose zone as the main source of speleothem carbon. *Quaternary Science Reviews*, *127*, 37–47. https://doi.org/10.1016/j.quascirev.2015.05.021

Orland, I. J., Edwards, R. L., Cheng, H., Kozdon, R., Cross, M., & Valley, J. W. (2015). Direct measurements of deglacial monsoon strength in a Chinese stalagmite. *Geology*, *43*(6), 555–558. https://doi.org/10.1130/G36612.1

Oster, J. L., Montañez, I. P., Guilderson, T. P., Sharp, W. D., & Banner, J. L. (2010). Modeling speleothem ??13C variability in a central Sierra Nevada cave using 14C and 87Sr/86Sr. *Geochimica et Cosmochimica Acta*, *74*(18), 5228–5242. https://doi.org/10.1016/j.gca.2010.06.030

Owen, R. A., Day, C. C., & Henderson, G. M. (2018). CaveCalc: A new model for speleothem chemistry & isotopes. *Computers and Geosciences*, *119*(July), 115–122. https://doi.org/10.1016/j.cageo.2018.06.011

Owen, R. A., Day, C. C., Hu, C. Y., Liu, Y. H., Pointing, M. D., Blättler, C. L., & Henderson, G. M. (2016). Calcium isotopes in caves as a proxy for aridity: Modern calibration and application to the 8.2 kyr event. *Earth and Planetary Science Letters*, *443*, 129–138. https://doi.org/10.1016/j.epsl.2016.03.027

Partin, J. W., Cobb, K. M., Adkins, J. F., Clark, B., & Fernandez, D. P. (2007). Millennial-scale trends in west Pacific warm pool hydrology since the Last Glacial Maximum. *Nature*, *449*(7161), 452–455. https://doi.org/10.1038/nature08125

Partin, J. W., Cobb, K. M., Adkins, J. F., Tuen, A. A., & Clark, B. (2013). Trace metal and carbon isotopic variations in cave dripwater and stalagmite geochemistry from northern Borneo. *Geochemistry, Geophysics, Geosystems*, *14*(9), 3567–3585. https://doi.org/10.1002/ggge.20215

Paterson, D., De Jonge, M. D., Howard, D. L., Lewis, W., McKinlay, J., Starritt, A., et al. (2011). The X-ray fluorescence microscopy beamline at the Australian synchrotron. In *AIP Conference Proceedings* (Vol. 1365, pp. 219–222). https://doi.org/10.1063/1.3625343

Pausata, F. S. R., Battisti, D. S., Nisancioglu, K. H., & Bitz, C. M. (2011). Chinese stalagmite δ18O controlled by changes in the Indian monsoon during a simulated Heinrich event. *Nature Geoscience*, *4*(7), 474–480. https://doi.org/10.1038/ngeo1169

Petit, J. R., Jouzel, J., Raynaud, D., Barkov, N. I., Barnola, J. M., Basile, I., et al. (1999). Climate and atmospheric history of the past 420,000 years from the Vostok ice core, Antarctica. *Nature*, *399*(6735), 429–436. https://doi.org/10.1038/20859

Piccini, L., Zanchetta, G., Drysdale, R. N., Hellstrom, J., Leone, G., Doveri, M., et al. (2008). The environmental features of the Monte Corchia cave system (Apuan Alps, central Italy) and their effects on speleothem growth. *International Journal of Speleology*, *37*(3), 153–172. https://doi.org/10.5038/1827-806x.37.3.2

Prell, W. L., & Kutzbach, J. E. (1987). Monsoon variability over the past 150,000 years. *Journal of Geophysical Research*, *92*(D7), 8411. https://doi.org/10.1029/JD092iD07p08411

Reimer, P. J., Bard, E., Bayliss, A., Beck, J. W., Blackwell, P. G., Ramsey, C. B., et al. (2013). Selection and Treatment of Data for Radiocarbon Calibration: An Update to the International Calibration (IntCal) Criteria. *Radiocarbon*, *55*(04), 1923–1945. https://doi.org/10.2458/azu_js_rc.55.16955

Ridley, H. E., Asmerom, Y., Baldini, J. U. L., Breitenbach, S. F. M., Aquino, V. V., Prufer, K. M., et al. (2015). Aerosol forcing of the position of the intertropical convergence zone since ad 1550. *Nature Geoscience*, *8*(3), 195–200. https://doi.org/10.1038/ngeo2353

Rohling, E. J., & Pälike, H. (2005). Centennial-scale climate cooling with a sudden cold event around 8,200 years ago. *Nature*, *434*(7036), 975–979. https://doi.org/10.1038/nature03421

Rosenthal, Y., Field, M. P., & Sherrell, R. M. (1999). Precise Determination of Element / Calcium Ratios in Calcareous Samples Using Sector Field Inductively Coupled Plasma Mass Spectrometry. *Analytical Chemistry*, *71*(15), 3248–3253.

Rudzka, D., McDermott, F., Baldini, L. M., Fleitmann, D., Moreno, A., & Stoll, H. (2011). The coupled δ13C-radiocarbon systematics of three Late Glacial/early Holocene speleothems; insights into soil and cave processes at climatic transitions. *Geochimica et Cosmochimica Acta*, *75*(15), 4321–4339. https://doi.org/10.1016/j.gca.2011.05.022

Ryan, C. G., Siddons, D. P., Kirkham, R., Dunn, P. A., Kuczewski, A., Moorhead, G., et al. (2010). The new Maia detector system: Methods for high definition trace element imaging of natural material. In *AIP Conference Proceedings* (Vol. 1221, pp. 9–17). https://doi.org/10.1063/1.3399266

Saltzman, M. R., & Thomas, E. (2012). Carbon Isotope Stratigraphy. *The Geologic Time Scale 2012*, *1–2*, 207–232. https://doi.org/10.1016/B978-0-444-59425-9.00011-1

Santos, G. M., Southon, J. R., Druffel-Rodriguez, K. C., Griffin, S., & Mazon, M. (2004). Magnesium Perchlorate as an Alternative Water Trap in AMS Graphite Sample Preparation: A Report On Sample Preparation at Kccams at the University of California, Irvine. *Radiocarbon*, *46*(1), 165–173. https://doi.org/10.1017/S0033822200039485

Santos, G. M., & Xu, X. (2017). Bag of Tricks: A Set of Techniques and other Resources to Help ^{14}C Laboratory Setup, Sample Processing, and Beyond. *Radiocarbon*, *59*(3), 785–801. https://doi.org/10.1017/RDC.2016.43

Schneider, T., Bischoff, T., & Haug, G. H. (2014). Migrations and dynamics of the intertropical convergence zone. *Nature*, *513*(7516), 45–53. https://doi.org/10.1038/nature13636

Scholz, D., & Hoffmann, D. L. (2011). StalAge - An algorithm designed for construction of speleothem age models. *Quaternary Geochronology*, *6*(3–4), 369–382. https://doi.org/10.1016/j.quageo.2011.02.002

Shrestha, B., Maskey, S., Babel, M. S., van Griensven, A., & Uhlenbrook, S. (2018). Sediment related impacts of climate change and reservoir development in the Lower Mekong River Basin: a case study of the Nam Ou Basin, Lao PDR. *Climatic Change*, *149*(1), 13–27. https://doi.org/10.1007/s10584-016-1874-z

Sinclair, D. J., Banner, J. L., Taylor, F. W., Partin, J., Jenson, J., Mylroie, J., et al. (2012). Magnesium and strontium systematics in tropical speleothems from the Western Pacific. *Chemical Geology*, *294–295*, 1–17. https://doi.org/10.1016/j.chemgeo.2011.10.008

Southon, J., Noronha, A. L., Cheng, H., Edwards, R. L., & Wang, Y. (2012). A high-resolution record of atmospheric14C based on Hulu Cave speleothem H82. *Quaternary Science Reviews*, *33*, 32–41. https://doi.org/10.1016/j.quascirev.2011.11.022

Spötl, C., Fohlmeister, J., Cheng, H., & Boch, R. (2016). Modern aragonite formation at near-freezing conditions in an alpine cave, Carnic Alps, Austria. *Chemical Geology*, *435*, 60–70. https://doi.org/10.1016/j.chemgeo.2016.04.017

Stocker, T. F., Qin, D., Plattner, G.-K., Tignor, M. M. B., Allen, S. K., Boschung, J., et al. (2013). *Climate Change 2013 The Physical Science Basis Working Group I Contribution to the Fifth Assessment Report of the Intergovernmental Panel on Climate Change Edited by*. Retrieved from www.cambridge.org

Stuiver, M., & Polach, H. A. (1977). Discussion Reporting of ^{14}C Data. *Radiocarbon*, *19*(3), 355–363. https://doi.org/10.1017/S0033822200003672

Teller, J. T., Leverington, D. W., & Mann, J. D. (2002). Freshwater outbursts to the oceans from glacial Lake Agassiz and their role in climate change during the last deglaciation. *Quaternary Science Reviews*, *21*(8–9), 879–887. https://doi.org/10.1016/S0277-3791(01)00145-7

Thomas, E. R., Wolff, E. W., Mulvaney, R., Steffensen, J. P., Johnsen, S. J., Arrowsmith, C., et al. (2007). The 8.2 ka event from Greenland ice cores. *Quaternary Science Reviews*, *26*(1–2), 70–81. https://doi.org/10.1016/J.QUASCIREV.2006.07.017

Tindall, J. C., & Valdes, P. J. (2011). Modeling the 8.2 ka event using a coupled atmosphere–ocean GCM. *Global and Planetary Change*, *79*(3–4), 312–321. https://doi.org/10.1016/J.GLOPLACHA.2011.02.004

Treble, P. C., Bradley, C., Wood, A., Baker, A., Jex, C. N., Fairchild, I. J., et al. (2013). An isotopic and modelling study of flow paths and storage in Quaternary calcarenite, SW Australia: Implications for speleothem paleoclimate records. *Quaternary Science Reviews*, *64*, 90–103. https://doi.org/10.1016/j.quascirev.2012.12.015

Treble, P. C., Fairchild, I. J., Griffiths, A., Baker, A., Meredith, K. T., Wood, A., & McGuire, E. (2015). Impacts of cave air ventilation and in-cave prior calcite precipitation on Golgotha Cave dripwater chemistry, southwest Australia. *Quaternary Science Reviews*, *127*, 61–72. https://doi.org/10.1016/j.quascirev.2015.06.001

Tremaine, D. M., & Froelich, P. N. (2013). Speleothem trace element signatures: A hydrologic geochemical study of modern cave dripwaters and farmed calcite. *Geochimica et Cosmochimica Acta*, *121*, 522–545. https://doi.org/10.1016/j.gca.2013.07.026

Trenberth, K. E., Stepaniak, D. P., & Caron, J. M. (2000). The global monsoon as seen through the divergent atmospheric circulation. *Journal of Climate*, *13*(22), 3969–3993. https://doi.org/10.1175/1520-0442(2000)013<3969:TGMAST>2.0.CO;2

Trumbore, S. (2000). Age of soil organic matter and soil respiration: Radiocarbon constraints on belowground C dynamics. *Ecological Applications*, *10*(2), 399–411. https://doi.org/10.1890/1051-0761(2000)010[0399:AOSOMA]2.0.CO;2

Wang, J. K., Johnson, K. R., Borsato, A., Amaya, D. J., Griffiths, M. L., Henderson, G. M., et al. (2019). Hydroclimatic variability in Southeast Asia over the past two millennia. *Earth and Planetary Science Letters*, *525*, 115737. https://doi.org/10.1016/j.epsl.2019.115737

Wang, X., Auler, A. S., Edwards, R. L., Cheng, H., Ito, E., & Solheid, M. (2006). Interhemispheric anti-phasing of rainfall during the last glacial period. *Quaternary Science Reviews*, *25*(23–24), 3391–3403. https://doi.org/10.1016/j.quascirev.2006.02.009

Wang, Y., Cheng, H., Edwards, R. L., He, Y., Kong, X., An, Z., et al. (2005). The Holocene Asian Monsoon : Links to Solar Changes and North Atlantic Climate, *2002*(May), 854–858.

Wang, Y., Cheng, H., Edwards, R. L., Kong, X., Shao, X., Chen, S., et al. (2008). Millennial- and orbital-scale changes in the East Asian monsoon over the past 224,000 years. *Nature*, *451*(7182), 1090–1093. https://doi.org/10.1038/nature06692

Wang, Y., Cheng, H., Edwards, R. L., An, Z. S., Wu, J. Y., Shen, C. C., & Dorale, J. a. (2001). A high-resolution absolute-dated late Pleistocene Monsoon record from Hulu Cave, China. *Science (New York, N.Y.)*, *294*(5550), 2345–2348. https://doi.org/10.1126/science.1064618

Wanner, H., Beer, J., Bütikofer, J., Crowley, T. J., Cubasch, U., Flückiger, J., et al. (2008). Mid- to Late Holocene climate change: an overview. *Quaternary Science Reviews*, *27*(19–20), 1791–1828. https://doi.org/10.1016/j.quascirev.2008.06.013

Ward, B. M., Wong, C. I., Novello, V. F., McGee, D., Santos, R. V., Silva, L. C. R., et al. (2019). Reconstruction of Holocene coupling between the South America Monsoon System and local moisture variability from speleothem δ 18 O and 87 Sr/ 86 Sr records. *Quaternary Science Reviews*, *210*, 51–63. https://doi.org/10.1016/j.quascirev.2019.02.019

Wong, C. I., & Breecker, D. O. (2015). Advancements in the use of speleothems as climate archives. *Quaternary Science Reviews*, *127*, 1–18. https://doi.org/10.1016/j.quascirev.2015.07.019

Wong, C. I., Banner, J. L., & Musgrove, M. (2011). Seasonal dripwater Mg/Ca and Sr/Ca variations driven by cave ventilation: Implications for and modeling of speleothem paleoclimate records. *Geochimica et Cosmochimica Acta*, *75*(12), 3514–3529. https://doi.org/10.1016/j.gca.2011.03.025

Wood, C. T., Johnson, K. R., Griffiths, M. L., Borsato, A. (in prep., a) Speleothem trace element responses over the last deglaciation and Holocene in Northern Laos. (target journal: *Quaternary Science Reviews*)

Wood, C. T., Johnson, K. R., Griffiths, M. L., Borsato, A., Czimcik, C., Walker, J., Xu, X. (in prep., b) Speleothem radiocarbon evidence for paleohydrologic changes in Mainland Southeast Asia (target journal: *Geochimica et Cosmochimica Acta*)

Xie, P., & Arkin, P. A. (1997). Global Precipitation: A 17-Year Monthly Analysis Based on Gauge Observations, Satellite Estimates, and Numerical Model Outputs. *Bulletin of the American Meteorological Society*, *78*(11), 2539–2558. https://doi.org/10.1175/1520-0477(1997)078<2539:GPAYMA>2.0.CO;2

Xu, X., Trumbore, S. E., Zheng, S., Southon, J. R., McDuffee, K. E., Luttgen, M., & Liu, J. C. (2007). Modifying a sealed tube zinc reduction method for preparation of AMS graphite targets: Reducing background and attaining high precision. *Nuclear Instruments and Methods in Physics Research Section B: Beam Interactions with Materials and Atoms*, *259*(1), 320–329. https://doi.org/10.1016/J.NIMB.2007.01.175

Yang, H., Johnson, K. R., Griffiths, M. L., & Yoshimura, K. (2016). Interannual controls on oxygen isotope variability in Asian monsoon precipitation and implications for paleoclimate reconstructions. *Journal of Geophysical Research: Atmospheres*, *121*(14), 8410–8428. https://doi.org/10.1002/2015JD024683

Yuan, D., Cheng, H., Edwards, R. L., Dykoski, C. A., Kelly, M. J., Zhang, M., et al. (2004). Timing, Duration, and Transitions of the Last Interglacial Asian Monsoon. *Science*, *304*(5670), 575–578. https://doi.org/10.1126/science.1091220

Zhang, H., Griffiths, M. L., Huang, J., Cai, Y., Wang, C., Zhang, F., et al. (2016). Antarctic link with East Asian summer monsoon variability during the Heinrich Stadial–Bølling interstadial transition. *Earth and Planetary Science Letters*, *453*, 243–251. https://doi.org/10.1016/j.epsl.2016.08.008

Zhang, H., Griffiths, M. L., Chiang, J. C. H., Kong, W., Wu, S., Atwood, A., et al. (2018). East Asian hydroclimate modulated by the position of the westerlies during Termination I. *Science (New York, N.Y.)*, *362*(6414), 580–583. https://doi.org/10.1126/science.aat9393

Zhou, H., Feng, Y. xing, Zhao, J. xin, Shen, C. C., You, C. F., & Lin, Y. (2009). Deglacial variations of Sr and 87Sr/86Sr ratio recorded by a stalagmite from Central China and their association with past climate and environment. *Chemical Geology*, *268*(3–4), 233–247. https://doi.org/10.1016/j.chemgeo.2009.09.003

Appendix 1

Glossary of acronyms used in the text

8.2 – 8.2 ka event *(8.2 kiloyear event)* – An abrupt, ~150-160 years long climate event ~8,200 years before present (yrs BP) during the Holocene. **1**, 12, **15**, **19**, 20, 22-23, 34-35, 45-47, 51-52, 55, 57, 63, 78, 82, 86-90, **96-98**, 101-103, 105-119, 121-122

AM – Asian Monsoon – The greater monsoon region of Asia, which includes the Indian Monsoon, the East Asian Monsoon, and the Southeast Asian Monsoon realms. **1**, 2-3, 6, **13-17**, 19-20, 22-24, 27, 45, 49

AMOC – Atlantic meridional overturning circulation – Term used to describe the typical circulation and meridional transportation of heat/energy in waters of the Atlantic Ocean; disrupted or halted by some abrupt climate events. **15-16**, 20, 24, 49, 115, 119

CAD – Carbonic acid dissolution – The normal mode of mildly acidic bedrock dissolution in cave settings; forms most caves over long periods of time. **59**, 75-77, 81, 89

DCP – Dead carbon proportion – The amount of fully decayed carbon sourced from bedrock in a speleothem, calculated by comparing the initial ^{14}C activity of a stalagmite to the

^{14}C activity of the atmosphere from the time of formation; sometimes controlled by open vs. closed system dissolution (hydrology), which will increase DCP in wet periods; may also be affected by input from decayed organic carbon sources. **1**, 11, 19, **54-59**, 63-64, 69-72, 74-78, 80-90, 92-93, 107-108, 123, 125-127

EASM – East Asian Summer Monsoon – The region of the Asian Monsoon covering the areas to the northeast of India and Southeast Asia (includes most of China). **6**, 14, 20, **23**, 26, 41, 45, 47, 50, **98**, 107, 111, 115, 117, 119

HS (HS1, HS2, HS3) – Heinrich stadials – Millennial scale climate events caused by large-scale melting of freshwater ice sheets and glaciers in the North Atlantic; causes Northern Hemisphere cooling, changes in ocean circulation, and a weakened Asian Monsoon. **15**, 18, 19-20, **34-35**, 40-45, 49-51, 57, 77-78, 82, 84-88, 90

ISM – Indian Summer Monsoon – Region of the Asian Monsoon affecting the country of India and the surrounding areas. **23**, 40

ITCZ – Intertropical convergence zone – Seasonally shifting band of intense convection and rainfall with a mean location north of the equator; may shift north or south during climatic changes. **16-17**, 20**, 48-50**, 52, 125

MSEA – Mainland Southeast Asia – The region of continental Southeast Asia that includes the countries of Cambodia, Laos, Myanmar, Thailand, and Vietnam. **1**, 18, 20, 22-23, 27, 40, 47-48, 52, 57, 85, 87, 90, 96-98, 110, 114-115, 117-119

NHSI – Norther Hemisphere Summer Insolation – The measure of incoming solar radiation in the Northern Hemisphere during Boreal Summer. **23**, 40, 47-48, 52

PCP – Prior calcite precipitation – Calcite ($CaCO_3$) that precipitates out of drip water in any area up-flow from the speleothem being analyzed. Increases levels of trace element ratios (Mg/Ca, Sr/Ca) during drier periods and may increase $\delta^{13}C$. **8-10**, 12, 18, 22, **25-26**, 35, 37-40, 42, 44-46, 51-53, 57, 78-80, 84-85, 87-88, 107-110

SAD – Sulfuric acid dissolution – Mechanism that enhances the dissolution of bedrock above a cave due to sulfuric acid sourced from sulfide mineral oxidation (e.g. pyrite); increases DCP to levels not possible by carbonic acid dissolution alone. **59**, **75-77**, 81, 83, 89, 127

SEAM – Southeast Asian Monsoon – The region of the Asian Monsoon affecting Mainland Southeast Asia (see MSEA entry), southwest of the East Asian Monsoon and east of the Indian Monsoon regions. **27**, 47, 49-50

WRI – Water-rock interaction – Control on speleothem trace element ratios defined by the amount of time drip waters interact with bedrock; increases trace element ratios during dry periods. **9-10**, **26**, 38-39, 44